Functional classification of cell types in the zebrafish optic tectum

Shallcross, Thomas

Awarding institution:
King's College London

Functional classification of cell types in the zebrafish optic tectum

Thomas Shallcross

Supervisors:

Dr. Martin Meyer (primary supervisor)

Dr. Matthew Grubb (secondary supervisor)

A thesis presented for the degree of

Doctor of Philosophy

Centre for Developmental Neurobiology

Institute of Psychiatry, Psychology & Neuroscience

King's College London

Contents

List of Figures

List of Tables

Acronyms

AP anterior to posterior.

DotS dot selectivity index.

dpf days post fertilisation.

DSRGC direction selective retinal ganglion cell.

DV dorsoventral.

GECI genetically encoded calcium indicators.

GEVI genetically encoded voltage indicators.

IPL inner plexiform layer.

kNN kth nearest neighbour.

LP lateral posterior thalamic nucleus.

NF narrow-field.

OKR optokinetic reflex.

OMR optomotor reflex.

PA posterior to anterior.

PBGN parabigeminal nucleus.

PV+ parvalbumin expressing.

PVN paraventricular nucleus.

RGC retinal ganglion cell.

SC superior colliculus.

scRNA-seq single cell RNA sequencing.

SIN superficial inhibitory neuron.

SOM+ somatostatin expressing.

SPV stratum periventriculare.

t-SNE t-distributed stochastic neighbour embedding.

V1 primary visual cortex.

WF wide-field.

WTA winner takes all.

Abstract

Classification of cell types in the brain remains a fundamental goal of neuroscience. A systematic classification of cell types is a means to reduce the dimensionality of the brain and is a prerequisite to understanding the nature of the neural codes underlying brain function.

Here a method is presented to functionally categorise cells within the optic tectum of larval zebrafish; a midbrain structure involved in guiding attention and movement relative to specific locations in egocentric space. Using an array of visual stimuli and functional imaging of the entire tectum with single neuron resolution, the aim of this thesis is to be able to classify tectal cell types and determine the 3D distribution of these neurons throughout the tectum. To examine whether tectal neurons can be classified by responses to specific combinations of visual features a non-parametric method of classification has been developed based on unsupervised density based clustering of tectal cell responses. From this method a number of biological findings emerged. First, neurons were found which are selective for a of conjunction visual features, namely size and direction. Second, there is evidence for dot selective neurons in the tectum. Third, there appears to be a non-uniform distribution of neuronal subtypes across the tectum, which may have implications for how information is processed across the visual scene.

The aim is to provide a cellular resolution description of tectal organisation and because the method is applied to live animals it paves the way for providing an unbiased description of the population codes underlying sensory representations in the tectum and tectally mediated behaviour.

Acknowledgements

Firstly, I would like to thank my supervisor Dr. Martin Meyer who supported me through this project. His guidance, enthusiasm, and mentoring have been irreplaceable throughout the whole experience, and I am truly grateful that I was able to conduct my PhD in his lab.

A great big thank you also to everyone in the Meyer Lab, both past and present: Dominic, Dylan, Jade, Kostas, Nikolas, Paul, Rachel, Richard, Tom, and Tom. I've had an amazing time working with you all. Not only have each of you taken the time out to help me with this project, but you've made the whole experience incredibly fun.

A special mention must go towards Giovanni; no amount of words could describe my gratitude for everything you have taught me, and helped me, with over the past few years. Thank you so much.

Thank you also to everybody in the Centre for Developmental Neurobiology, it's been such a great community to be a part of.

Lastly, I would also like to say a massive thank you to my mum and dad who have supported me over the past 29 years in anything and everything that I have chosen to do. I would not be where I am today without you.

‘A little learning is a dang’rous thing;
Drink deep, or taste not the Pierian spring:
There shallow draughts intoxicate the brain,
And drinking largely sobers us again.’
Alexander Pope (1711)

‘I need another drink’
Thomas Shallcross (2019)

Chapter 1

Introduction

1.1 Neuronal diversity and classification

Neuronal classification has been conducted since the inception of modern neuroscience (Ramon y Cajal 1909) and has continued to challenge neuroscientists to the present day, with multimillion dollar projects devoted to recording and classifying neuronal diversity within the brain (Jones et al. 2009). The aim of neuronal classification is to categorise neurons into discrete types with the hope that this will help further our understanding of computation and behaviour. Whilst neuronal classification in and of itself will not be sufficient to allow us to understand the brain, classifying cells can help us to advance our knowledge of neuroscience in several ways: First, using agreed upon criteria to define neurons allows a common language to be spoken amongst researchers, ensuring that it is possible to compare results across studies. Second, by classifying neurons as types, rather than treating them as individual units, it allows us to reduce the complexity and dimensionality of the brain, something which is necessary if we are to understand how the billions of neurons within our brain encode information. Third, it can further our understanding of neurological diseases by informing us whether specific neuronal types are affected. Finally, classification allows us to assign specific roles to identified neuronal types, which will help us understand the computations underlying behaviour (Zeng and Sanes 2017).

A fundamental problem in the field of neuronal classification is the question of what determines a neuronal type. Intuitively, classification aims to place neurons with similar properties together into a single group, whether that be via analysis of morphology, genetics, or physiology. However, when measuring these properties, what level of similarity is sufficient to place two neurons together? At one extreme, it could be argued that every neuron is different and therefore belongs in its own class. At the other extreme, the simple identification of a cell as neuronal implies that neurons form a class of their own, distinguished from other biological cell types. Whilst neither of these two extremes is particularly useful for the purposes of classification, it does highlight the problem faced when attempting to objectively classify neurons in a reproducible and robust manner, not only across multiple brain regions, but also across multiple species. The aim of classification, therefore, is to be able to find a middle ground between these two extremes that helps us to define a relevant and useful parts list of the brain.

A related problem to the question of classification is how best to apply quantitative, objective methods to define neuronal types. Historically, data acquisition was slow and laborious making it difficult to apply much more than descriptive characteristics to the data. However, the development of modern data acquisition techniques has allowed the analysis of hundreds, or thousands, of neurons in a single experiment, opening up the possibility of applying quantitative computational methods. Machine learning algorithms have been successfully utilised with genomic, physiological and morphological data (Armañanzas and Ascoli 2015), although due to the ill defined nature of neuronal classification the choice of method to use is far from simple and requires a not insignificant level of knowledge from the researcher.

1.1.1 Parameters used to define neuronal types

When classifying neuronal types a number of different parameters can be used, which generally can be split into the three broad categories of morphological, molecular and physiological. A brief account of how these categories can be used to define neuronal types is given below.

Morphology

Morphology has been used for over 100 years to classify cells, since Cajal's seminal work classifying neuronal types in the cerebellum (Ramon y Cajal 1909). Neuronal morphological analysis can include measuring a number of parameters, including neurite shape, complexity and projection pattern, as well as soma size and location. Historically, the primary method of morphological analysis has been sparse labelling of either random or genetically defined neurons across many different samples, followed by morphological reconstruction. The underlying assumption of morphological analysis is that the structural features analysed are informative about the functional role of the neuron, and indeed in many cases this has proven to be true. For example, bipolar cells of the retina can be classified based on what laminar of the inner plexiform layer (IPL) they stratify. From this morphological classification it is also possible to predict whether the bipolar cell will respond to light onset (ON) or offset (OFF), or both (ON-OFF). A more fine grained morphological analysis has demonstrated the presence of 12 bipolar cell types in mice, which differ in terms of the stratification levels of their axons (Ghosh et al. 2004, Wassle et al. 2009) (Fig. 1.1.1a), with the stratification level of a particular type also corresponding to that types response kinetics (Baden et al. 2013).

Whilst sparse labelling and reconstruction has proven incredibly useful, it is difficult to directly compare features, such as anatomical location and projection pattern, from neurons that have been labelled across multiple different specimens. In order to address this problem a method was developed which combines sparse labelling across many samples with image registration, thus allowing information from multiple specimens to be collated into a common reference frame (Jefferis et al. 2007) (Fig. 1.1.2). Bringing neurons from many samples into a common reference frame, or standard space, allows a direct quantitative comparison of neurons collected from multiple samples. This method has enabled the creation of a digital atlas of neuronal morphologies across the whole brain in drosophila (Chiang et al. 2011), zebrafish (Kunst et al. 2019), honeybee (Rybak et al. 2010), and locust (Jundi et al. 2010), as well as brain regions in mouse (X. Li et al. 2018) and rat (Egger et al. 2012) (Fig. 1.1.3). The development of classification algorithms for morphological data has en-

abled patterns of connectivity to be analysed across the brain (Costa et al. 2016, Kunst et al. 2019), something which is necessary for the development of realistic circuit models (Fig. 1.1.4). Indeed, analysis of this morphological data has already been used to dissect a cellular resolution pathway for the computation underlying the analysis of optic flow in the zebrafish larvae (Kramer et al. 2019), uncover the topographic organization of the zebrafish tectal motor map (Helmbrecht et al. 2018), and develop a anatomically realistic model of information flow within the rat vibrissal cortex (Lang et al. 2011).

Molecular

Since a neuron's biophysical properties are determined by its molecular identity many studies have attempted to classify neurons based on their underlying transcriptomic or proteomic profile. A number of advances in molecular biology have enabled the unbiased genome-wide profiling of RNA within single cells (Wagner et al. 2016), including the development of single cell RNA sequencing (scRNA-seq) (Tang et al. 2009) which allowed a more detailed description of neuronal transcriptomic diversity than ever before. Further advances in these techniques have increased both their sensitivity and throughput, allowing tens of thousands of single cells to be analysed in a highly parallel manner (Macosko et al. 2015). Clustering using scRNA-seq has not only validated cell types that had already been classfied by other means, but has also led to the discovery of new cell types. For example, using morphological analysis mouse retinal bipolar cells had been classified into 12 types (Ghosh et al. 2004, Wassle et al. 2009). Using high throughput scRNA-seq Shekar et al (2016) were able to analyse 25 000 bipolar cells, finding a 1:1 correspondence between previously defined morphological types and their own transcriptionally defined types (Fig. 1.1.1b - 1.1.1c). They were also able to elucidate a further two types not previously defined (Euler et al. 2014, Shekhar et al. 2016). Importantly, the vast majority of bipolar cells could be classified, and there was little evidence of any intermediate types, indicating that, for bipolar cells at least, neurons exist as discrete types rather than being spread across a continuum.

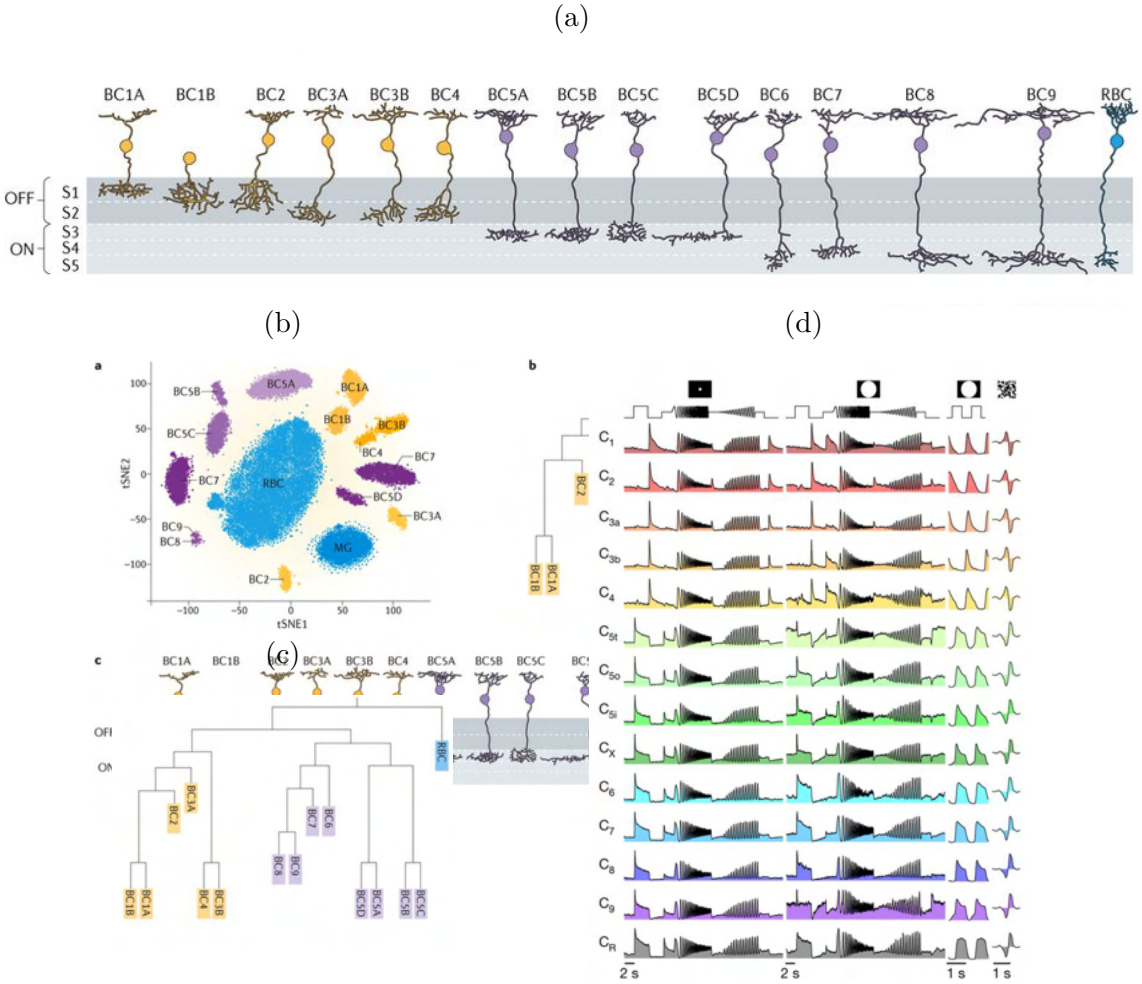

Figure 1.1.1: *Bipolar cell types in the mouse retina and the criteria by which they can be classified.* (a) Morphology: bipolar cells can be classified based on their morphological parameters, in particular their level of stratification within the IPL layer (Wassle et al. 2009). BC1B was discovered using transcriptomic profiling (Shekhar et al. 2016). Morphological analysis also only distinguished between 3 BC5 types (Euler et al. 2014), whilst a further subdivision became apparent using transcriptomics (Shekhar et al. 2016). (b) Transcriptomic: t-distributed stochastic neighbour embedding (t-SNE) plot showing the clustering of 25 000 bipolar cells using Drop-seq, a high throughout method of single-cell RNA sequencing (Shekhar et al. 2016). (c) Hierarchical clustering of the bipolar cell types based on their transcriptomic similarity. (d) Physiology: Using the previously described morphological types, bipolar cells were clustered based on their glutamate release. The plot shows the mean glutamate response (n=8,452 ROIs) of each cluster in response to a variety of stimuli (Baden et al. 2013). Figures (a), (b) and (c) are from (Zeng and Sanes 2017). Figure (d) is from (Baden et al. 2013)

Physiological

A further method of classification is conducted by analysing the underlying physiological properties of the neurons. Classic electrophysiological studies were able to classify visually responsive neurons based on how they responded to a variety of

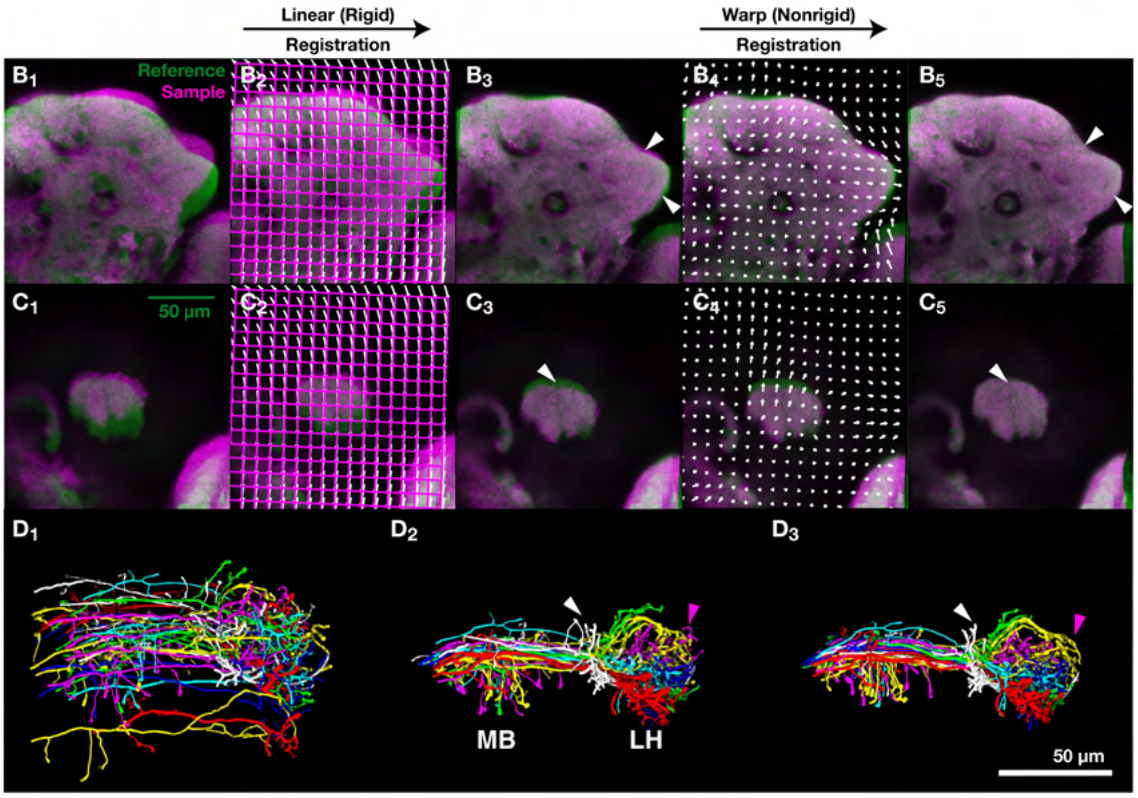

Figure 1.1.2: *Registration allows images from different specimens to be brought into a common reference space.* The drosophila Lateral Horn (LH) (B1) and Mushroom Body (MB) Calyx (C1) from two different brains, a reference brain (green) is used as a template to which the sample brain (magenta) is aligned. The first step in the registration is a rigid body transformation (B1 and C1). The result (B3 and B4) is then warped using non-rigid body alignment (B4 and C4) to allow for non-linear differences, which may occur due to the slightly different sizes or shape of the two specimens. This two step process results in alignment of the two samples (B5 and C5). The white arrow heads indicate where there has been an improvement in alignment. (D) The registration parameters are applied to the neurons from each sample to bring all the neurons into a common anatomical reference frame. Figure taken from (Jefferis et al. 2007).

visual stimuli, leading to the discovery of orientation and direction selective neurons (Hubel and Wiesel 1959), as well as the various feature detectors of the frog optic nerve, including contrast and edge detectors (Lettvin et al. 1968). With the advancement of molecular genetics bringing about the ability to label restricted populations of neurons, electrophysiology studies have been able to delineate more precise sub-populations based on a variety of electrophysiological parameters. For example, Parvalbumin (PV+) expressing neurons are a subtype of cortical interneuron thought to modulate the responsiveness of pyramidal neurons. Using a line which labels PV+ neurons with GFP, 4 neuronal types were discovered, each of

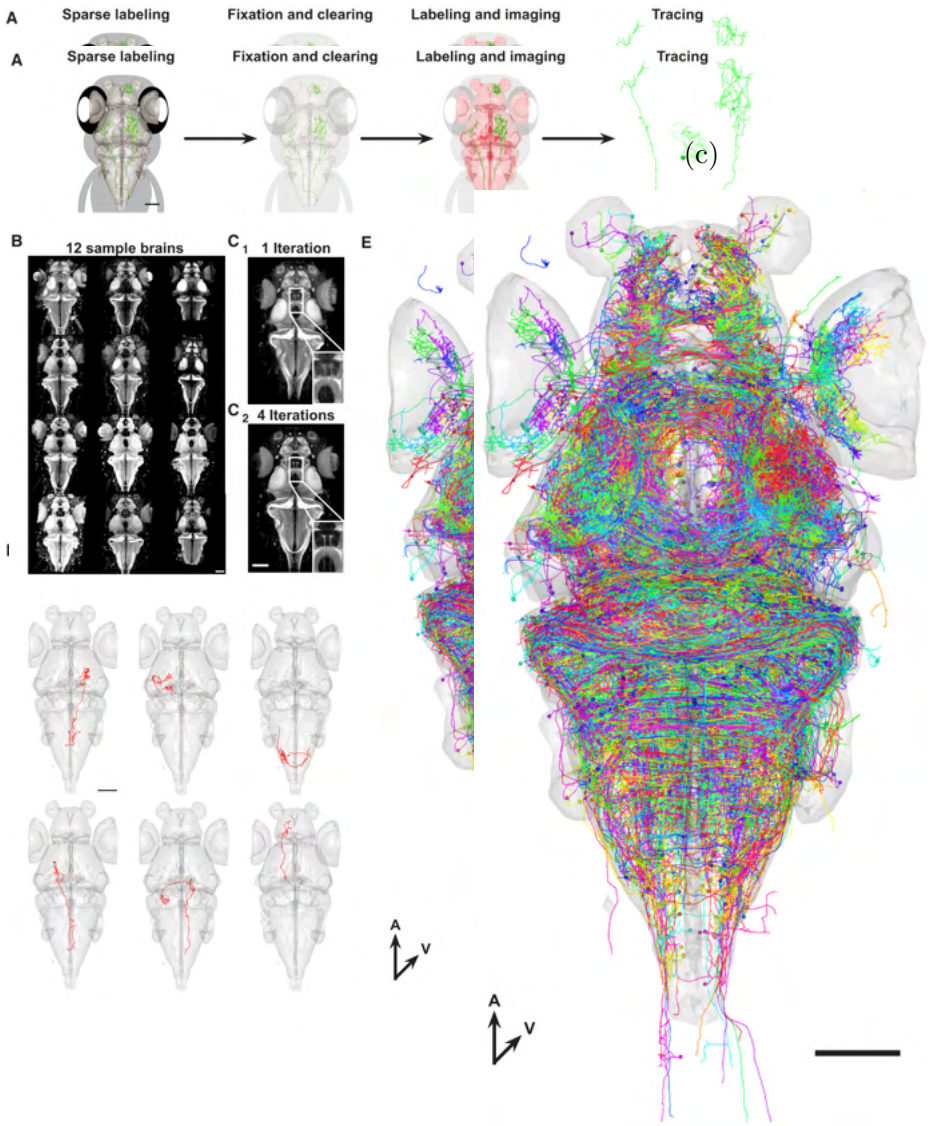

Figure 1.1.3: *Registration allows the creation of a whole brain single neuron atlas.* (a) Image of 12 brains which were registered to one another to create a template brain for the atlas. (b) Example of individual neurons from different brains which have been aligned to the template brain. (c) Overlay of all neurons ($n = 1955$) onto the template brain. Colours assigned randomly. Scale bars show 100 µm. Figures taken from (Kunst et al. 2019)

which differed in terms of passive membrane properties, action potential shape, and excitatory inputs (Helm et al. 2013). Similarly, somatostatin expressing (SOM+) cortical interneurons were split into 3 types based on morphological and electrophysioloigcal properties. One of these corresponded to an already known cell type, whilst the two others had not been previously described (McGarry et al. 2010).

Whilst single cell patching can give a wealth of information about electrophysiological properties, the method is time consuming and labourious, often resulting in low powered analysis. One way to circumvent this problem is to perform optical imaging of neural activity using genetically encoded calcium indicators (GECI) (Miyawaki

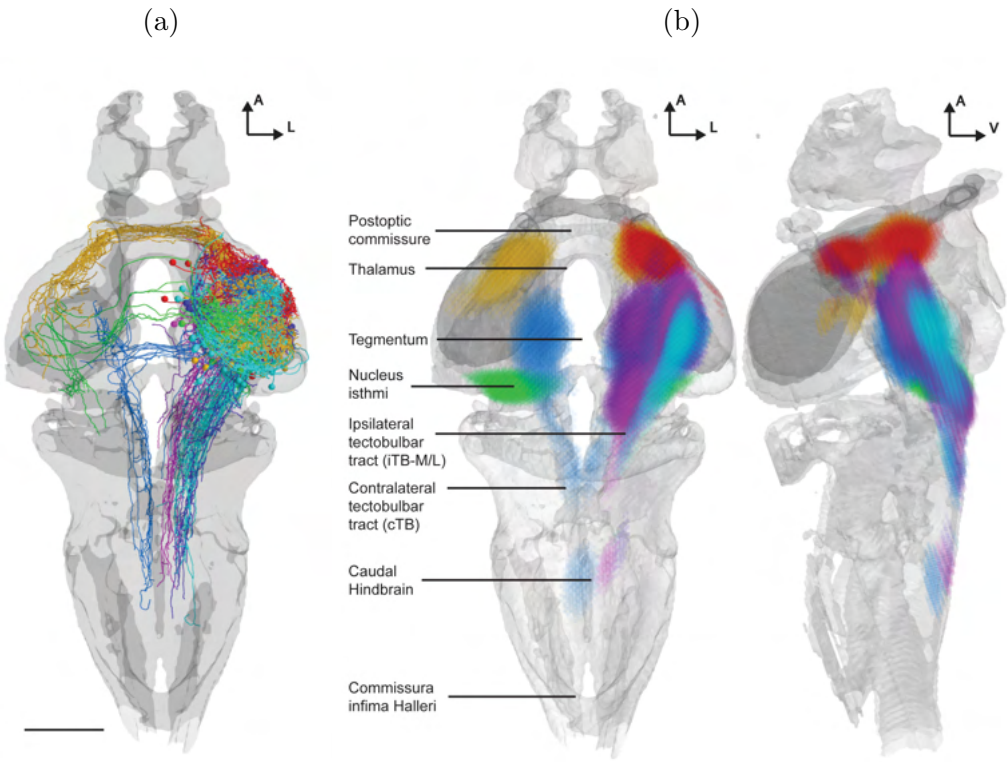

Figure 1.1.4: *Single neuron data can be classified according to projection pattern.* (a) Single tectal projection neurons ($n = 133$) were registered to the template and clustered based on their innervation targets, which revealed seven classes of neuron. The neurons are coloured according to their projection class. (b) Colour density maps of the main arborization targets for each class of neuron. Scale bar shows 100 µm. Figures taken from (Helmbrecht et al. 2018)

et al. 1997), or more recently, genetically encoded voltage indicators (GEVI) (Kannan et al. 2019). Optical imaging allows the acquisition of the activity of hundreds to thousands of neurons simultaneously. This not only greatly increases the amount of data it is possible to collect, but also allows the visualisation of circuit level dynamics which often give rise to emergent properties, something which cannot be analysed when recording from single cells. Similar to morphological and genomic analysis, neuronal types in the retina have been successfully mapped using optical imaging methods, with the functional diversity of bipolar cells mapping clearly onto their morphological counterparts (Fig. 1.1.1d) (Franke et al. 2017). Further studies have recorded activity from the output cells of the mouse retina, the direction selective retinal ganglion cell (DSRGC), to delineate approximately 32 functional types (Baden et al. 2016). These types are thought to correspond to feature detectors, each of which extracts a specific aspect of the visual scene, such as direction of

motion or size, to send to the brain. Functional classification from *in vivo* recordings have allowed the analysis of the distribution of functional response types across different brain regions such as the laminar organisation of direction selective inputs to the zebrafish optic tectum (Nikolaou et al. 2012). Furthermore, simultaneous recording of *in vivo* neural activity and behaviour has also allowed a classification of neuronal cell types based not only on their responses to sensory stimuli, but also based on how they correlate to a behavioural output, thereby helping researchers to understand the neural activity underlying sensorimotor transformations (Bianco and Engert 2014, Carrillo-Reid et al. 2019, Chen et al. 2018, Dunn et al. 2016b, Miller et al. 2014, Temizer et al. 2015).

Overall cell type classification has provided a useful method to reduce the dimensionality of the brain and has enabled researchers to begin to understand the underlying organisational principles which govern brain function.

1.1.2 Using classification to understand visuomotor transformations

Our perception of the world is dictated by the information that is transmitted from our sensory organs to the rest of the brain. However, mapping from sensory input to neural activity and then onto behaviour is a challenge. How sensory information is transferred, transformed and distributed throughout the brain to give rise to an appropriate behavioural response is not fully understood. Correlating large scale neural activity to both sensory input (Miller et al. 2014, Roland et al. 2017, See et al. 2018) and motor output (Gahtan et al. 2002, Leonardo and Fee 2005) demonstrates that the key to understanding sensorimotor transformations is to focus on the population activity across many neurons (Buzsáki 2010, Yuste 2015). To understand the population coding it is possible to use neuronal classification and then correlate the population activity in defined neuronal subtypes with behavioural output. One area of research in which this approach has been successfully applied is in understanding the visuomotor transformations underlying the processing of optic flow in the larval zebrafish (Kramer et al. 2019, Kubo et al. 2014, Naumann et al.

2016, Orger et al. 2008, Wang et al. 2019).

As an animal moves through its environment the relative movement of objects in the visual scene results in the experience of optic flow. Neuronal circuits process this optic flow to produce two stabilising reflexes: The optomotor reflex (OMR) stabilises the perceived position of the animal relative to visual objects, whilst the optokinetic reflex (OKR) stabilises the image of a moving object on the retina (Fig. 1.1.5). The OMR and OKR can both be elicited from 5 days post fertilisation (dpf) larval zebrafish using wholefield gratings (Brockerhoff et al. 1995, Neuhauss et al. 1999). The OMR is elicited by translational optic flow and results in different motor components depending on the direction of the optic flow: forward motion results in forward swims, lateral motion results in turning behaviour, and backward motion results in a reduction in swimming (Naumann et al. 2016). The OKR is elicited by rotational optic flow and results in the eyes undergoing a smooth pursuit followed by a saccade.

To understand the neural circuits which process optic flow, a detailed kinematic analysis of the behaviour must first be performed in response to a range of optic flow stimuli, such as wholefield gratings moving in various directions (Brockerhoff et al. 1995, Naumann et al. 2016, Neuhauss et al. 1999, Orger et al. 2008). This detailed analysis allows a dissection of the stimulus features which are necessary to elicit specific types of behavioural output. For example, whilst it was known that fish will turn to match their swimming direction towards the direction of optic flow, Naumann et al (2016) discovered each eye does not contribute equally to the behaviour. The eye experiencing medial optic flow (optic flow towards the midline of the fish) contributed more to the turning behaviour, compared to the eye experiencing lateral optic flow (optic flow away from the midline of the fish). From these behavioural observations a number of hypothesised neural computations can be generated. For example, there must be neurons which show binocular integration, as well neurons representing the medial-lateral asymmetry seen in turning behaviour (Naumann et al. 2016, Orger et al. 2008).

After behavioural analysis, the neural activity across multiple brain regions is recorded, in response to the same optic flow stimuli. Neurons are then classified based on their

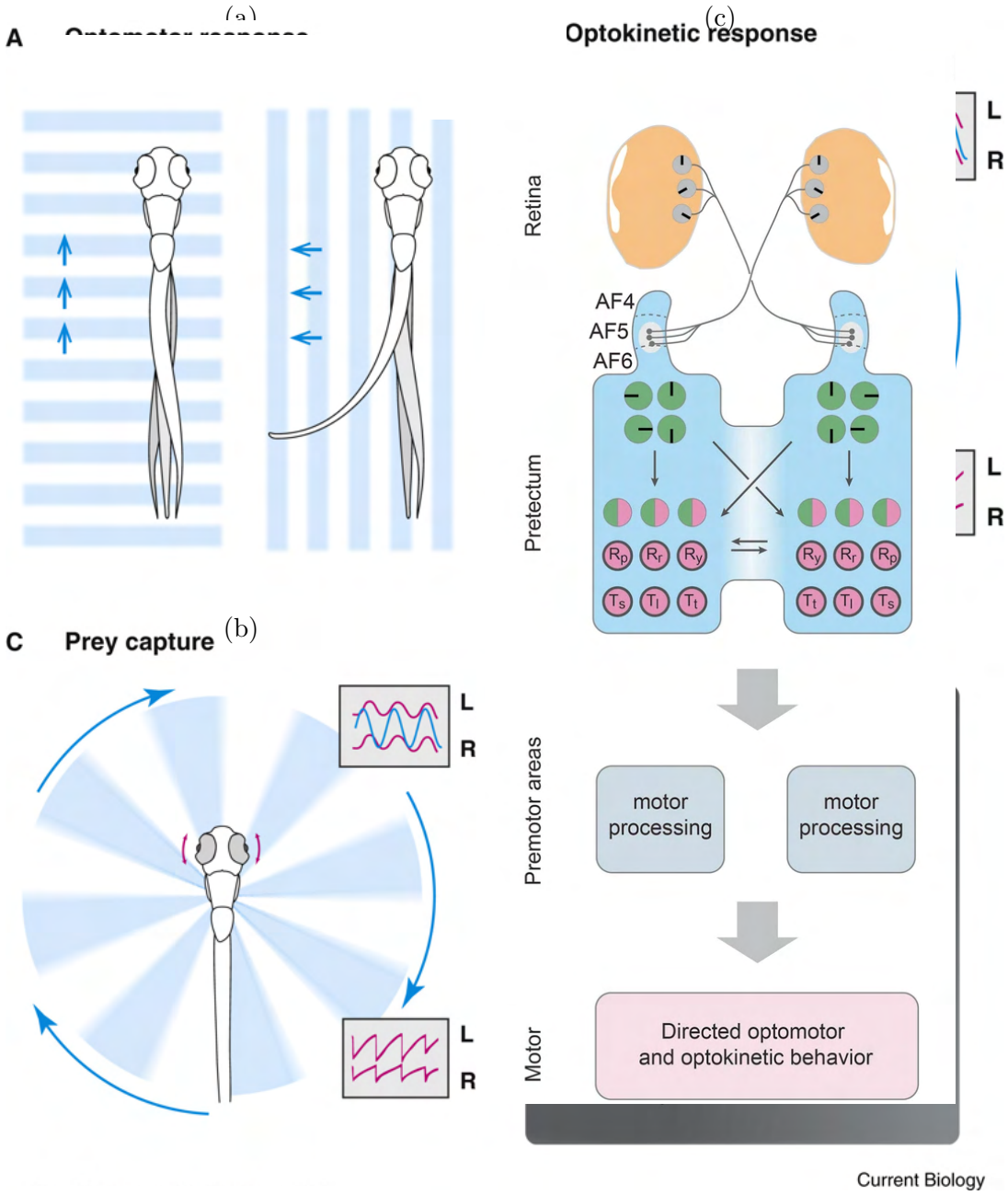

Figure 1.1.5: *The OMR and OKR responses in zebrafish.* (a) The OMR response stabilises the position of the fish in the water and can be elicited using translational optic flow. The fish swims forward to along with the optic flow, and will turn to bring its swimming pattern to match that of the optic flow. (b) The OKR stabilises the position of an object on the retina and can be elicited using rotational optic flow. The fish alternates between smooth pursuit followed by a fast saccade rest. (c) A proposed circuit model for the binocular processing of optic flow. Monocular input from the RGCs projects to arborisation field 5 (AF5). The 3 DSRGCs (Nikolaou et al. 2012) are transformed to 4 DSRGCs in the pretectum (Wang et al. 2019). Information from the contralateral eye is integrated in the pretectum allowing binocular selectivity (magenta responses). R_p, R_r, R_y: neurons selective for rotations about the pitch, roll and yaw axes. T_s, T_t, T_l: neurons selective for translation along the sideslip, thrust, and lift axes. Figures (a) and (b) are taken from (M. Orger 2016), figure (c) is taken from (Wang et al. 2019)

stimulus response properties, such as direction selectivity or whether they respond to binocular or monocular stimuli (Kubo et al. 2014, Naumann et al. 2016, Wang et al. 2019). Neural activity in the defined subtypes can then be correlated with the hypothesised neural computations necessary to perform the visuomotor transformations. For example, whilst RGCs were exclusively monocular, neurons in the pretectum and hindbrain showed binocular integration, as well as asymmetries in their response to medial and lateral motion (Naumann et al. 2016, Wang et al. 2019). Furthermore, based on their behavioural data Orger et al (2008) predicted that neurons involved in forward swims would be selective for forward motion stimuli, and show a bilateral symmetric distribution in the brain. These properties were found in neurons located in the nucleus of the medial longitudinal fasiculus. Ablations of neurons can provide further evidence that they are involved in a certain aspect of behaviour. For example, neurons hypothesised to be involved in turning were unilaterally ablated, which resulted in a complete elimination of turning only towards the ablated side, whilst also not affecting forward swims (Orger et al. 2008). From these results circuit level models can be generated of how distributed brain activity can give rise to specific behaviours (Fig. 1.1.5c) (Kubo et al. 2014, Naumann et al. 2016, Wang et al. 2019). These experiments provide an outline for how defining neuronal subtypes based on their responses to specific stimuli can help understand visuomotor transformations, and although the data lack the underlying neuronal connectivity to validate the circuits models, more recent work combining functional imaging with single neuron labelling has begun to test these models (Kramer et al. 2019).

1.1.3 Methodological approaches to classifying neurons

The advances in data collection and computing power have allowed neuronal classification to move from a strictly qualitative description of the data, based on the experimenters observations (Lettvin et al. 1959), towards a more quantitative endeavour (Costa et al. 2016). This shift towards quantitative methods is not without its problems; as mentioned above the exact definition of a neuronal type is not explicitly defined, and as a consequence, the methods used to define neuronal types can be

extremely varied, with each method having various underlying assumptions about the data. For example, across 8 different studies which all focused on classifying cortical interneurons there was a total of 7 different methodologies used (Defelipe et al. 2013, Druckmann et al. 2013, Helm et al. 2013, Hosp et al. 2014, Karagiannis et al. 2009, López-Cruz et al. 2014, Santana et al. 2013). The methodological approaches to defining neuronal types can be split into two broad categories: supervised and unsupervised learning.

Supervised learning

In supervised learning the underlying neuronal types are predefined; the goal is to be able to determine to which type a neuron belongs based on a number of parameters. For example, a set of morphological parameters from a group of labelled excitatory and inhibitory neurons can be analysed. This is known as the training set. Based on those morphological parameters, a classifier then learns to associate neurons of the training set to either the excitatory or inhibitory group, based on their morphological parameters. This will then allow the classifier to infer the neurotransmitter identity of neurons in a different dataset, where the neurotransmitter identity is not known *a posteriori*. Thus, for a given set of data, supervised classification aims to classify each neuron based on its description by n parameters. A classifier function f learns to assign each neuron to one of the predetermined classes m, based on the n set of parameters, using the training data

$$f : \mathbf{x} \rightarrow m \tag{1.1}$$

where $\mathbf{x} = (x_1, ..., x_n)$ is an n-dimensional vector of all measured parameters for each neuron and $\mathbf{m} = \{1, 2, ..., m\}$ are all possible neuronal types (Armandas and Ascoli, 2015). There are many types of classifer which can map $\mathbf{x}$ onto m, including linear classifiers, support vector machines and neural networks.

Unsupervised learning

In unsupervised learning, also known as clustering, the underlying neuronal types are not predefined. This makes the process somewhat difficult since, unlike in super-

vised learning, there is no ground truth which can be referred to. It is, however, a situation in which researchers commonly find themselves: having a set of measured parameters from a heterogeneous group of neurons without any prior knowledge of what type they belong to. The aim of clustering, therefore, is to infer the underlying neuronal types by grouping together neurons based on the similarity between their measured parameters, such as gene expression profiles or morphology. Again, there are many types of clustering algorithm including k-means, hierarchical, and density based clustering. Each of the algorithms makes a number of assumptions about the underlying data, such as its distribution or type. For example, k-means assumes the clusters are spherical, with each cluster having an equal variance. If the data do not approximate these assumptions then the output is unlikely to be meaningful. Furthermore, most algorithms have one or more parameters which must be set, and which can dramatically affect the outcome. For example, in k-means the number of clusters must be chosen prior to clustering. The choice of clustering algorithm is, therefore, heavily dependent on the data, with no one algorithm able to satisfy all problems (Kleinberg, 2003).

1.2 The Optic Tectum

The aim of this thesis is to develop a method to classify neuronal cell types in the zebrafish optic tectum based on their responses to an array of visual features. The following is brief account of what is known about the optic tectum in fish and other species.

The optic tectum is a midbrain structure known as the superior colliculus (SC) in mammals. It receives a variety of sensory inputs from multiple modalities, and is the primary retinorecipient area in non-mammalian species. It integrates these inputs to direct a number of species specific behaviours. In all vertebrates examined the best known role of the optic tectum is to direct movements to a particular region of space, whether this be a saccade of the eyes in primates (Robinson 1972), movement of the tail in fish (Herrero et al. 1998), or locomotion in the alligator (Schapiro and Goodman 1969). However, research also indicates the optic tectum plays an

important role in higher cognitive functions including attention and decision making (Basso and May 2017, Zhaoping 2016). The basic architecture of the optic tectum is similar across species, with the anatomical structure being split up into several laminae (Fig. 1.2.1a). The exact number and naming of the laminae varies across species, but in general the more superficial layers receive visual input, whilst deeper layers receive input from other sensory modalities, a variety of other brain regions, and are important for initiating goal directed movements (May 2006). In teleostean fish the optic tectum can be split up into 2 main regions: a deep region known as the stratum periventriculare (SPV), and a superficial neuropil region (Fig. 1.2.1b). The SPV contains the cell bodies of all the tectal neurons, whilst the neuropil region contains the axons and dendrites, and is anatomically divided into multiple laminae (Fig. 1.2.2c). Neurons in the SPV extend their neurites up into the neuropil region where they branch out forming synpases with incoming afferents.

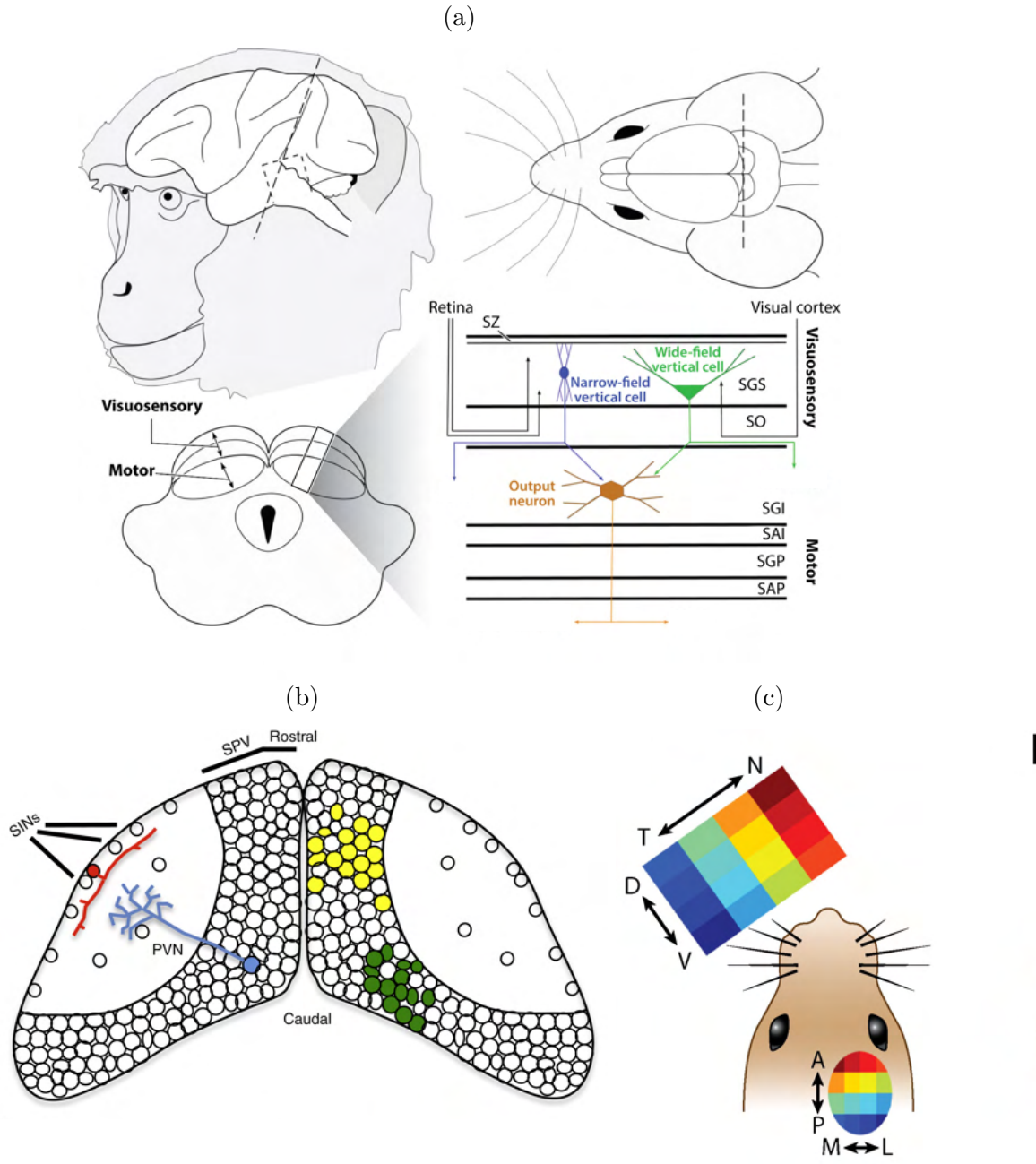

Figure 1.2.1: *Anatomy of the superior colliculus/optic tectum.* (a) The location of the SC in primate and mouse. An axial cut reveals the laminar structure. The stratum zonale is the most superficial layer. The Stratum griseum superficiale (SGS) and stratum opticum (SO) receive visual input. The stratum griesum intermediale (SGI), stratum album intermediale (SAI) and stratum album profundum (SAP) comprise the motor output. Two morphological types of the SC are the NF neuron, and the WF neuron. (b) A schematic of the tectum with the paraventricular nucleus (PVN) projecting its neurites into the neuropil (blue neuron) and the superficial inhibitory neuron (SIN) situated along the most dorsal aspect of the tectum (red neuron). Right shows the spatially localised assemblies active during during prey capture behaviour (Bianco and Engert 2014). (c) The retinotopic organisation of the SC. Figure (a) taken from (Basso and May 2017), figure (b) taken from (M. Orger 2016), and figure (c) taken from (Cang et al. 2018).

1.2.1 Maps within the tectum

The tectum plays a role in both processing incoming sensory information, as well as generating the appropriate motor output (Basso and May 2017). The neural circuits which are responsible for processing this information are highly organised into multiple maps contained within different regions of the tectum.

Mapping visual input

Across all species analysed there is an ordered retinotopic mapping of connections from the eye to the tectum such that adjacent regions of visual space are represented by adjacent tectal neurons (Fig. 1.2.1c) (Chandrasekaran et al. 2005, Cornide-Petronio et al. 2011, Romano et al. 2015). Furthermore, the representations of visual features are segregated into layers, in a feature specific manner, such that the tectum receives visual input from the retina in the form of multiple parallel retinotopically organised maps, stacked on top of one another. For example, in mouse the most dorsal region of the retinorecipient area receives input from DSRGCs and local motion detectors (Kim and Basso 2010, Zhang et al. 2012), with those selective for anterior motion arborising in more superficial layers compared to those which respond preferentially to vertical motion (superior and inferior) (Kay et al. 2011). Furthermore, the more ventral retinorecipient layers receive non-direction selective retinal input (Fig. 1.2.2a) (Hattar et al. 2006, Huberman et al. 2008, Hong et al. 2011). This segregation of feature maps is also found in the zebrafish, with DSRGCs targeting specific laminae in the dorsal optic tectum based on their preferred direction of motion (Fig. 1.2.2b - 1.2.2d) (Nikolaou et al. 2012). There is a further size dependent mapping in zebrafish, with RGCs responding preferentially to large stimuli targeting deeper retinorecipient layers, and small size selective RGCs targeting the more superficial layers (Preuss et al. 2014).

Mapping motor output

The more ventral laminae, however, consist of a motor map whereby the location of maximal activity within the optic tectum determines the direction of a saccade (Robinson 1972). The direction and amplitude of the saccade is determined by the

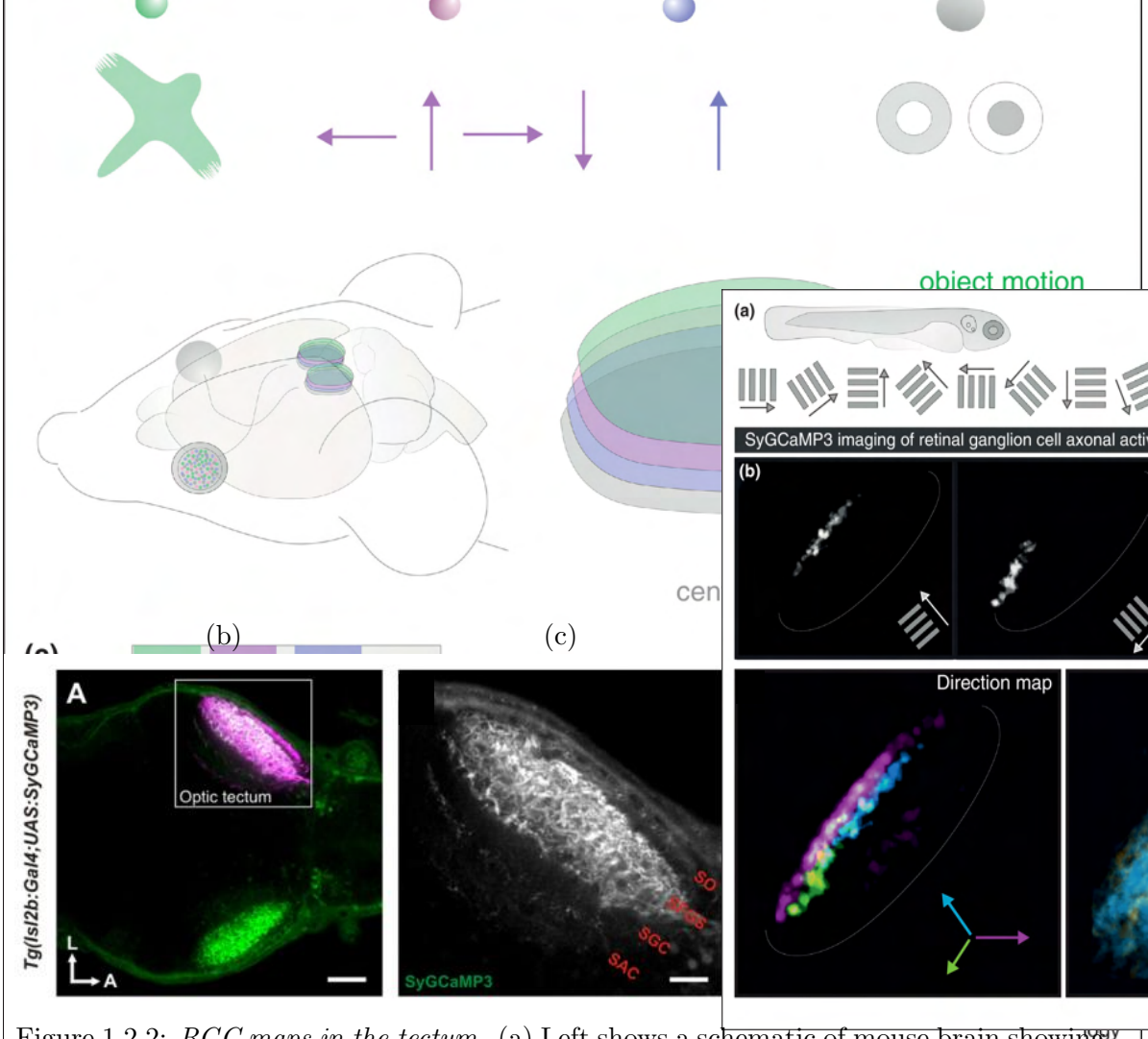

Figure 1.2.2: *RGC maps in the tectum.* (a) Left shows a schematic of mouse brain showing the superior colliculus (SC). Right shows laminar organisation of the SC based on the neurons' feature selectivity. (b) Dorsal view of transgenic zebrafish expressing SyGCaMP3 in the neuropil of the optic tectum (Nikolaou et al. 2012). (c) The laminar organisation of the tectal neuropil (SO,stratum opticum; SFGS, stratum fibrosum et griseum superficiale; SGC, stratum griseum centrale; SAC, stratum album centrale). (d) Direction selective RGC inputs into the optic tectum, colour coded according to their direction preference, arranged in a laminar manner. Scale bars show 50 µm in (b) and 20 µm in (c). Figures taken from (Dhande and Huberman 2014, Nikolaou et al. 2012).

location of stimulation, irrespective of the initial position of the eye in the orbit (Robinson 1972). A phenomenon which seems generally conserved across species (Salas et al. 1997).

Since the direction of the saccade is congruent with the overlying retinotopic map (Salas et al. 1997, Wurtz and Goldberg 1971), it was proposed that there is a direct link between visual and motor maps, with the idea that a saccade would be directed towards the location specified by the visually responsive neurons (Basso and May 2017). This idea is supported by anatomical labelling studies in primate (Mooney et al. 1988, Rhoades et al. 1989, Tardif et al. 2005) and electrophysiological record-

ings in ferret (Doubell et al. 2003) and tree shrew (Lee and Hall 1995), all of which have confirmed a direct connection between the retinotopic and underlying motor maps. However, since saccades can be elicited without visual stimulation, such as from memory (Zivotofsky et al. 1996), auditory stimulation (Engelken and Stevens 1989), or tactile stimulation (Groh and Sparks 1996) it has been proposed that the motor map doesn't encode information simply in retinotopic coordinates, but generates a map based in motor coordinates that is common across sensory modalities. Sparks (1988) developed the motor-error hypothesis which states that saccade related collicular activity is encoded in terms of the trajectory of movement required to look at an object, rather than the location of the target in space (Sparks 1988). Electrophysiological studies in primate support this hypothesis by confirming that activation of the overlying visually responsive neurons is not necessary for the generation of a saccade (Wurtz and Goldberg 1971) and saccade related neurons give rise to the same direction and amplitude of saccade, irrespective of whether they are activated by either somatosensory and visual stimuli (Groh and Sparks 1996). However, it is not clear whether a similar encoding strategy occurs in other species.

Mapping saliency

Since an individual tectal neuron only encodes a very coarse saccade vector, they cannot be used to generate precise saccades (Mcilwain 1991). It was, therefore, thought that a weighted sum of population activity across the tectum was used to increase the accuracy of a saccade (Mcilwain 1991). However, this method of decoding is appropriate only when there is a single visual target, a situation which is rarely found in nature. More recent work on the tectum has begun to explore how the population activity is decoded when there are multiple competing stimuli, to ensure that the most salient stimulus is chosen (Li and Basso 2005). The saliency of an object can be defined as the degree to which it attracts attention. For example, a red sock among green socks stands out perceptually; the red sock has high saliency and it said to 'pop-out' (Fig. 1.2.3). The degree to which a visual feature causes an object to pop-out is assessed by the ability of an animal to find the object amid distractors. This can be measured quantitatively as the animals saccade response time. It has been shown that the optic tectum can signal the relative levels of saliency

among multiple competing stimuli in primate (White et al. 2017), owls (Mysore et al. 2011), archerfish (Ben-Tov et al. 2015), and mice (Ahmadlou et al. 2017). The optic tectum then initiates a motor program towards (or away from) the location of the most salient object. How the underlying neural activity is decoded to choose the most salient stimulus is still not fully understood. There is some evidence from studies in owl that a winner takes all (WTA) approach is used (Mysore et al. 2011), however, studies in primate have indicated that a Bayesian model, the maximum *a posteriori* estimate, is more accurate at decoding saccade choice from the neural activity (Kim and Basso 2010).

It has been proposed that in primates the area of the brain responsible for actually generating this saliency map is the primary visual cortex (V1), with a copy then passed on to the SC (Zhaoping 2016). The mechanism by which this map is generated is thought to be iso-feature suppression, whereby neurons tuned to the same stimulus feature suppress one another's activity (Allman et al. 1985). Thus, using the sock analogy again, the activity of the neurons which signal the location of the multiple green socks would be suppressed, whereas the neurons which signal the location of the single red sock would escape this suppression and thus signal high saliency. V1 is thought to be a suitable place for generating a saliency map as its neurons are tuned to multiple visual features such as orientation and direction (Gur et al. n.d.). This poses the question of where the saliency map is generated in species which lack a neocortex, such as the fish? The optic tectum itself has been suggested as a candidate (Zhaoping 2016); unlike in primates the optic tectum of lower vertebrates, such as fish and mouse, contains a high number of feature detectors, including those for direction, orientation, size and contrast (Bianco and Engert 2014, Del Bene et al. 2010, Grama and Engert 2012, Hunter et al. 2013, Preuss et al. 2014, Sajovic and Levinthal 1982a). Furthermore, it has been demonstrated the optic tectum of the archerfish displays iso-feature suppression to moving stimuli (Ben-Tov et al. 2015), and that features such as colour, size, orientation, and motion are efficient at guiding archerfish attention (Reichenthal et al. 2019). Further work delineating the features which mediate visual pop-out in fish, and how they are represented in the tectum, would help elucidate the role the tectum plays in generating saliency maps.

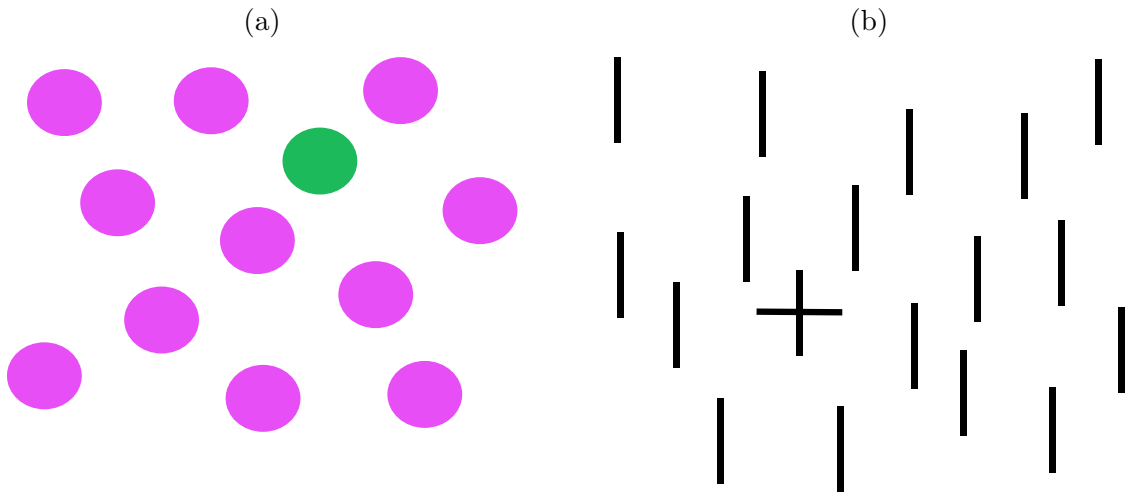

Figure 1.2.3: *Different visual features can contribute to object saliency.* Both the green circle (a) and cross (b) stand out perceptually from the surrounding objects.

1.2.2 Tectal mediated visually guided behaviours

Since the tectum contains both a map of visual space and motor behaviour it has proved to be a useful model to attempt to understand the population coding underlying visuomotor transformations. In particular, the tectum has been shown to be important in mediating both approach and avoidance related behaviours across many species (Blanchard et al. 1981, DesJardin et al. 2013, Ewert 1974, Finlay et al. 1980, Furigo et al. 2010, Gahtan et al. 2005, Herrero et al. 1998, Roeser and Baier 2003, Temizer et al. 2015). These instinctive behaviours are important for an animal to survive and include the detection, recognition of, and escape from a predator or orientation towards a prey. Whilst the role of the tectum in these behaviours has been known about for decades, the cellular mechanisms and computations which give rise to such behaviours are still not fully understood.

Approach behaviour

A number of studies have demonstrated the importance of the tectum in mediating approach behaviours. For example, ablation of the zebrafish tectum results in a deficit in orienting movements towards the prey (Gahtan et al. 2005) but leaves other visuomotor behaviours intact (Roeser and Baier 2003). Tectal lesions also reduces reorientation and pursuit of prey in hamsters (Finlay et al. 1980) and rats

(Furigo et al. 2010). Activation of the tectum has also been shown to induce approach behaviours, with tectal stimulation in toads being able to recapitulate the stereotyped patterns of motor behaviour involved in hunting: orienting, approaching, fixating, snapping and mouth wiping (Ewert 1974). The stimulation elicted the movements in the correct order, with the orienting movements directed towards the appropriate areas of the visual field, depending on stimulation location (Ewert 1987). Furthermore either tectal microstimulation in goldfish (Herrero et al. 1998) or optogenetic activation in zebrafish (Helmbrecht et al. 2018) is able to induce orienting and approach swims, with the directionality of the swim correlating with the site of stimulation along the antero-posterior axis of the tectum.

Avoidance behaviour

The tectum is also thought to play a role in visually evoked defensive behaviour, with tectal ablation inhibiting escapes from predator-like stimuli in zebrafish (Temizer et al. 2015) and rats (Blanchard et al. 1981), and activation of the deep and intermediate layers of the SC resulting in defensive-like behaviours in non-human primates (DesJardin et al. 2013). In mouse, both escaping and freezing behaviour can result from opotogenetic tectal stimulation (Shang et al. 2015). These behaviours can also be elicited using visual stimuli, with a looming stimulus inducing an escape response (Yilmaz and Meister 2013), and a sweeping overhead stimulus, which is thought to mimic an overhead bird of prey, inducing freezing behaviour (De Franceschi et al. 2016) (Fig. 1.2.4a). These results highlight the ability of the tectum to mediate multiple different defensive behaviours depending on the context of the situation. Furthermore, the looming stimulus must be located in the upper visual field for the mouse to respond (Yilmaz and Meister 2013), which, given its topographic mapping, may indicate some regional specialisation in the way the tectum processes visual information. This is supported by the finding that microstimulaiton of regions of the tectum corresponding to the upper visual field elicited avoidance behaviours in rat, whilst simulation of regions representing the lower visual field resulted in orienting behaviour (Sahibzada et al. 1986). There is further evidence of regional specialisation in the zebrafish tectum where it was found that optogenetic activation evoked escape responses only in the posterior portion of the tectum (Helmbrecht et al. 2018).

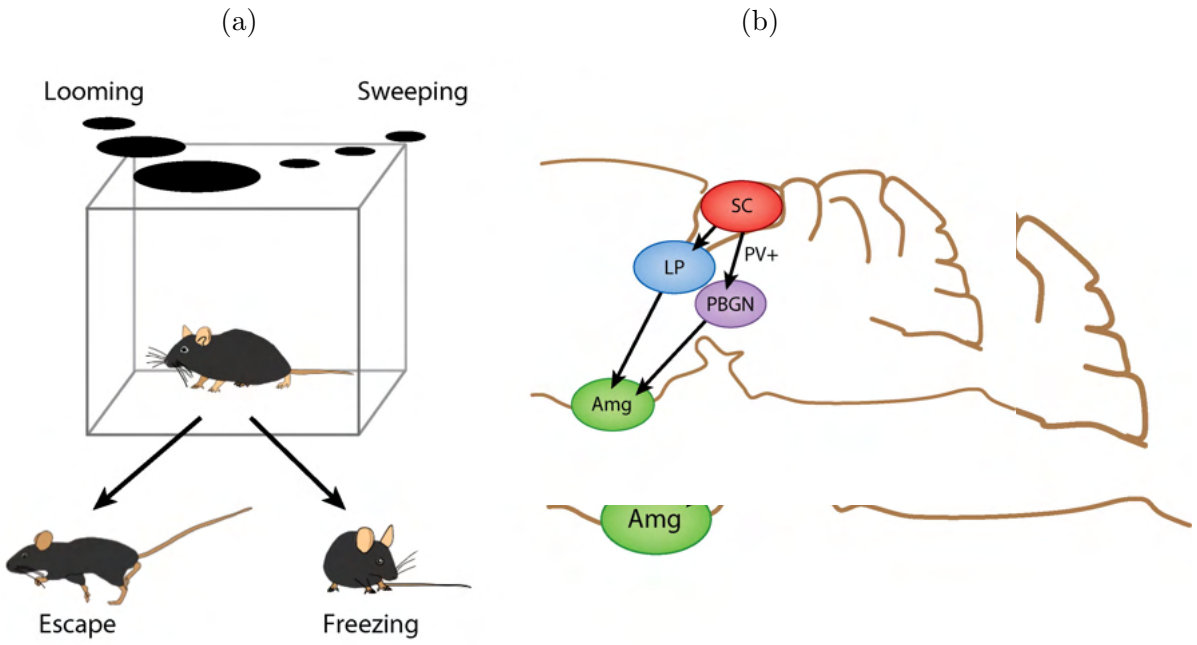

Figure 1.2.4: *Opposing behaviours mediated by two separate pathways from the SC.* (a) A looming stimulus, which mimics an approaching predator, will elicit an escape response, whilst a sweeping stimulus, which mimics an overhead bird of prey, results in freezing behaviour (Yilmaz and Meister 2013, De Franceschi et al. 2016). (b) The two opposing behaviours are mediated via two separate pathways (Shang et al. 2018. Activation of neurons which project to the LP results in freezing behaviour (Shang et al. 2018, Wei et al. 2015), whilst activation of neurons which project to the PBGN results in escape behaviour (Shang et al. 2018). Figures taken from (Cang et al. 2018).

1.2.3 Linking cell types to behaviour

Experiments to uncover the cellular substrate responsible for these behaviours have been attempted since the seminal work of Barlow and Lettvin. Their work on the frog's retina identified 4 groups of neuron: contrast, edge, dimming, and net convexity detectors (Barlow 1953, Lettvin et al. 1968). Each of these subtypes responded selectively to a specific visual feature, with last also being known as a bug detector, as they were thought to detect the presence of prey. These feature detectors allow neurons to extract ethologically relevant information, and ignore irrelevant background noise. The presence of the bug detectors led to the idea that there are specialised neurons in the visual system which are capable of perceiving complex stimuli such as prey and predator. This hypothesis predicts the presence of a hierachical network, with multiple levels of feature convergence. The higher up in the network, the more selective a neuron becomes, eventually giving rise to highly

specialised neurons (Ewert 1987) (Fig. 1.2.5a), which are necessary and sufficient to drive the corresponding behaviour.

While later work by Ewert failed to find prey selective neurons in the retina of the toad, he did record from neurons in the optic tectum which responded preferentially to prey like stimuli (Ewert 1974). Ewert, however, didn't favour a strict interpretation of the feature detector hypothesis (Ewert 1987, Ewert 1997). Instead, he proposed a 'feature-analysing network' (Fig. 1.2.5b), involving parallel information processing, as he thought this would better allow for the flexible behavioural repertoire that is seen even in simple organisms. According to this hypothesis assemblies of neurons, each of which responds to a different facet of the sensory stimulus, coordinate the perception of prey or predator. The detection of prey would, therefore, be an emergent property of the system, brought about through the mutual interaction of multiple neuronal subtypes. For example, one population may be responsible for object recognition and a second population for object localisation. He proposed two ideas: first, that the activation of specific combinations of these neuronal subtypes would give rise to specific behaviours, such as avoiding, turning, snapping etc, and second, that individual subtypes would be able to participate across multiple assemblies (Ewert 1987, Ewert 1997).

Approach behaviour

More recent advances in genetics and electrophysiology have enabled these hypotheses to be tested (Basso and May 2017, Cang and Feldheim 2013, Ito and Feldheim 2018, Oliveira and Yonehara 2018). In particular work by Hoy et al (2019) has lent support for Ewert's 'feature-analysing network' hypothesis by demonstrating that the combined action of multiple neuronal subtypes is necessary for successful hunting behaviour. They inactivated two classically defined collicular cell types, wide-field (WF) and narrow-field (NF) neurons (Fig. 1.2.1a) (Ramon y Cajal 1909), and found that each type was responsible for distinct aspects of hunting. Inactivation of WF neurons resulted in a decrease in prey detection and approach initiation, whilst inactivation of NF neurons resulted in a deficit in orientation and pursuit of prey (Hoy et al. 2019). These behaviours corresponded well with the known morphological and physiological properties of WF and NF neurons. WF neurons have large dendritic

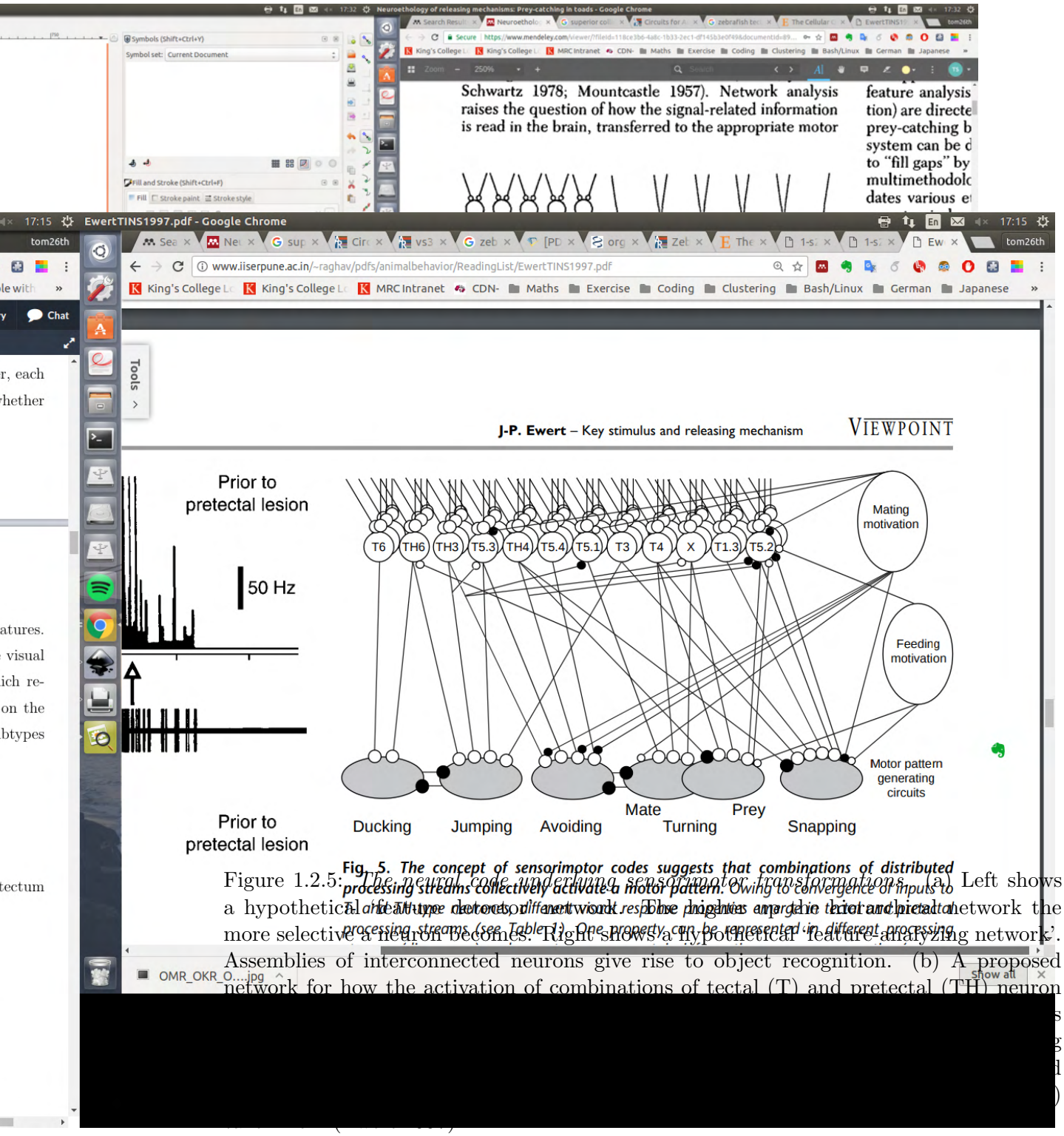

Figure 1.2.5: *The neural code underlying sensorimotor transformations.* (a) Left shows a hypothetical 'feature detector network'. The highlighted neuron and its lateral and more selective a neuron becomes. Right shows a hypothetical 'feature-analyzing network'. Assemblies of interconnected neurons give rise to object recognition. (b) A proposed network for how the activation of combinations of tectal (T) and pretectal (TH) neuron

arbours, with correspondingly large receptive fields, and prefer moving over stationary dots, whilst NF neurons have smaller arbours, smaller receptive fields and are commonly direction selective (Gale and Murphy 2014).

Avoidance behaviour

Work in mice has also begun to unravel the cellular basis of avoidance behaviours. In one study Shang et al (2015) demonstrated that a group of genetically defined

neurons, expressing PV, responded to looming stimuli, with their peak response close to the estimated time to collision of the stimulus. Furthermore, optogenetic activation of these PV+ neurons could induce two behaviours associated with threatening stimuli: freezing and escape (Shang et al. 2015). It was later discovered that these neurons formed two divergent pathways, which either projected to the parabigeminal nucleus (PBGN) or lateral posterior thalamic nucleus (LP) (Shang et al. 2018) (Fig. 1.2.4b). Selective activation of the PBGN pathway was associated with escape, whilst activation of the LP pathway was associated with freezing (Shang et al. 2018, Wei et al. 2015). Since a looming stimulus activates both sets of neurons simultaneously, a winner takes all strategy may be employed to elicit one of the defensive behaviours. Which behaviour is elicited may be determined by a number of contributing factors including the stimulus features, environmental context, or differences in arousal state. The fact that loom detectors are able to participate in two mutually exclusive behaviours lends further support for a parallel feature analysing network that allows for behavioural flexibility.

Despite these recent findings, the neuronal activity which underlies tectal mediated behaviour is still not fully understood. For example, whilst the PV+ neurons could be classified as looming detectors (Shang et al. 2015, Shang et al. 2018), many other neurons in the SC also respond to a looming stimulus (Zhao et al. 2014). Furthermore, PV+ neurons in the SC form a group of neurons with mixed morphological and electrophysiological properties (Villalobos et al. 2018), indicating they may fulfil multiple computational and behavioural roles. Indeed, based on the morphological analysis reported by Shang et al (2015), their PV+ population may contain NF neurons, which were shown to be important in mediating prey capture (Hoy et al. 2019). Furthermore, both the PV+ neurons involved in escape and the NF neurons involved in orientation towards prey were shown to project to the PBGN (Hoy et al. 2019, Shang et al. 2018), which is thought to play a role in object localisation (Cui and Malpeli 2006). This, therefore, raises the possibility that there is an overlap in the population of neurons which play a role in these dichotomous behaviours. Recording the neural activity across all of the neurons in the SC would allow an unbiased analysis of the population activity which gives rise to these behaviour. However, due to its size and lack of optical accessibility it is impossible to do this

in mammals. In this respect, zebrafish larvae have proved to be a useful organism, since, due to their small size and optical transparency it is possible to record from every neuron in the tectum simultaneously (Ahrens et al. 2013). The use of zebrafish to understand the cellular basis of tectal mediated visuomotor transformations will be discussed in the next section.

1.2.4 Using zebrafish to understand the optic tectum

By 7 dpf zebrafish already show a range of visually guided behaviours, including hunting and escape (Patterson et al. 2013, Dunn et al. 2016b). These two mutually exclusive behaviours can each be defined using a number of behavioural kinematics, with hunting being characterised by eye convergence and small orientating movements of the tail, known as J-turns (Patterson et al. 2013), and escapes being characterised by a fast, high angle, stereotyped motor routine, known as a C-turn (Dunn et al. 2016b). Furthermore both these behaviours can be elicited in head-fixed larvae, using artificial stimuli presented onto a screen, with hunting behaviour being assayed using small dots, between 1° and 10° (Bianco et al. 2011, Bianco and Engert 2014), and escape behaviour assayed using a looming stimulus, with an escape initiated once the loom reaches a critical size of visual angle (Dunn et al. 2016b, Temizer et al. 2015).

A further advantage of using zebrafish larvae as a model organism is, due to its small size and optical accessibility, the ability to conduct whole tectal, or even whole brain, imaging at a single neuron resolution (Ahrens et al. 2013, Portugues et al. 2014). This functional imaging can be combined with presenting the zebrafish with various visual stimuli, as well as recording a behavioural output, therefore allowing the correlation between neural activity and behaviour to be recorded (Bianco and Engert 2014, Vladimirov et al. 2014). Overall this makes zebrafish larvae an ideal system in which to interrogate the cellular basis of visuomotor transformations.

Previous research has demonstrated the importance of population activity in mediating both hunting and escape behaviours (Bianco and Engert 2014, Dunn et al. 2016b, Temizer et al. 2015). Using eye convergence as a proxy for prey capture

behaviour, Bianco et al (2014) found spatially compact groups of neurons which would respond during, or just before, eye convergence (Fig. 1.2.1b). Furthermore, in response to a looming stimulus, it was shown that the critical angular size which initiates an escape routine can be decoded from the population neural activity (Dunn et al. 2016b, Temizer et al. 2015). However, recording from the population activity in response to behaviourally relevant stimuli, by itself, doesn't distinguish between the 'feature detector' or 'feature analyser network' hypotheses (Fig. 1.2.5): is the perception of prey and predator mediated by highly specialised feature detectors, assemblies of multiple neuronal subtypes, or a combination of both? In order to address this it is necessary to know the information that is encoded by those neurons which mediate hunting and escape. In order to do this, tectal neurons should be classified based on their response to an array of visual stimuli (Fig. 1.2.6a), once the neurons have been classified it will be possible to reveal the subtype composition of the population activity which drives behaviour (Fig. 1.2.6b). Whilst previous research in the zebrafish tectum has demonstrated the presence of a number of feature detectors tuned to direction (Hunter et al. 2013, Grama and Engert 2012), orientation (Hunter et al. 2013), size (Del Bene et al. 2010, Preuss et al. 2014), and polarity (Sajovic and Levinthal 1982a) each of these features was analysed independently making it impossible to know whether there are neurons which show selectivity for a conjunction of visual features. Furthermore, it is not known what role these feature detectors play in mediating behaviour. Whilst there is evidence of prey detectors in the zebrafish tectum (Bianco et al. 2011), it is not clear how their activation is related to behaviour, and they only represent a small fraction of tectal neurons. Furthermore, since hunting and escape related activity is yet to be imaged in the same animal it is currently unknown whether there is an overlap in the neural activity which mediates both behaviours.

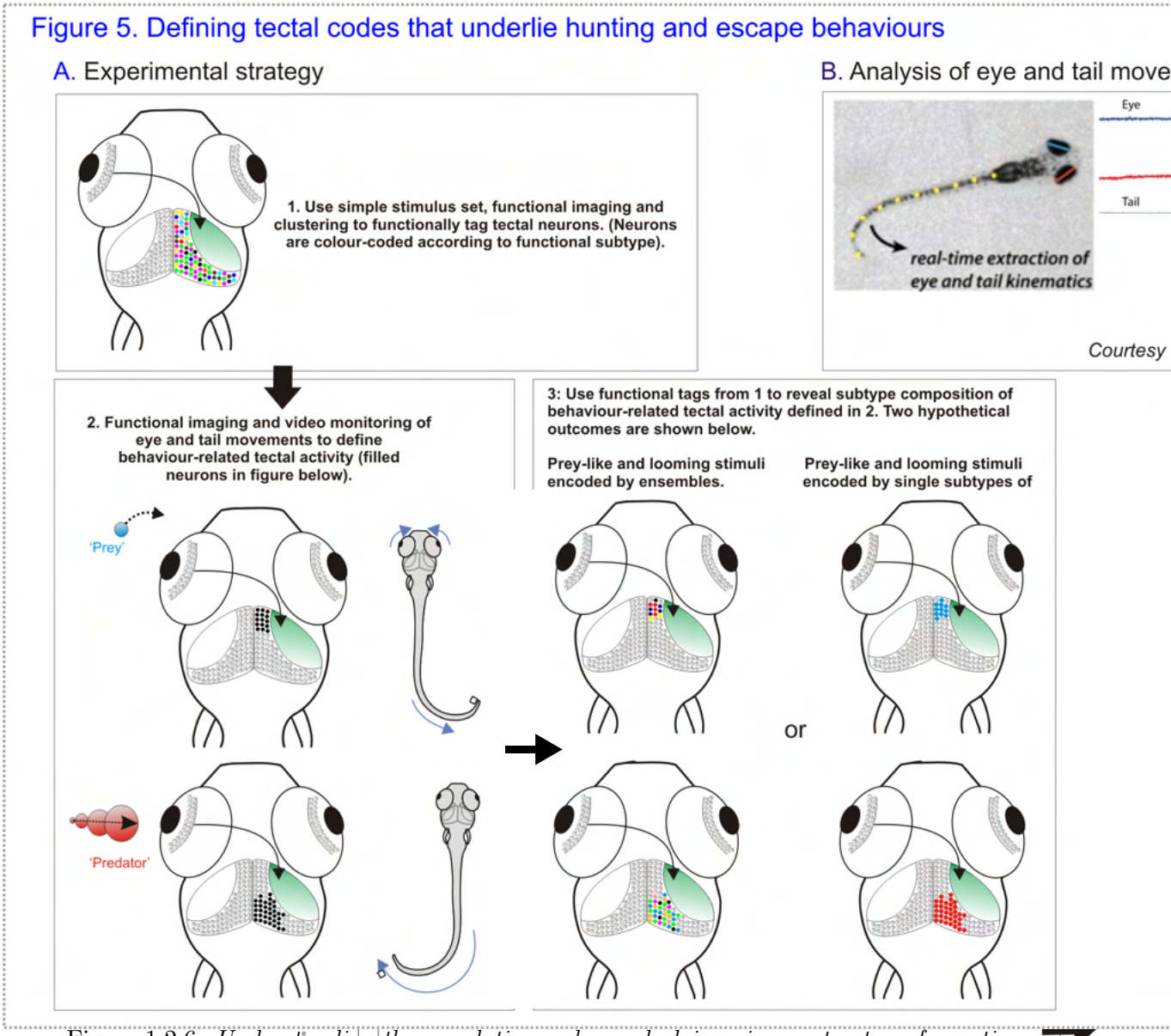

Figure 1.2.6: *Understanding the population codes underlying visuomotor transformations.* (a) Neurons in the tectum can be classified based on their response profiles to an array of visual stimuli. Neurons colour coded according to classification type. (b) To understand the population activity which gives rise to prey capture and predator avoidance, tectal activity is recorded, whilst monitoring behaviour (left). The functional classification from (a) is then used to reveal the subtype composition of the population code. Two possible outcomes are: prey and predator stimuli are encoded by assemblies (middle) or prey and predator stimuli are encoded by single neuronal subtypes (right).

1.3 Thesis Aims

In order to accomplish the goals set out above it is necessary to be able to classify tectal neurons *in vivo*. Therefore, one of the primary aims of this thesis was to develop a method to cluster tectal neurons based on their functional responses to visual stimuli. In order to achieve this a non-parametric unsupervised density based clustering algorithm was adapted (Rodriguez and Laio 2014), such that it was suitable to utilise on calcium imaging data (chapter 3). It was also necessary to develop tools to pre-process the data prior to clustering (chapter 3 and 5), as well as validating the resultant clusters (chapter 4). Furthermore a number of biological questions were addressed such as:

1. what is the selectivity of tectal neurons to the conjunction of direction and size (chapter 4)?

2. how are the resultant neuronal clusters distributed along the anteroposterior and dorsoventral axis (chapter 4)?

Chapter 2

Materials and Methods

2.1 Animals

Zebrafish were maintained at 28.5°C on a 14 hr ON/10 hr OFF light cycle in Danieau solution [58mM NaCl, 0.7 mM KCl, 0.4 mM $MgSO_4$, 0.6 mM $Ca(NO_3)_2$, 5 mM HEPES, pH 7.6]. The transgenic line used in this study was *Tg(elavl3:H2B-GCaMP6s)* (Dunn et al. 2016a). The fish were crossed with the pigmentation mutant, *nacre*, which lacks all neural crest derived melanophores (Lister et al. 1999), and therefore allows optical access to the larval brain. This work was approved by the local Animal Welfare and Ethical Review Body (King's College London), and was carried out in accordance with the Animals (Experimental Procedures) Act, 1986, under license from the United Kingdom Home Office.

2.2 Lightsheet

2.2.1 Microscope

Lightsheet imaging was conducted on a custom made lightsheet microscope built by Dr. Martin Meyer (King's College London) based on the designs by Panier et al. 2013. Mechanics and optics were constructed using ThorLabs components.

Excitation was provided by an OBIS Coherent 488 nm laser focused onto a galvanometer mirror (6215H/8315K, Cambridge Technology) oscillating at 200 Hz horizontal over 800 μm to create an illumination sheet. A second galvanometer mirror (6215H/8315K, Cambridge Technology) scanned along the z-axis and is associated with a low NA illumination objective (5 x 0.16NA, Zeiss EC Plan-Neofluar) to focus the laser onto the sample. The detection arm consists of a 20x/1.0 NA water immersion XLUMPlanFLN objective (Olympus) controlled with a Piezo Controller NV 40/1 CLE (Piezosystem jena) to allow the lightsheet to align with the focal plane. Fluorescence is detected using a high speed sCMOS camer (PCOedge 4.2). The 20x magnification yielded a view of 0.8 x 0.8 mm^2, with a pixel dimension of 0.39 μ^2. The components were synchronised using a data acqusition card (NI-DAQ - USB 6259, National Instruments, CA), using custom built software developed in LabView by George Debreagas and Rafael Candelier.

2.2.2 Visual stimuluation

7 dpf zebrafish larvae were paralysed in α-bungarotoxin (1 mg/ml; Tocris) prepared in Danieau solution. Once paralysed, larvae were mounted in 2% low melting point agarose (Sigma) on a custom made platform dorsal side up. The fish were immersed in Danieau in a custom built chamber and positioned such that the right eye was facing a semi-circular screen covered in a diffusive filter. The screen covers 153° x 97°of visual space, along the horizontal and elevational axes respectively, with the screen positioned 40 mm from the larva's eye. Visual stimuli were projected using a P2JR pico-projector (AAXA Tech). The stimuli were custom written by Dr. Giovanni Diana (King's College London) in C++ using the opencv package.

2.2.3 Imaging

Functional time-series (320 x 320 pixels) were acquired at a rate of 20 Hz, 2x2 pixel binning (0.8 μm x 0.8 μm resolution). The light sheet displays a hyperbolic profile along the light propagation axis. The diffraction-limited minimum (z-dimension)

thickness of the light sheet (characterized by imaging 100 nm diameter fluorescent beads) was 2.5 μm at the focal plane of the illumination objective. This value increases to 9 μm at a distance of 80 μm from the waist.

2.2.4 Image Analysis

Image registration was performed to correct for motion artifacts using a rigid-body algorithm using the SPM8 package in Matlab (http://www.fil.ion.ucl.ac.uk/spm/). Image analysis was conducted using custom C++ scripts written by Dr. Giovanni Diana (King's College London). Signal extraction was conducted on a voxel wise basis. A sliding window of 20 frames (B) scans along the timeseries and calculates a baseline that corrects for low frequency drifts (ΔF = F - B). To ensure responses are not included in the baseline calculation another sliding window compares the fluorescent value at frame N with the mean value of the previous 5 frames, R. A response is detected if the value at frame N is $2\sigma > R$, and continues until N falls back to $2\sigma < R$. Periods when the voxel is responding are not used to calculate the baseline. Cell segmentation and creating a binarised response vector for each neuron was done as described in (Diana et al. 2018).

2.3 Two-photon

2.3.1 Microscope

2-photon imaging was conducted using a custom built microscope (Independent NeuroScience Services, INSS). Excitation was provided using a Mai Tai HP ultrafast Ti:Sapphire laser (Spectraphysics) tuned to 940 nm. The microscope was equipped with a 16x/1.0 NA water immersion objective (Nikon) mounted on a Piezo Controller (Physik Instrumente). The fluorescence was detected using a gallium arsenide phosphide (GaAsP) detector (ThorLabs). Scanning and image acquisition was controlled using Scanimage Software (Vidrio Technologies).

2.3.2 Visual stimulation

Visual stimulation was conducted the same as for the lightsheet, except that the fish was positioned 20 mm from the screen.

2.3.3 Imaging

Images (256 x 256 pixels) were acquired at a rate of 50 Hz, with a pixel resolution of 1.26 μm x 1.24 μm, allowing for the acquisition of 7 focal planes per volume, with a step size of 10 μm, at a volumetric rate of 7.28 Hz.

2.3.4 Image Analysis

Image registration, cell segmentation, and calcium signal extraction was conducted using suite2P (Pachitariu et al. 2017).

2.4 Data processing

Density based clustering was conducted using custom written C++ scripts (Dr. Giovanni Diana, King's College London). Pre- and post-processing of the data was conducted using custom written R scripts.

2.4.1 Cross validation

The neurons from each fish were clustered independently in the first round of clustering. This gives rise to multiple cluster centres from each fish, which are then used to cluster the fish together in the second round of clustering (see chapter 3 for a detailed explanation of the clustering procedure). The cross validation is done on the second round of clustering: centres from the first round of clustering were randomly allocated to 1 of 5 groups. This data was re-clustered 5 times, each time

excluding one of the groups. The Jaccard index was then used to calculate the similarity between every cluster from the original data and every cluster from a cross validated group. This essentially quantifies the fraction of common centres contained between a pair of clusters. The Kuhn-Munkres algorithm was then used to find the matching clusters between the original and cross validated data. A low similarity measure between the original and cross validated clusters is because there are some centres not common to both clusters. Ideally, this should represent a large shift in the cluster landscape. However, it could also be due to the fact that some of the data has been removed in the cross validation group. To ensure the reduction in similarity is actually quantifying a shift in the cluster landscape, and not just the data which was removed, when caclculating the Jaccard Index the equivalent centres which were removed prior to clustering in the cross validated data were also removed from the original data after having been clustered.

2.4.2 Fitting anterior-posterior axis and calculating null distribution

For each fish the xy coordinates of the neurons were extracted. The coordinates were rotated 20° anti-clockwise to attempt to make the SPV layer parallel to the x axis of the image. The x-axis was split into 10 bins and the centre of mass of all the neurons in a bin was calculated. Linear interpolation was then used to generate a total of 20 points along the AP axis.

A null distribution along the AP axis was also calculated for each stimulus. To do this, the number of neurons which were classified as robust to each visual stimulus was found. The same number of neurons were then randomly selected from all of the segmented neurons. The Euclidean distance between each neuron and all of the 20 points along the AP axis was then calculated, and each neuron was assigned to the point closest to it. The average distance along the AP axis was then calculated for these randomly selected neurons. This process was repeated 200 times, for each of the 3 visual stimuli used.

Chapter 3

Density Based Clustering

3.1 Introduction

As mentioned in the introduction the classification of neurons into subtypes, whether by morphological, genetic, or physiological criteria has been a useful tool in many areas of neuroscience, with the eventual aim of this classification being to link neuronal subtypes with computation and behaviour.

In the visual system, many studies have focused on defining subtypes based on a neuron's response to a defined visual feature such as the orientation of an object. For example, some neurons in the retina and downstream visual areas show predictable tuning profiles when an object with an elongated axis is rotated within their receptive fields'. These neurons, which are said to be orientation selective, show high firing rates when presented with an object at their preferred angle and minimal firing rates when presented with an object orthogonal to the preferred angle. These data are often analysed in a parametric manner with an explicit underlying statistical model of how the data are distributed, such as a Gaussian distribution for orientation selectivity (Cronin et al. 2010 Mazurek et al. 2014). Whilst parametric analysis allows for a quantitative description of neuronal selectivity to the given visual feature (Carandini and Ferster 2000, Nikolaou et al. 2012), it will exclude a large number of neurons whose tuning properties don't fit the model. Furthermore, it becomes more

difficult to develop a single appropriate model for the simultaneous classification of neurons tuned to multiple stimuli such as shape, size, and contrast etc. Since the aim of the thesis is to be able to classify large numbers of visually responsive neurons to an array of different kinds of visual features it would, therefore, be advantageous to develop an unbiased non-parametric method for cell type classification that is based on tuning profiles, irrespective of their shape.

A number of studies have turned to non-parametric cluster analysis in an effort to classify neurons without any prior knowledge of how many subtypes to expect (Bianco and Engert 2014, Chen et al. 2018, Helmbrecht et al. 2018, Kunst et al. 2019, Niell and Smith 2005). These clustering methods have classified large numbers of neurons based on multiple input parameters, such as stimulus response properties and morphology. This has led to the discovery of novel neuronal subtypes and has enabled the dissection of a number of neural circuits, such as demonstrating there are neurons tuned to prey like stimuli (Bianco and Engert 2014), revealing the topographic organisation of the zebrafish tectal motor map (Helmbrecht et al. 2018) and uncovering a cellular resolution pathway for the computation underlying the analysis of optic flow (Kramer et al. 2019).

Given the promise that non-parametric cluster analysis has already demonstrated, it seems an appropriate method to be able to cluster visually responsive neurons in an unbiased manner, and to wide variety of visual stimuli. Therefore, the following chapter shows:

1. The rationale and adaptation of a density based non-parametric clustering method (Rodriguez and Laio 2014).

2. The necessary steps taken to preprocess *in vivo* functional imaging data prior to clustering.

3. Validation experiments to demonstrate that applying the clustering method to *in vivo* functional imaging data produces biologically meaningful clusters.

3.2 Results

3.2.1 Outline of density based clustering

The outline of the clustering procedure follows the algorithm set out in Rodriguez and Laio 2014. The basic assumption is that clusters of data points in n-dimensional space can be thought of as approximating some arbitrary density distribution. Clusters are defined as areas of high density, and cluster centres are defined as regions of local density maxima, which are sufficiently separate from other maxima (Fig. 3.2.1).

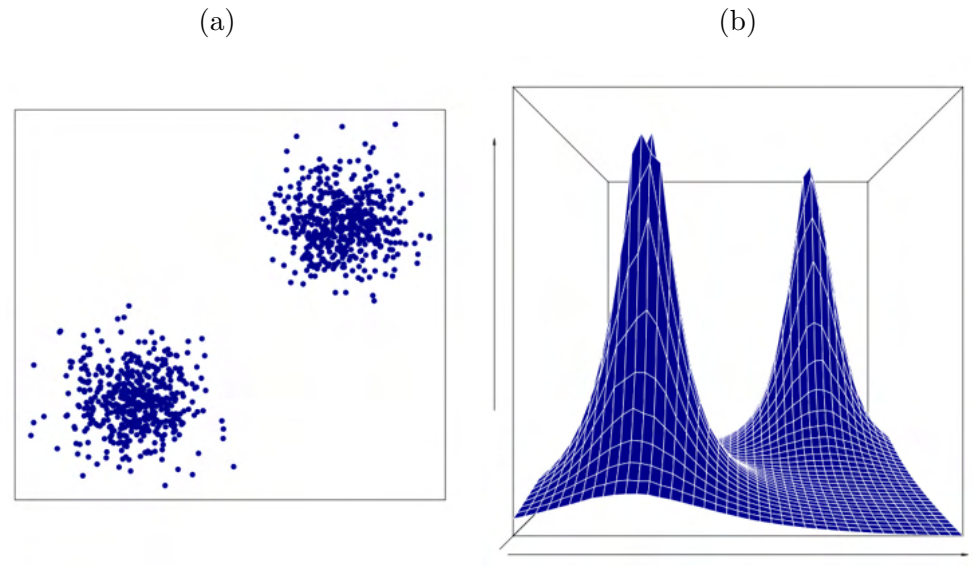

Figure 3.2.1: *Points in n-dimensional space can be thought of as approximating some arbitrary density distribution.* (a) Points embedded in a two-dimensional space drawn from one of two multivariate Gaussian distributions, each of which represents a cluster. (b) The density can be estimated from the data; increases in the density represent clusters and the peaks represent cluster centres.

The clustering procedure aims to find the centre of each cluster i.e. the point of highest density within a cluster. These cluster centres can be thought of as peaks in the density landscape (Fig 3.2.1b). The number of cluster centres defines the number of clusters. Therefore, unlike many clustering methods, this algorithm has the advantage that the number of clusters are not defined prior to clustering. The way this is achieved is as follows. For each data point i two quantities are calculated:

1. its local density (ρ_i)

2. its Euclidean distance from the nearest point of higher density (δ_i).

Unlike Rodriguez and Laio, who use a kernel density estimator, ρ_i is defined using a kth nearest neighbour (kNN) approach, where the density is approximated by calculating the Euclidean distance between point i and its k^{th} nearest neighbour ($dKNN$):

$$\rho_i \propto \frac{1}{[dKNN]^n} \tag{3.1}$$

where n is equal to the dimensionality of the data. This method of estimating the density can therefore be thought of as asking what is the minimum volume necessary to encapsulate the k nearest neighbours of data point i, and serves as a useful relationship for defining the cluster centres (see eq. 3.3).

δ_i is calculated as the minimum distance to any point of higher density, j:

$$\delta_i = \min_{j:\rho_j > \rho_i} (d_{ij}) \tag{3.2}$$

The point with highest density is given $\rho_i = \max_j(d_{ij})$, that is the maximum distance between the highest density point and any other point. Intuitively, it is expected that points of low density tend to be far away from points of higher density simply because there are fewer points close by. Conversely, high density points tend to be close to points of higher density. Therefore, a negative correlation is expected when plotting δ vs ρ. This correlation breaks down, however, when in a local maximum of the density since it is necessary to travel further than expected to find a point of higher density, at which point we get δ_i much larger than expected, given ρ_i. These outliers become the cluster centres and define the number of clusters. The remaining points are then assigned to a cluster which is the same as their nearest neighbour of higher density. Using this method, cluster centres are therefore defined as local maxima of the density, sufficiently separated from points with higher densities.

Fig. 3.2.2 demonstrates how the algorithm works on some synthetic data. Fig. 3.2.2a shows 160 points in a two-dimensional space, with each point being taken from one of three multivariate Gaussian distributions. Each one of these distributions can be thought of as a cluster to be identified. After calculating δ_i and ρ_i for each point in the 2d space the logarithm of these values can then be plotted as shown in 3.2.2b. As can be seen there is generally a negative linear correlation between δ and ρ with the exception of three points, which have a larger δ than expected, given ρ (coloured dots in Fig. 3.2.2b). These three points correspond to the local maximum of the density for each cluster and are therefore classed as the cluster centres. Fig. 3.2.2c shows where those centres are located in the 2d space. The plot in Fig. 3.2.2b is referred to as the 'decision plot'. To objectively determine from the decision plot which points are considered centres the logarithm of Eq. 3.1 can be taken to fit the straight line:

$$\log(\rho) = -n \log(dkNN) + C \tag{3.3}$$

When $C = 0$ anything above the line represents a point with a higher δ than expected given ρ (red dashed line in Fig. 3.2.2b). Increasing the value of C increases the threshold for a point to be considered a cluster centre. In this example a value of $C = 3$ was chosen (black dashed line in Fig. 3.2.2b).

Once the cluster centres are defined, the rest of the data points are associated to the same cluster as their nearest neighbour of higher density. The algorithm will necessarily associate all points to a cluster (Fig. 3.2.2d). However, this assignment can become somewhat arbitrary for points of low density (Fig. 3.2.2f). To account for this, points are removed from clusters that are considered outliers. To classify whether a point is an outlier is a two step procedure. First, a point is considered an outlier if its k^{th} nearest neighbour is not also in the same cluster as itself (Fig 3.2.2e). Second, for each cluster, the outlier with maximum density is found. This density is then used as a minimum threshold for all points within the cluster. Any points in the cluster which do not have a density greater than the threshold will also be classified as outliers. As can be seen in Fig. 3.2.2f this approach causes any points

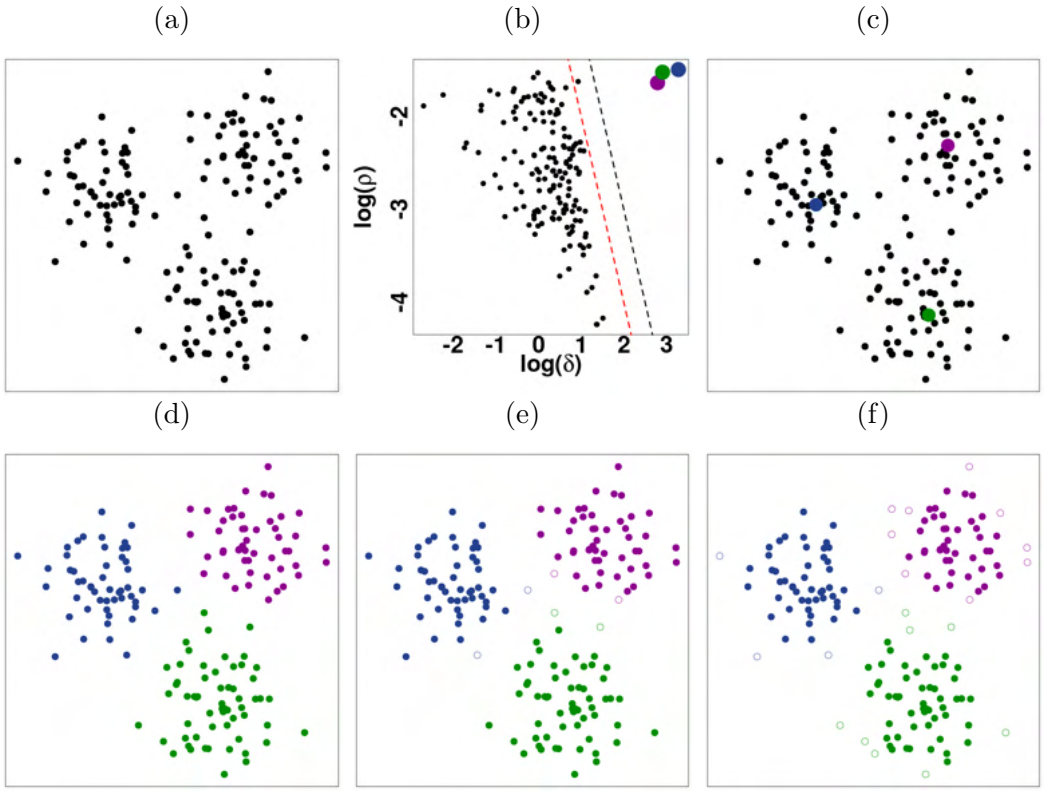

Figure 3.2.2: *Demonstration of the clustering algorithm.* (a) Points drawn from one of three multivariate Gaussian distributions, each of these distributions represents a cluster. (b) Plotting $\log(\delta)$ vs $\log(\rho)$ for each data point yields three outliers (large dots), which represent the centres of each cluster. (c) The location of the cluster centres, each colour coded according to (b). (d) Once the centres have been found the remaining points are associated to one of the cluster centres. (e) Points whose k^{th} nearest neighbour is not in the same cluster are removed as outliers (open circles) (f) The outlier with maximum density for each cluster is calculated and any point in that cluster which doesn't have a greater density is also removed (open circles).

around the outside of the cluster to removed i.e those points which don't represent the cluster to which they have been assigned.

Being able to find the cluster centres is predicated on choosing the correct value of k in the kNN local density estimation. A small value of k will lead to a very fine scale estimation of the local density, however, this may give rise to peaks in the density which actually just correspond to noise in the data (Fig. 3.2.3a). As the value of k increases the density estimation incorporates a larger area of the data, which leads to a smoother distribution of the density (Fig. 3.2.3b & 3.2.3c). In terms of the number of clusters, a small k will give rise to many clusters since there are many local density maxima (Fig. 3.2.3a) whilst a large k will give rise to fewer clusters,

(a) kNN = 2 (b) kNN = 200 (c) kNN = 1000

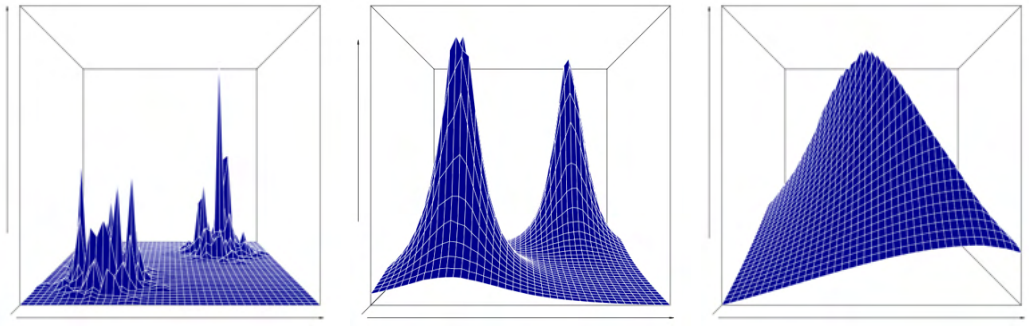

Figure 3.2.3: *The estimated density of the data, using different values of k.* The underlying data is the same as in Fig. 3.2.1a

since there are fewer local maxima (Fig. 3.2.3b). The actual value of k must be decided empirically for each dataset, and in this thesis is generally chosen such that no two clusters share very similar tuning properties.

The advantage of using this clustering method is that: first, any arbitrary distribution can be defined as a cluster and second, clusters of varying density are able to be successfully isolated. These are two things which other clustering approaches often fail to capture but may be important to successfully cluster the functional imaging data. For example, unlike k-means clustering, the density based clustering algorithm was able to successfully recover the clusters on data which is not Gaussian distributed (Fig. 3.2.4 - top row) or which have unequal variance (Fig. 3.2.4 - bottom row).

One requirement of the clustering algorithm is to be able to find common subtypes of neuron across multiple fish. This can be hindered somewhat due to experimental variability. Since there will be a certain amount of noise across experiments, the same subtype of neuron in each fish may not fully overlap in their response profile (Fig. 3.2.5a). This noise can come from multiple sources, including variations in the developmental stage or internal state of the fish, or from variations in the experimental procedure, such as time of day and temperature. This has the effect of creating 'artificial' peaks in the density. In the case of Fig. 3.2.5, if these two fish are clustered together, as outlined above, each cluster will only be present within one fish (Fig. 3.2.5a). To prevent this from happening and to allow clustering

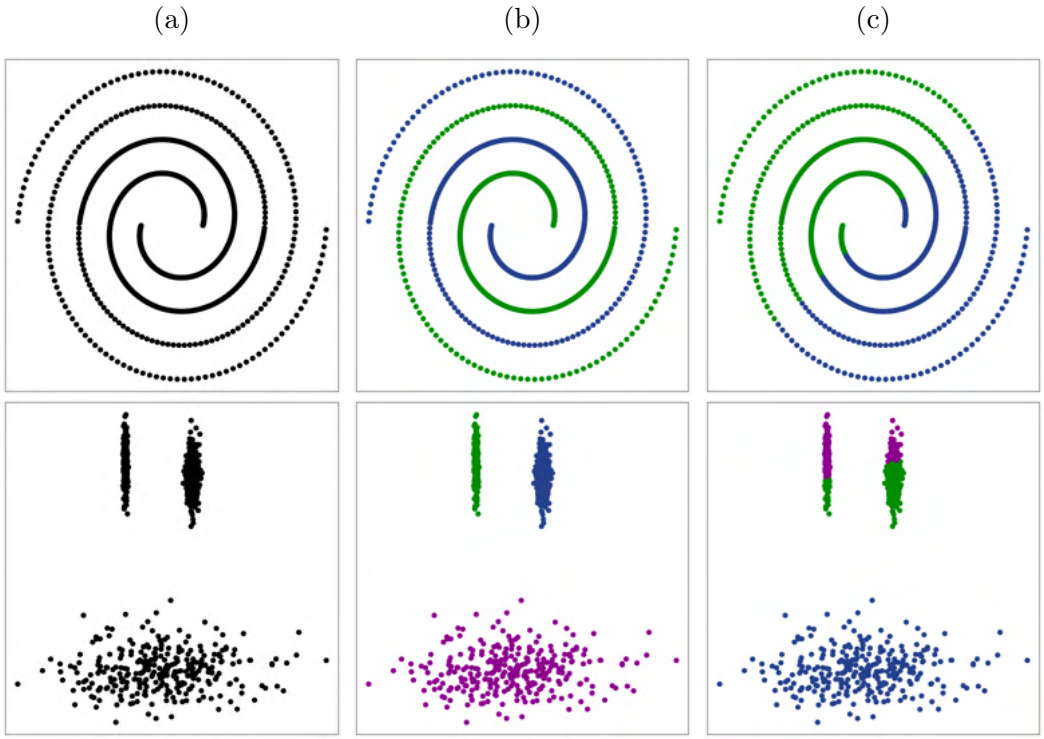

Figure 3.2.4: *The density based clustering algorithm is able to outperform k-means.* Top row: clusters come from an arbitrary distribution. Bottom row: clusters have an unequal variance. (a) The unlabelled data. (b) Cluster assignment using the density based algorithm. (c) Cluster assignment using k-means. Notice how k-means incorrectly assigns points to clusters in both cases, even when supplied with the correct number of clusters

of common subtypes across fish, the method has been adapted into a two step density-based agglomerative clustering method. First, all neurons from each fish are clustered separately using a fine scale density estimation (using a kNN value of 2) (Fig. 3.2.5b). The centres of these clusters from each fish are then combined and clustered together, using a more coarse grained density estimation (using a kNN value between 2 and 7) (Fig. 3.2.5c). This method can be thought of as reducing the effect of experiment to experiment variability and enables the algorithm to detect subtypes that are common across fish.

The cluster centres generated from the first round of clustering represent small groups of neurons which behave in a very similar manner. There is, however, a degree of uncertainty associated with how well that cluster centre represents that small group of neurons. This uncertainty can be propagated through to the second round of clustering by calculating the variance of the centres and using this as a weight when calculating the Euclidean distance between centre C and C' in the

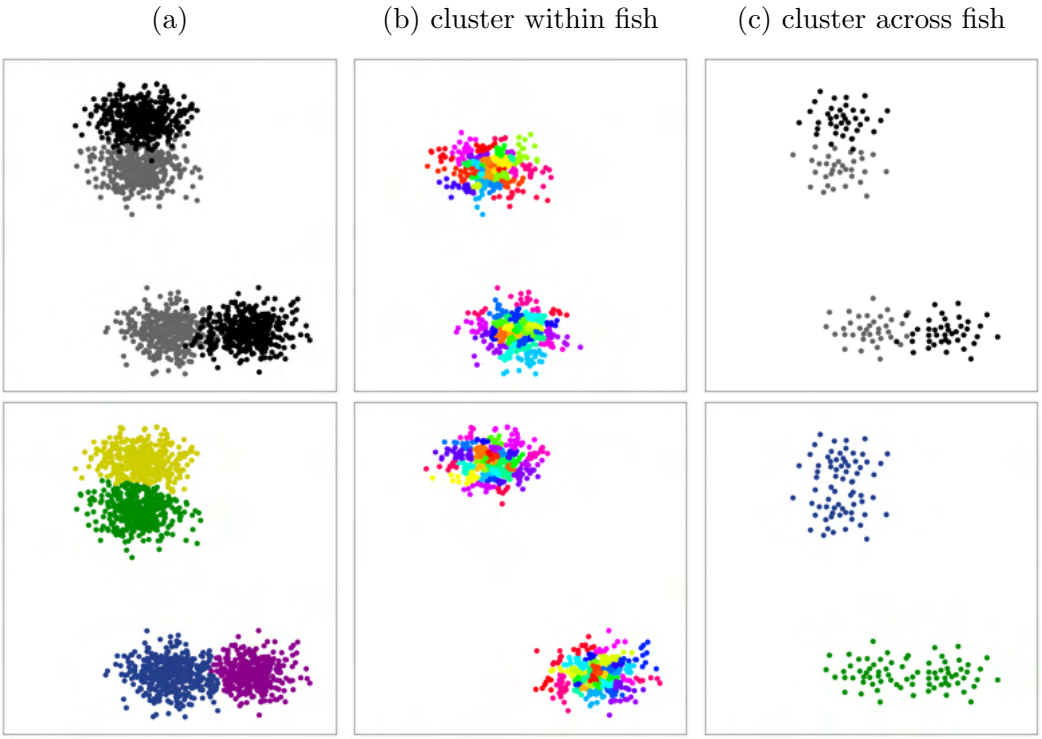

Figure 3.2.5: *Schematic of the two step clustering procedure.* (a) Black and grey points can be thought of as data from from two separate experiments. Due to experiment variability the black and grey clusters do not perfectly overlap, despite representing the same cluster. What should be considered two clusters are clustered into four separated clusters (bottom panel). (b) To reduce the effect of experiment to experiment variability each fish is initially clustered separately using a fine scale (small k) density estimation. (c) The centres from this first round of clustering are combined and clustered together in a second round of clustering which this time gives rise to two clusters, both of which are present across both fish.

second round of clustering as follows:

$$d_{CC'} = \sqrt{\sum_i \frac{(r_i^C - r_i^{C'})^2}{(\sigma_i^C)^2 + (\sigma_i^{C'})^2}} \tag{3.4}$$

where r_i^C represents the response of centre C to stimulus i and $(\sigma_i^C)^2$ represents the standard deviation of the responses from the neurons in centre C to stimulus i. This means that, given a certain Euclidean distance, centres which have less variance are penalised less, compared to clusters with higher variance.

3.2.2 Pre-processing *in vivo* functional imaging data for density based clustering

To apply this clustering procedure to functional imaging data visual stimuli were presented in a pseudo-randomised order to one eye of elavl3:H2B-GCaMP6s expressing zebrafish, and the responses from the contralateral tectum were recorded. The following is an outline of the pre-processing steps applied to the functional imaging data. An array of different visual stimuli were used across multiple experiments, for details about the stimuli see section 3.2.3, chapter 4, and chapter 5. Lightsheet microscopy was performed with an acquisition rate of 20 Hz on a single plane. Following data acquisition the calcium signal from each pixel was extracted (materials & methods). The neurons were segmented (Fig. 3.2.6) (Diana et al. 2018) and the calcium signal from each pixel in a segmented neuron was averaged together. For each cell, the maximum fluorescent calcium signal was then calculated across each stimulus. For each neuron, these values were concatenated to give a response vector, which is as long as the number of visual stimuli presented. The response vector therefore encapsulates a neuron's response to the visual barrage. The response vector was then Z-scored to normalise each neuron. The normalised response vector was used for the clustering procedure, where the number of data points is equal to the number of neurons and the dimensionality is equal to the number of different stimuli (Fig. 3.2.7).

Since the aim of the clustering procedure is to classify visually responsive neurons it is important to make sure the neuronal responses that are clustered are locked to the visual stimuli and are not just firing spontaneously. To remove any neuron which is not responding in a time-locked manner to the visual stimulus, the activity of the neuron was compared to a random noise model. In order to do this, the calcium signal from each neuron was binarised such that the time frames when there is a maximum likelihood of the neuron firing are equal to 1 and the rest of the time frames are equal to -1 (Fig. 3.2.6c) (Diana et al. 2018). If x_i is the binarised state of neuronal activity at timepoint i and s_i represents whether or not a visual stimulus is being shown at timepoint i (1 = visual stimulus, -1 = no visual stimulus), and N is the total number of frames, for each neuron it's correlation coefficient can then

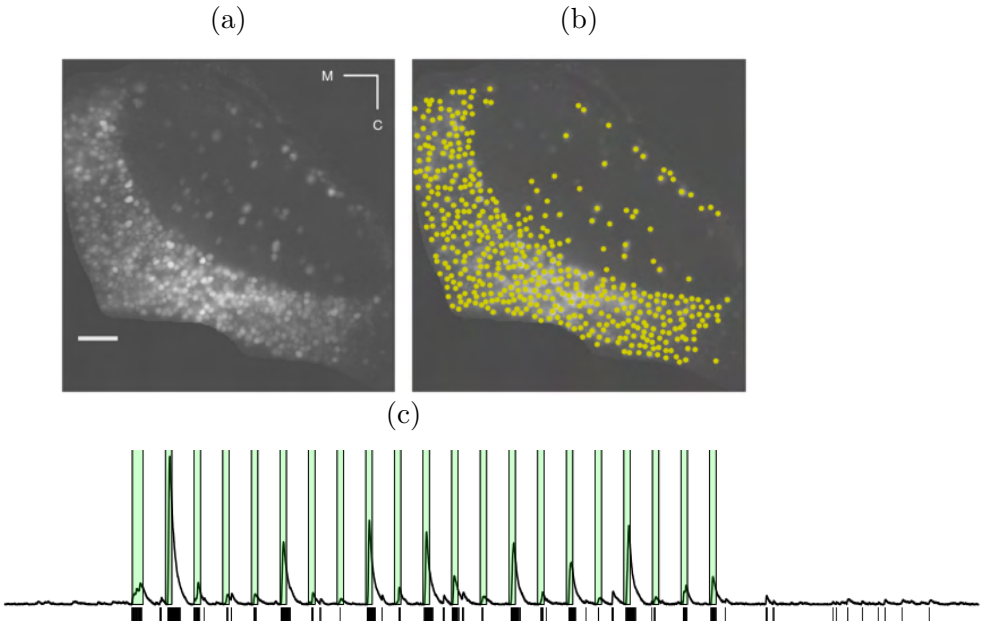

Figure 3.2.6: *Cell segmentation and signal extraction.* (a) An image of the zebrafish tectal hemisphere and (b) the centroids of the segmented cells. (c) An example of the calcium trace from one neuron. Below the calcium trace is the binarised response vector, where black dashes indicate frames where there is a maximum likelihood of the neuron firing (Diana et al. 2018). Green bars indicate when a visual stimulus was being presented. Scale bars show 15µm unless otherwise specified.

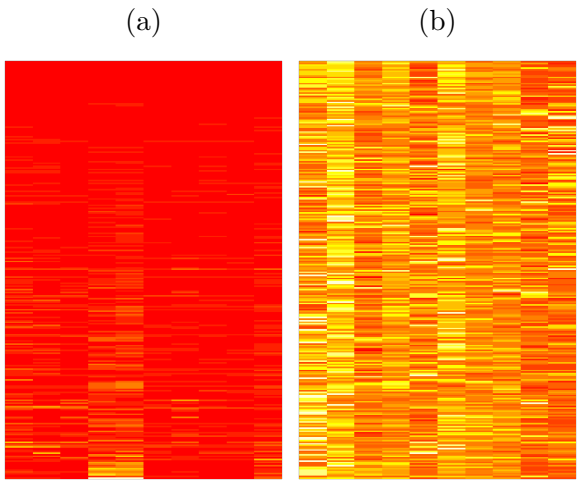

Figure 3.2.7: *The response vectors for all neurons in one fish.* Each row represents one neuron's response vector. Each column is a stimulus and also represents the dimensionality of the data. (a) un-normalised and (b) z-scored response.

be calculated by:

$$NCC = \frac{1}{N}\sum_{i=1}^{N} s_i x_i \tag{3.5}$$

where a value of 1 would indicate that the neuron is firing only (and always) during the presentation of the visual stimuli and a value of -1 would indicate the opposite, that the neuron fires only (and always) outside of the time during which the visual stimuli are presented. To remove neurons which are firing randomly the average NCC of a neuron given its probability of being active, p_x, is calculated:

$$\langle NCC \rangle = \langle s \rangle \langle x \rangle \tag{3.6}$$

where

$$\langle s \rangle = \frac{N_1 - N_{-1}}{N} \quad \begin{cases} N_1 & \text{total visual stimulus frames,} \\ N_{-1} & \text{total no visual stimulus frames.} \end{cases} \tag{3.7}$$

and

$$\langle x \rangle = 2p_x - 1 \tag{3.8}$$

where

$$p_x = \frac{\sum_{x_i > 0} x_i}{N} \tag{3.9}$$

from this the standard deviation is given by:

$$\frac{1}{N}\sqrt{4p_x(1-p_x)} \tag{3.10}$$

The NCC was calculated for each neuron and the neuron was removed if this value was not at least six standard deviations higher than $\langle NCC \rangle$. This ensures that neurons are only kept if they are more likely to fire during the presentation of a visual stimulus than outside of the presentation of a stimulus, given their probability of firing. Thus, visually responsive neurons can be selected for.

Fig. 3.2.8a shows a heatmap of NCC values across a zebrafish tectal hemisphere. As can be seen there is a concentration of higher NCC values located in the centre of

the hemisphere, compared to the periphery, indicating there is an non-homogenous distribution of reliable visually responsive neurons across the tectum, with a higher concentration in the midpoint. Fig. 3.2.8b shows all of the neurons which were kept following thresholding based on $\langle NCC \rangle$. Figs.3.2.9a and 3.2.9b show calcium traces from example neurons that were either kept or removed, respectively. As can be seen, neurons that were kept after thresholding respond in a timelocked manner during the presentation of the stimulus, whilst neurons which were removed show high levels of non-stimulus locked activity.

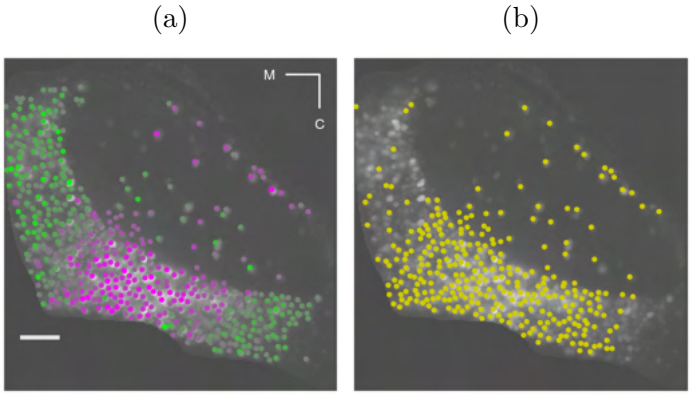

Figure 3.2.8: *NCC distribution across the tectum.* (a) heatmap of the NCC values across the tectum, more purple indicates a higher NCC value. (b) All of the neurons that were kept after thresholding based on the NCC.

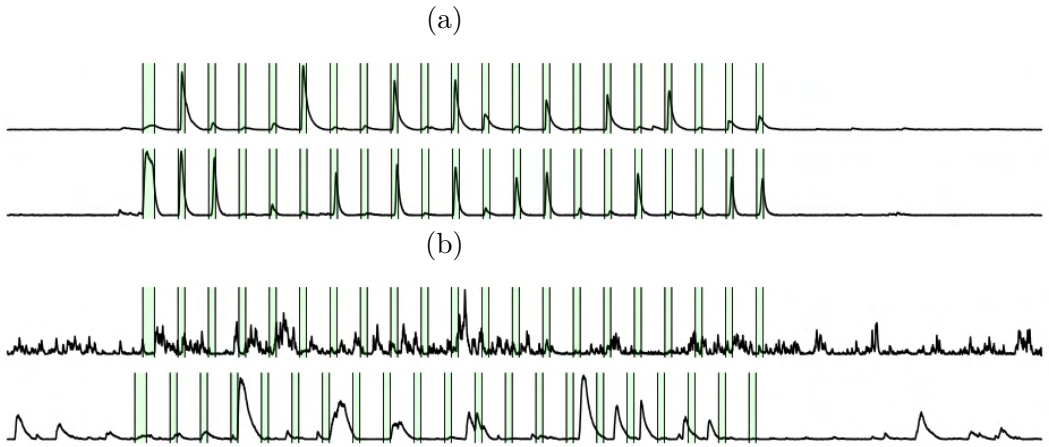

Figure 3.2.9: *Examples of neurons that were removed after thresholding based on the NCC value.* Neurons in (a) were kept and neurons in (b) were removed. Green bars indicate when a visual stimulus was being presented.

3.2.3 Application of the density based clustering algorithm to *in vivo* calcium imaging data

In an effort to ensure this clustering method is appropriate to apply to *in vivo* calcium imaging data a simple ground truth experiment was conducted by taking advantage of the topography within the zebrafish optic tectum, whereby objects located at different positions in the nasotemporal visual field are represented by neurons located along the antero-posterior axis in the tectum. Two gratings of 15° spatial frequency moving at 1 Hz in the 270° direction were presented sequentially to the zebrafish. One grating was localised to the nasal visual field and the other was localised to the temporal visual field (Fig. 3.2.10a). If the clustering procedure is working correctly then topographically organised clusters should be generated along the antero-posterior axis of the tectum. Fig. 3.2.10b shows the location of the three clusters generated in the tecta of the imaged fish. As can be seen two of the clusters are spatially compact and span the antero-posterior axis, with responses selective for either the nasal or temporal visual fields (Fig. 3.2.10c-3.2.10d). The third cluster is also localised to the posterior tectum but is more sparse, with the response profile being less selective between the two stimuli (Fig. 3.2.10e). Therefore the clustering procedure generated biologically meaningful clusters which were in the expected locations, despite not providing information to the clustering algorithm about neuron or stimulus location.

Further to this, the clustering algorithm was able to identify 4 direction selective and 2 orientation selective populations of neuron when the zebrafish were presented with drifting sinusoidal gratings of 15° spatial frequency at 1 Hz in each of the 4 cardinal directions (Fig. 3.2.11). This is in line with previous research which took a parametric approach to study direction and orientation selectivity in the tectum (Hunter et al. 2013), further validating the applicability of the algorithm to *in vivo* calcium imaging data. The clustering procedure also picked out a further 3 clusters not found using the parametric approach (Fig. 3.2.12).

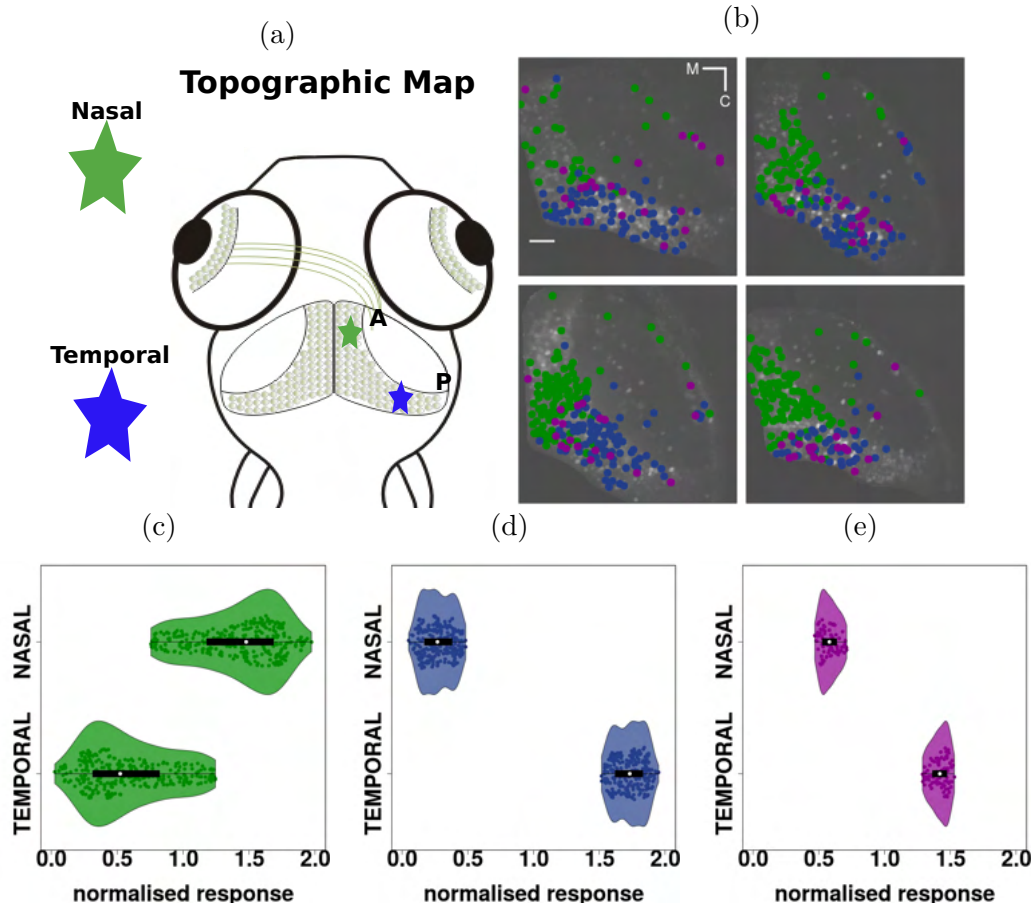

Figure 3.2.10: *Validation of the clustering algorithm using topography.* (a) Schematic of the zebrafish visual system with objects located in the nasal visual field being represented in the anterior portion of the tectum (green stars), whilst objects located in the temporal visual field being represented in the posterior portion of the tectum (blue stars). (b) The location of the neurons in the three clusters which were generated in response to the spatially localised stimuli. The clusters form a rough topographic map along the antero-posterior axis of the tectum. (c-e) Each plot shows the response of every neuron belonging to that cluster (green, blue and purple dots), as well as the median response of all the neurons in the cluster (white dot) $n = 4$ fish.

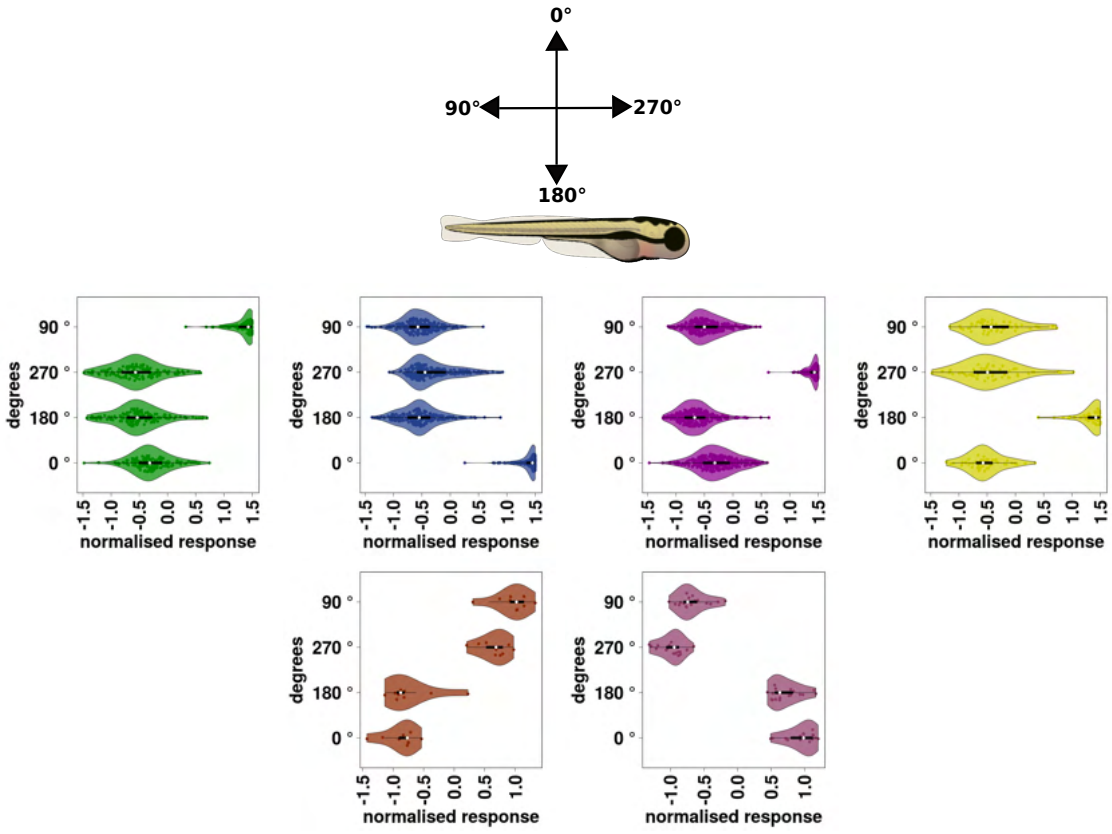

Figure 3.2.11: *The clustering algorithm is able to recover the 4 direction selective populations in the tectum.* Schematic shows directions of stimuli relative to the zebrafish body axis. Each plot shows the normalised response of all the neurons in a cluster when the fish were presented with drifting sinusoidal gratings of 15° spatial frequency at 1 Hz in each of the four cardinal directions. The top row shows four populations each of which respond to one of the four cardinal directions. The bottom row shows two populations which respond to either horizontal and vertical orientations. $n = 8$ fish. Zebrafish larvae schematic taken with permission from Lizzy Griffiths (http://zebrafishart.blogspot.com/2013/05/heres-new-drawing-this-time-of-baby.html)

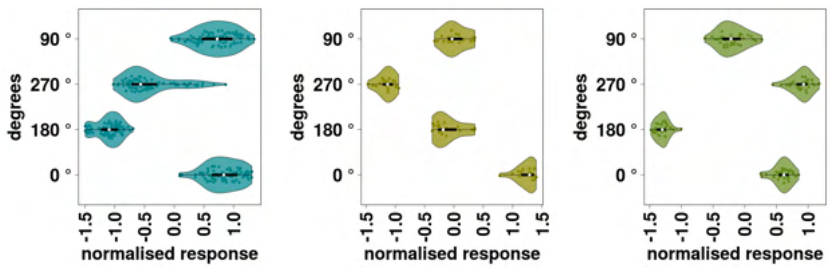

Figure 3.2.12: *The clustering algorithm reveals novel clusters in response to directional stimuli.* Each plot shows the normalised response of all the neurons in a cluster when the fish were presented with drifting sinusoidal gratings of 15° spatial frequency at 1 Hz in each of the four cardinal directions. $n = 8$ fish.

3.2.4 Summary

1. A density based clustering algorithm has been adapted from Rodriguez and Laio (2014) which defines clusters as regions of local density maxima. The procedure has been adapted into a two step agglomerative density based method to allow the detection of common neuronal subtypes across multiple fish.

2. The algorithm is able to successfully define clusters using synthetic data, where k-means clustering fails.

3. Neurons which are reliably locked to visual stimuli can be selected for using the NCC.

4. Clustering on *in vivo* calcium imaging data produces biologically meaningful clusters.

3.3 Discussion

The data presented here demonstrate the applicability of a density-based clustering algorithm to cluster *in vivo* calcium imaging data. The clustering algorithm is superior to other commonly used algorithms such as k-means in several ways:

1. It makes no assumptions about the underlying distribution of the data and can cluster arbitrary distributions.

2. The algorithm can successfully isolate clusters even when there are clusters of different densities, something which other density-based clustering algorithms such as DBSCAN struggle with (Kriegel et al. 2011).

3. There is no need to define the number of clusters prior to clustering.

The algorithm is, however, sensitive to the initial choice of k when estimating the density. This parameter must be chosen empirically with larger values of k leading to a progressively smoother density landscape and fewer cluster centres being chosen. This, therefore, means that more neurons would be incorporated into each cluster,

leading to a reduction in the similarity within the cluster. Whilst it is difficult to choose k objectively, a value is generally chosen such that no two clusters appear to be similar by eye. Recent work has also attempted to mitigate this problem by finding optimisation methods for the choice of k (Marques and M. Orger 2019).

To determine which points are to be considered centres in the decision plot a threshold must be chosen. As the threshold is increased the number of clusters decreases as clusters are merged, and the number of neurons within each cluster increases. A smaller threshold will lead to more clusters with each clustering containing fewer neurons which are more similar one another. The choice of this threshold is somewhat arbitrary but with an appropriate density estimation ideally there is a clear separation of points which are considered centres from the rest of the data, which means the number of clusters will be robust over a wide range of threshold values. However, it should be stressed that the choice of these thresholds is far from objective and highlights the exploratory nature of cluster analysis.

3.3.1 Validating the algorithm on *in vivo* data.

Whilst it is relatively easy to validate a clustering algorithm on synthetic data which has some ground truth, it is more difficult to apply this same logic to real-world date. Nevertheless, by taking advantage of known functional cell types in the tectum and retinotectal topography, it has been possible to validate the clustering algorithm using *in vivo* calcium imaging data. First, the clustering algorithm was able to define spatially compact and topographically organised clusters despite the fact that the clustering procedure was not provided with information on the position of the neurons or visual stimuli. Second, the method was able to recapitulate the findings of previous research which has demonstrated that there were four directions selective, and two orientation selective populations of neuron in tectum (Hunter et al. 2013). The fact that this non-parametric method is able to recapitulate the findings from a parametric method is an encouraging sign that the algorithm is generating biologically meaningful clusters.

3.3.2 Distribution of visually responsive neurons in the tectum

Since the algorithm will necessarily cluster all points, it is important to sufficiently pre-process the data to make sure only neurons which are responding to visual stimuli are being clustered. To this end, a neuron's response profile was compared to a random noise model and any neuron which was not time-locked to the visual stimuli was removed. Interestingly, when looking at the spatial distribution of these neurons, it was found that neurons in the centre were more locked to the timing of the stimulus compared to neurons at the poles. This indicates that there is a non-uniform distribution of visually responsive neurons in the zebrafish tectum. Although it is far from clear what these neurons are doing there are some possible explanations. It is possible there is a higher concentration of pre-motor neurons at the poles, or the neurons there receive input from some other sensory organ (Thompson et al. 2016). An alternative explanation is that the neurons are more immature. It is known that newborn neurons are continually added to the tectum throughout the life of the zebrafish (Galant et al. 2016), and at 7 dpf this proliferative zone is located in the caudal pole of the tectum, with the newborn neurons showing intrinsic excitability, but little response to visual stimulation (Boulanger-Weill et al. 2017), similar to many of the neurons removed.

Overall the results suggest the algorithm is providing biologically meaningful clusters and provides justification to use the method to look for novel neuronal types to more complex visual features.

Chapter 4

Choosing visual stimuli

4.1 Introduction

There are certain visual features that are crucial for a visual system to extract, such as object size, shape, and direction of motion, as well as whether that motion is self-generated, or created by the movement of an object within the visual scene. Combinations of these extracted visual features are then used to drive an appropriate behavioural response. For example, in many animals a looming stimulus can elicit avoidance behaviours (Vries and Clandinin 2012, Dunn et al. 2016b, Jang et al. 2016, Rind et al. 2016, Temizer et al. 2015, Yilmaz and Meister 2013), whilst hunting behaviour can be elicited using an array of species dependent stimuli , such as small moving dots in zebrafish (Duong et al. 2017, Ewert 1974, Bianco et al. 2011, Monroy and Nishikawa 2011). However, the precise qualities of the stimulus which are essential to give rise to a behaviour are not always well defined. For example, whilst a moving spot of a certain size, speed, and direction can trigger hunting, the importance of shape is not known. Would a vertical or horizontal bar of the appropriate size, speed, and direction also trigger hunting? If so, then shape is perhaps a less important trigger feature for releasing hunting behaviour (Ewert 1974).

A further question is how these visual features are encoded in the neuronal pop-

ulation. Whilst numerous studies demonstrate the presence of neurons capable of detecting individual features, such as stimulus direction, orientation, or size, how these visual features are combined in the brain to give rise to behaviour is less well understood. A study in zebrafish revealed 'prey detector' neurons that are selective for the conjuction of size, speed, and direction of a moving spot, but these represented only a small fraction of the tectal population and the influence of stimulus shape was not explored (Bianco and Engert 2014). Similarly, tectal cells selective for motion direction (Hunter et al. 2013) and size (Preuss et al. 2014) have been identified, but the selectivity of these cells for other visual features is not known. Probing the tectal population with a diverse range of visual stimuli and using clustering approaches will hopefully allow these questions to be answered. More generally, this approach will help with understanding how visual features are encoded by the tectal population and provide insight into the functional diversity of tectal cell types.

Whilst such approaches can be very informative, there is a key limitation which is addressed in this chapter: the number of visual stimuli that can be used to probe the tectal population should ideally be limited for several reasons. First, as the number of stimuli increases the length of the recording and the size of the dataset increases. Second, some stimuli may not elicit reliable or robust responses in the tectum which means their inclusion in the stimulus set is redundant. Finally, as the number of stimuli increase so to does the dimensionality of the data and therefore clustering performance decreases. For these reasons it is necessary to perform pilot experiments to determine the most effective visual stimuli to use for clustering. Therefore, in this chapter a range of visual stimuli were explored to test how the tectum is tuned to two important visual features: shape and size.

4.2 Results

4.2.1 Selectivity for shape of local motion stimuli

How the shape of a local motion stimulus affects tectal responses is not clear. On one hand, a dot has a well defined size in all directions, but as it only covers a

portion of the screen, it may not move through the receptive field of all neurons. On the other hand, an elongated, vertically oriented bar would move through the receptive field of all neurons, since it traverses the whole of the screen, however, this also means it may extend beyond the receptive field of size selective neurons. These two types of local motion stimuli were therefore compared to determine if tectal neurons are selective for the shape of a visual stimulus. The stimuli moved in two directions: anterior to posterior (AP), or posterior to anterior (PA). The stimuli were composed of either black dots, which ranged in diameter from 5° to 30°, moving along the visual azimuth, or black bars which had a corresponding width, and a height which traversed the whole screen. The responses for each of the stimuli were extracted as outlined in the previous chapter and a dot selectivity index (DotS) index calculated:

$$DotS = \frac{R_{dot} - R_{bar}}{R_{dot} + R_{bar}} \tag{4.1}$$

There was a preference for dots across the neuronal population for all sizes and directions (Fig. 4.2.1). The location of dot selectivity in the tectum indicates that the PVNs show the highest dot selectivity, with the SINs appearing to have increased selectivity for the bars (Fig. 4.2.1b). When looking at the SINs in isolation, the distribution is more evenly split between bar and dot selectivity, with a tendency to show preference for bars over dots (Fig. 4.2.2). Overall there does seem to be selectivity for the shape of the stimulus, with most neurons preferring dots.

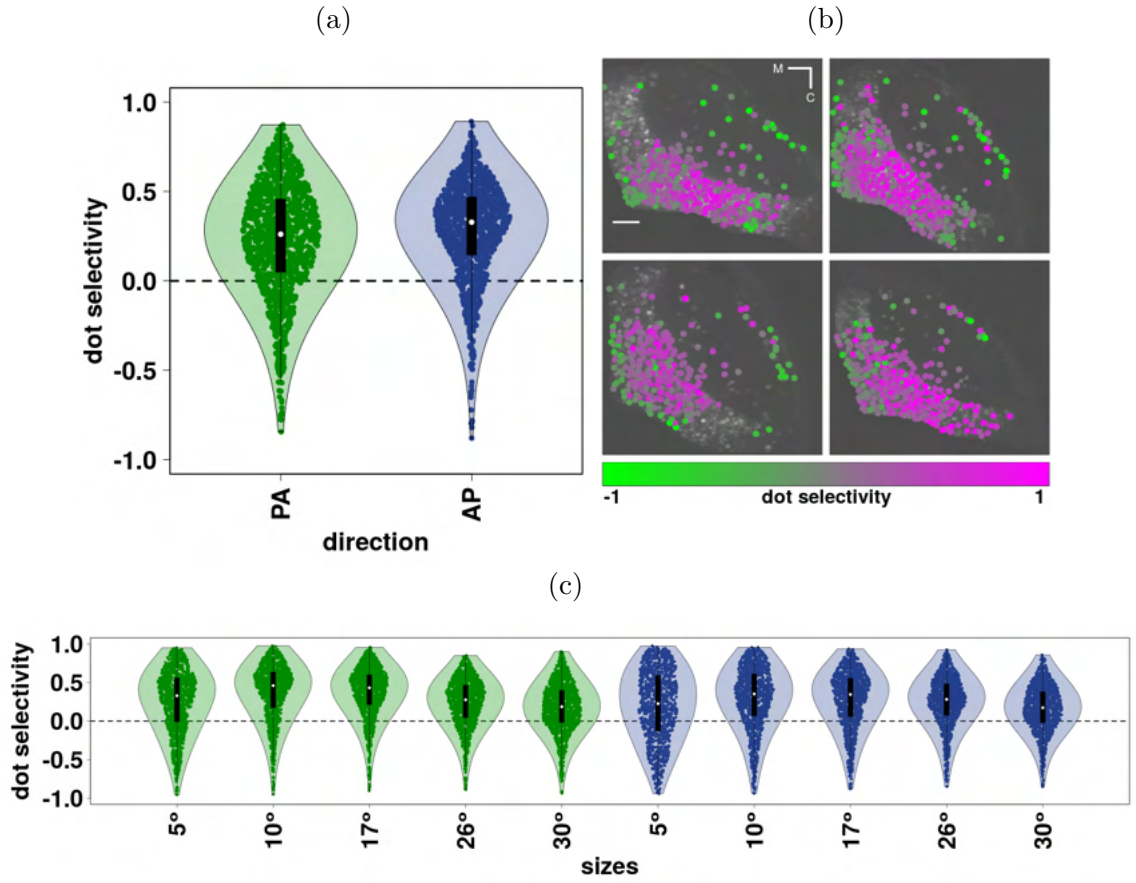

Figure 4.2.1: *Non-uniform distribution of dot selectivity in the tectum.* (a) Distribution of DotS for all cells in the tectum, averaged across sizes for the two directions. (b) Heatmap of the distribution of DotS throughout the tectum, more purple indicates more dot selective. (c) Each violin plot shows the distribution of DotS for all neurons in the tectum for all sizes and directions of stimuli. $n = 4$ fish.

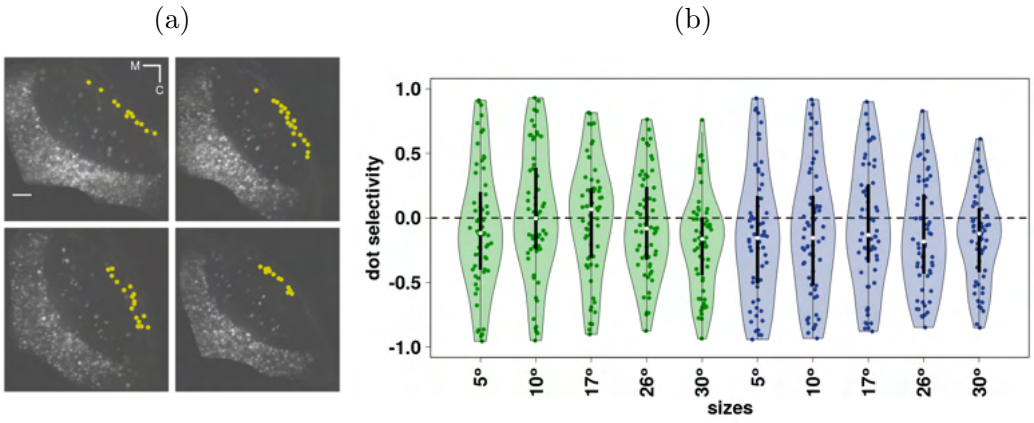

Figure 4.2.2: *Dot selectivity is uniformly distributed in the SINs.* (a) Location of SINs in 4 different fish (b) Distribution of DotS for all SINs across all sizes and directions $n = 4$ fish.

4.2.2 Neurons show mixed selectivity to different sizes and directions of a moving dot

Having established that, overall, dots induce a preferential activation of the tectal neurons, the responses of all the neurons were clustered, only taking into account their response to the dot stimuli. The data was processed and clustered as outlined in the previous chapter. This gave 13 clusters, which were reduced down to 7 clusters once neurons considered outliers were removed (Fig. 4.2.3) as outlined in the previous chapter (Fig. 3.2.2). Briefly, a neuron is removed if its k^{th} nearest neighbour is not also in the same cluster as itself ($k = 3$), or if its density is not greater than the minimum ρ (density) required (see chapter 3). It should be noted that it is possible for all neurons in a cluster to be removed, and hence the cluster itself to be removed; in this case the densities of all the neurons in the cluster are not greater than the minimum ρ (density) necessary to be kept in that cluster. The centres of the clusters which have been removed lie close to the threshold for being considered a cluster centre in the decision plot (Fig. 4.2.3b), indicating they have a lower peak in the density landscape compared to the remaining clusters.

An overview of the 7 remaining clusters can be seen in Fig. 4.2.4 and a summary given in Table 4.1. A more detailed overview of each cluster can be seen in Fig. 4.2.5 - 4.2.11. The clusters show a mixture of selectivity for the visual features with some showing a conjunction in their selectivity for size and direction. For example, cluster 2 shows a preference for small dots moving AP, whilst cluster 4 shows preference for large dots moving PA. Conversely, cluster 3 shows a preference for large size dots, irrespective of direction, whilst cluster 5 shows a preference for PA motion, irrespective of size. Most clusters appear in at least half of the fish, with only cluster 7 appearing in one fish (Table. 4.1). There does, however, tend to be a unequal distribution in the number of cells present in a given cluster across fish. In cluster 1, for example, most of the cells are present in one fish, with far fewer in the other two fish (Fig. 4.2.5). The neurons within a cluster seem to be generally dispersed throughout the tectum, with no obvious bias in their distribution. The clustering algorithm, therefore, seems to have successfully isolated a number of clusters which are selective for a mixture of the visual features shown.

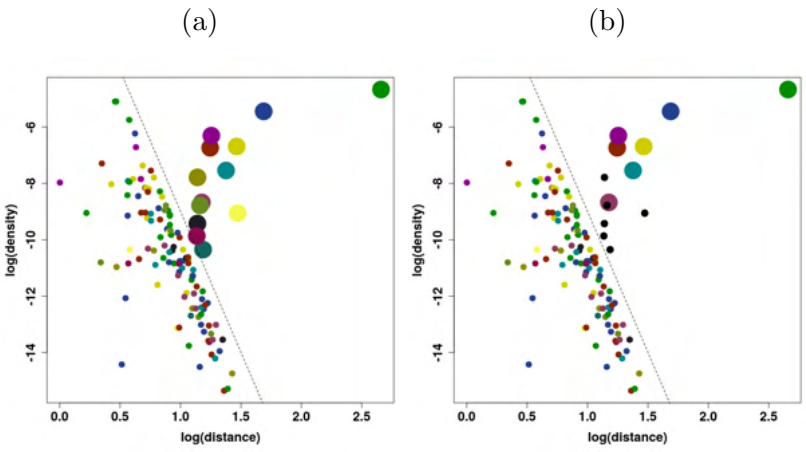

Figure 4.2.3: *Determining the cluster centres.* (a) Decision plot for determining cluster centres. The threshold chosen is 0.5 (dotted black line). Everything above the line represents a cluster centre. (b) The clusters which are retained after removing outliers (small black dots above threshold).

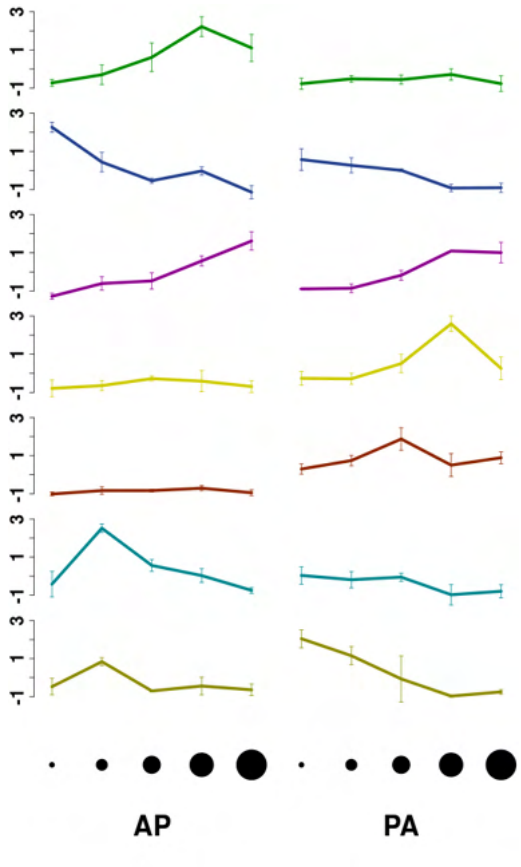

Figure 4.2.4: *Size and directional tuning of clusters.* Normalised average response of clusters, colour coded according to cluster membership, across all 10 stimuli. Error bars show standard deviation. $n = 4$ fish.

cluster	cells/fish	fish	description
1	46 ± 47	3 of 4	AP motion and large size selective
2	28 ± 29	2 of 4	AP motion and small size selective
3	12 ± 9	2 of 4	Large size selective
4	17 ± 15	4 of 4	PA motion and large size selective
5	16 ± 12	2 of 4	PA motion selective
6	16 ± 15	2 of 4	AP motion and small size selective
8	14	1 of 4	PA motion and small size selective

Table 4.1: *Summary of clusters.* Summary of the average number of cells per fish for each cluster, how many fish each cluster is found in and a short description of the cluster. AP - anterior to posterior, PA - posterior to anterior. All neurons in cluster 7 were removed as outliers.

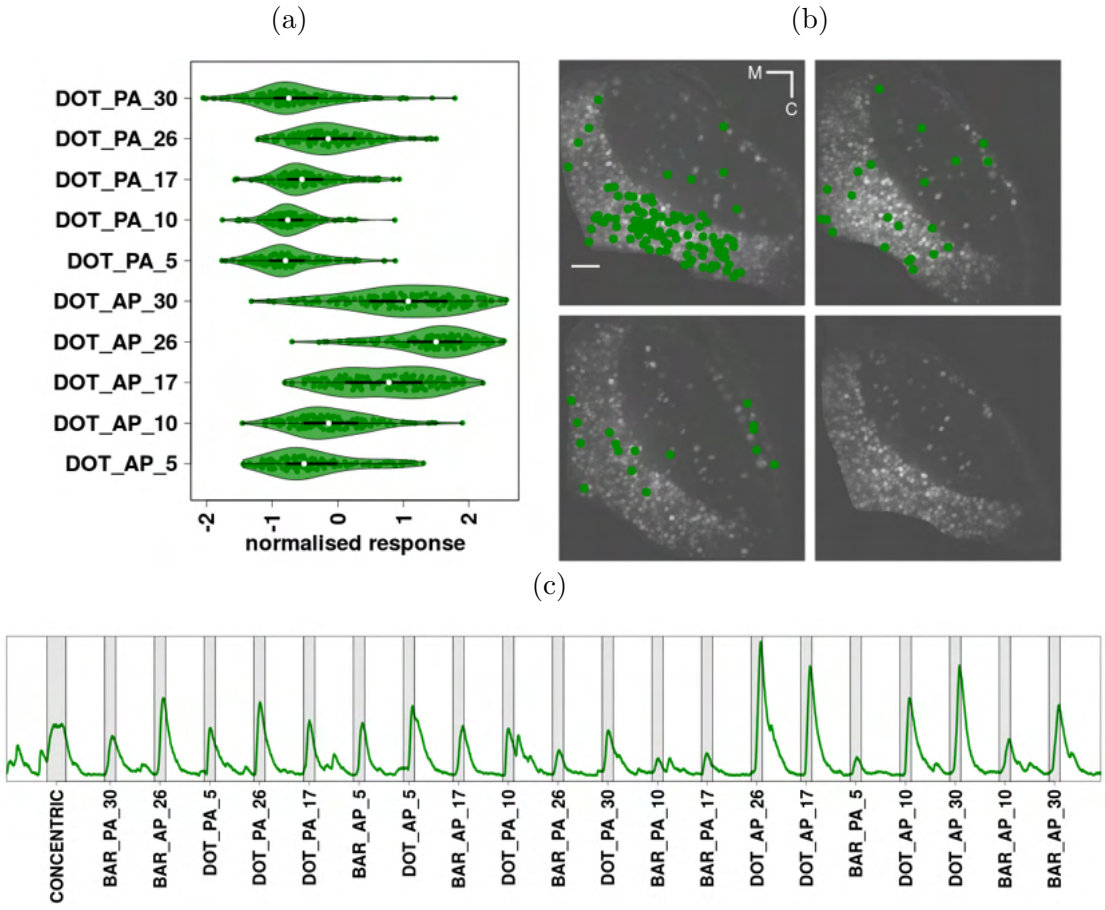

Figure 4.2.5: *Overview of cluster 1.* (a) normalised response to the stimuli of all the neurons in a cluster, the white dot shows the median response. (b) The location of the neurons in the tectum. (c) Example calcium traces averaged from all neurons in one fish. $n = 4$ fish.

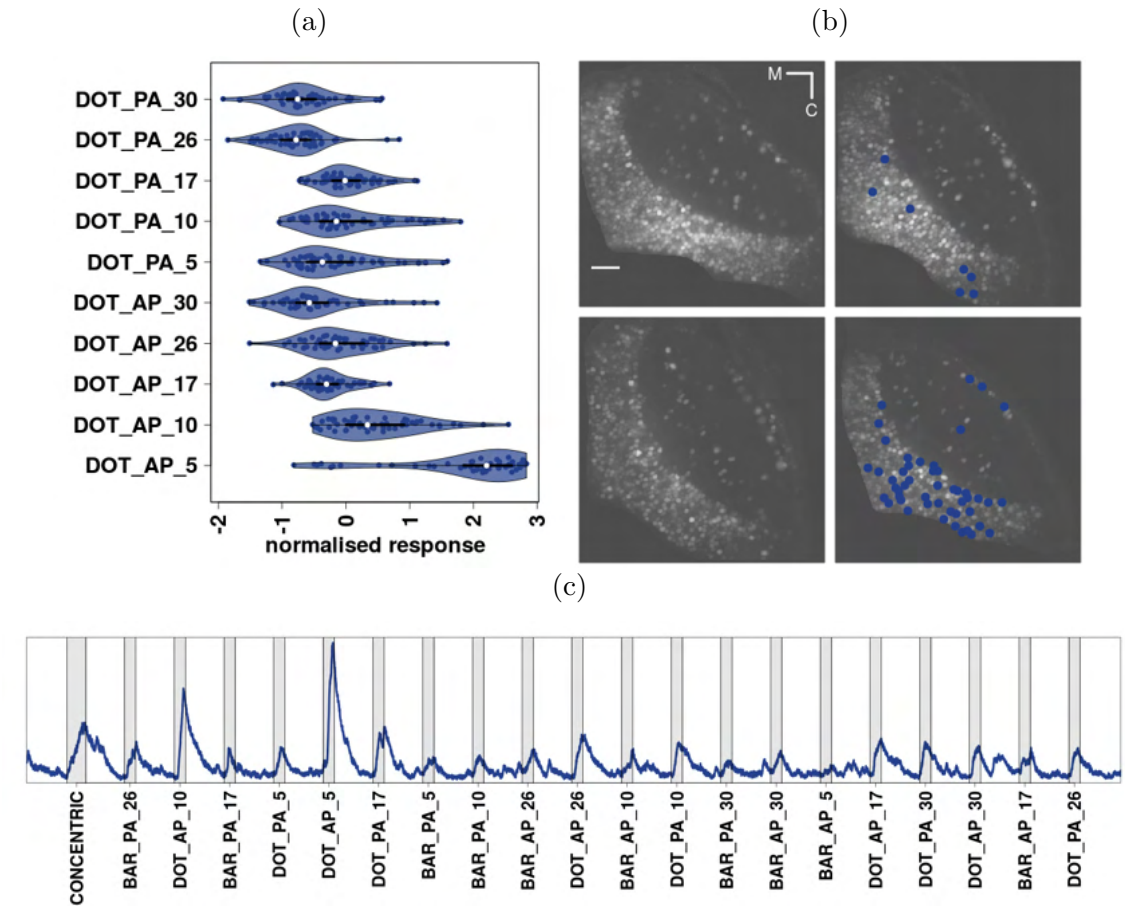

Figure 4.2.6: *Overview of cluster 2.* (a) normalised response to the stimuli of all the neurons in a cluster, the white dot shows the median response. (b) The location of the neurons in the tectum. (c) Example calcium traces averaged from all neurons in one fish. $n = 4$ fish.

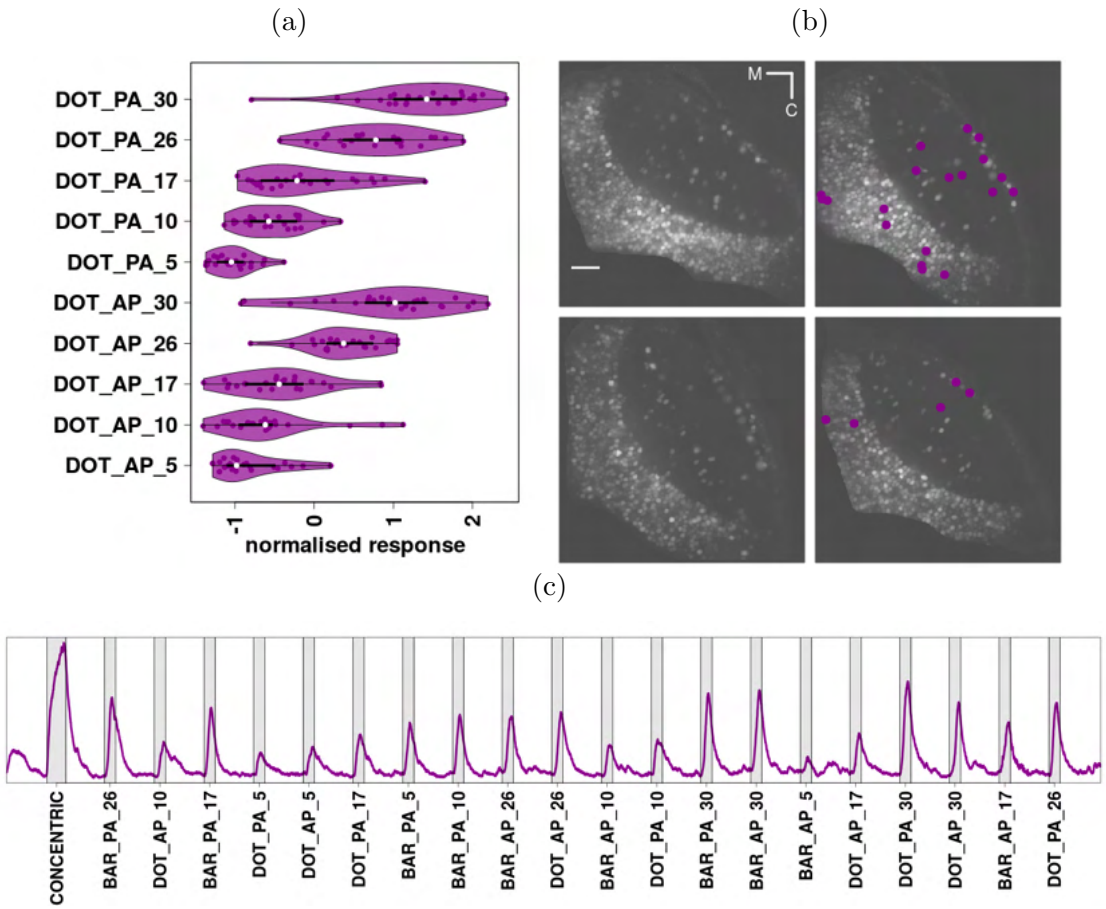

Figure 4.2.7: *Overview of cluster 3.* (a) normalised response to the stimuli of all the neurons in a cluster, the white dot shows the median response. (b) The location of the neurons in the tectum. (c) Example calcium traces averaged from all neurons in one fish. $n = 4$ fish.

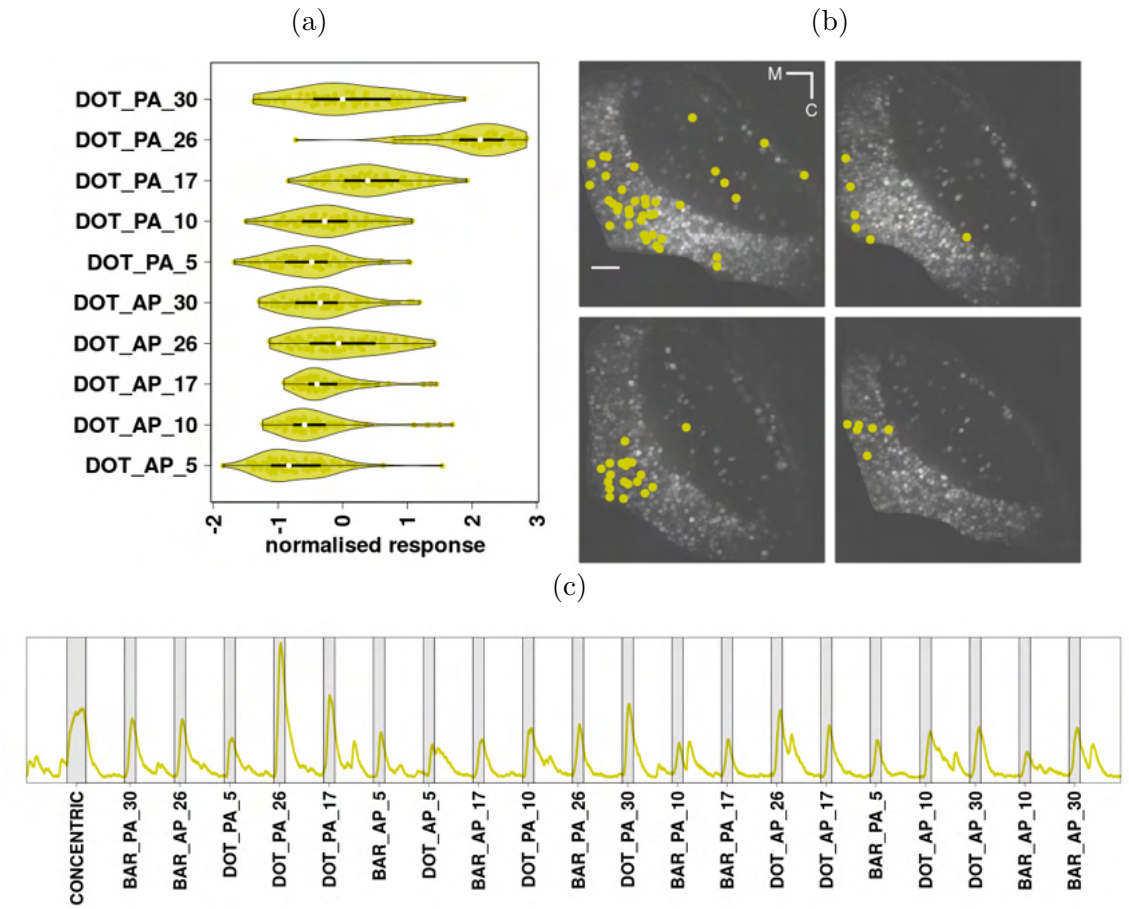

Figure 4.2.8: *Overview of cluster 4.* (a) normalised response to the stimuli of all the neurons in a cluster, the white dot shows the median response. (b) The location of the neurons in the tectum. (c) Example calcium traces averaged from all neurons in one fish. $n = 4$ fish.

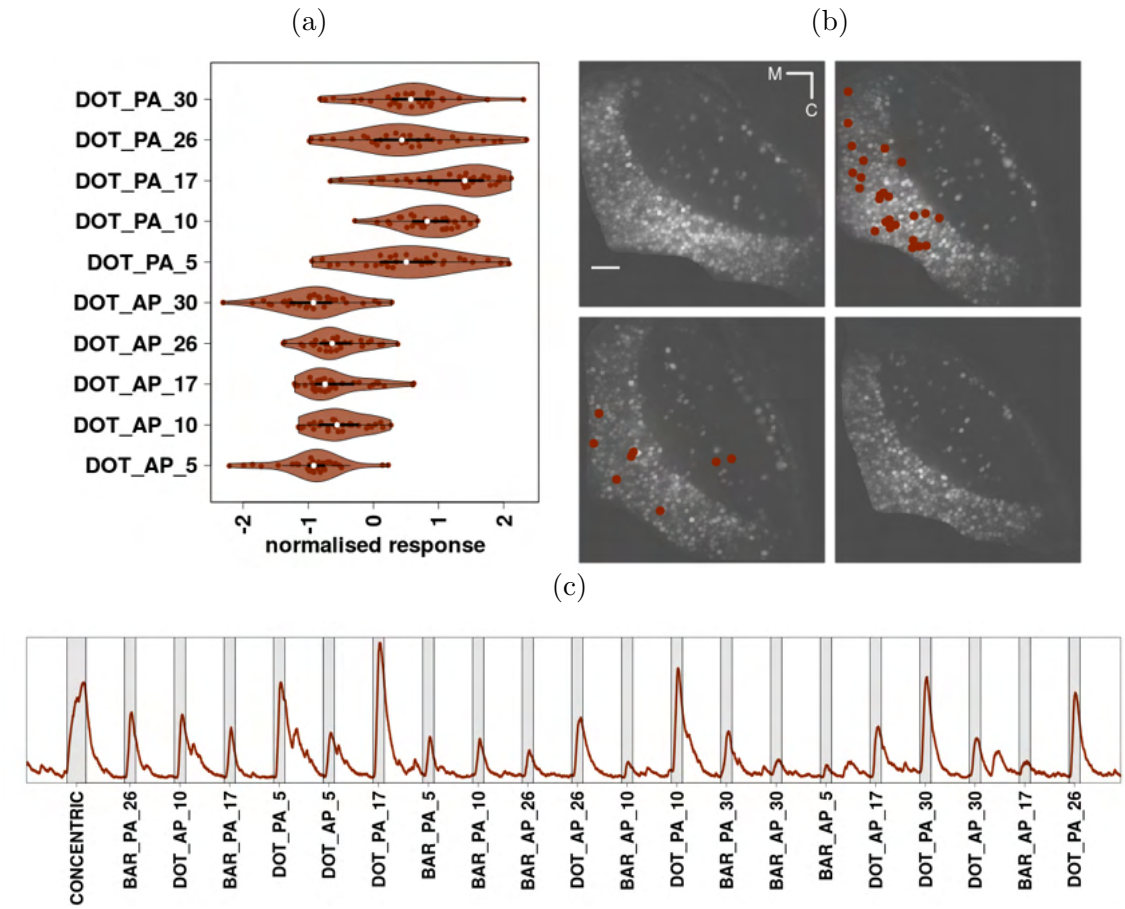

Figure 4.2.9: *Overview of cluster 5.* (a) normalised response to the stimuli of all the neurons in a cluster, the white dot shows the median response. (b) The location of the neurons in the tectum. (c) Example calcium traces averaged from all neurons in one fish. $n = 4$ fish.

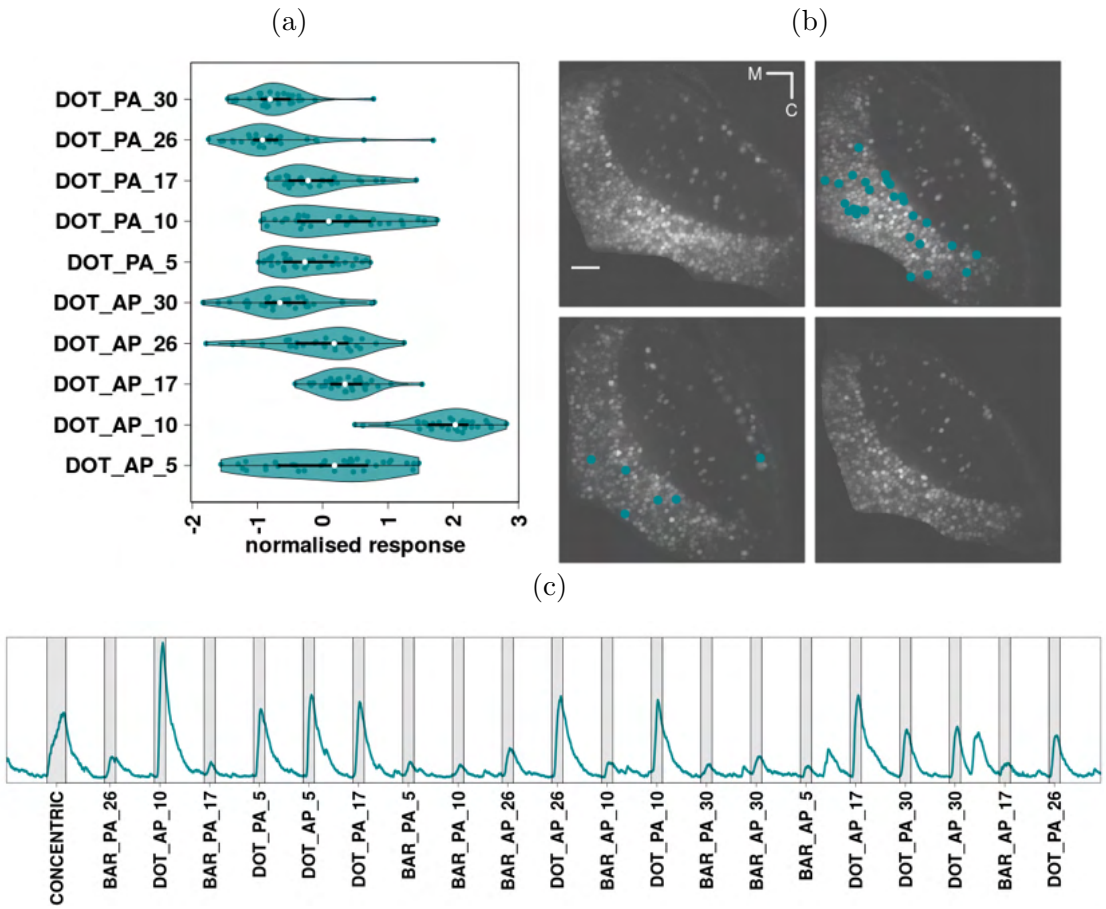

Figure 4.2.10: *Overview of cluster 6.* (a) normalised response to the stimuli of all the neurons in a cluster, the white dot shows the median response. (b) The location of the neurons in the tectum. (c) Example calcium traces averaged from all neurons in one fish. $n = 4$ fish.

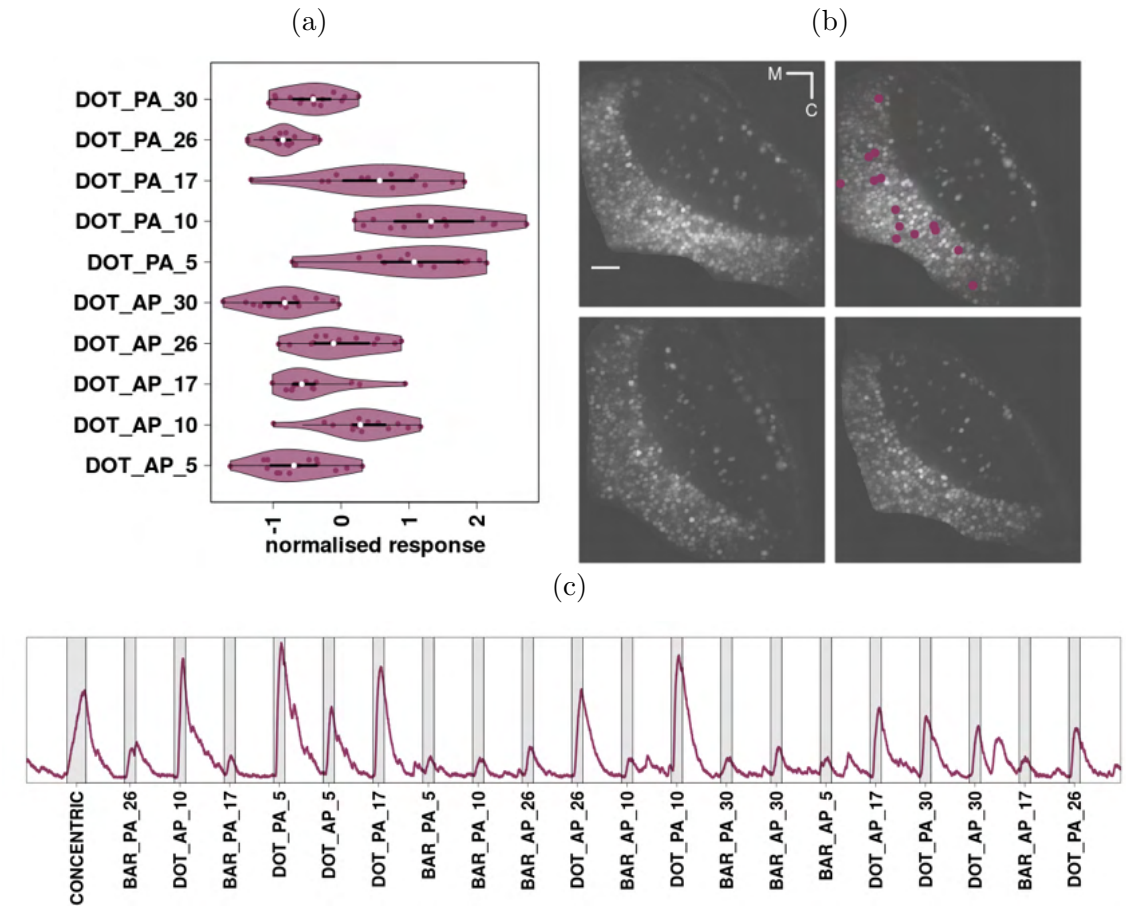

Figure 4.2.11: *Overview of cluster 8.* (a) normalised response to the stimuli of all the neurons in a cluster, the white dot shows the median response. (b) The location of the neurons in the tectum. (c) Example calcium traces averaged from all neurons in one fish. $n = 4$ fish.

4.2.3 Validation of clusters

Unsupervised clustering on real data often lacks any ground truth comparison to analyse how 'good' the outcome is. However, a number of metrics can be used to validate the clusters. First, the within cluster correlation was calculated and found to be higher than would be expected by chance (Fig. 4.2.12a - 4.2.12c). However, since the aim of the algorithm was to allow the clustering of arbitrary distributions, the structure of the high dimensional data was also inspected by projecting it into a 2-dimensional space using metric multidimensional scaling (MDS). The proximity of the neurons in this space reflects their functional similarity. The neurons were then colour coded according to their cluster membership (Fig. 4.2.12d). Neurons within the same cluster tend to congregate together in the 2d projection, indicating functionally similar neurons are being grouped together. There is a degree of overlap between certain clusters, for example clusters 2 (blue) and 6 (teal) tend to overlap (top left of Fig. 4.2.12d). However, when looking at the response profiles of these clusters, it can be seen that they are similar, with both of them showing a preference for small sized dots moving in an AP direction. Furthermore, the clusters which are furthest away from each other tend to have the least similar response profiles, for example cluster 1 (green) and 5 (brown) show preference for objects moving in an AP and PA direction, respectively.

A further validation is to check the stability of the clusters against the removal of data. If there is sufficient data and the clusters are well defined, removing a certain percentage of the data should not cause a dramatic shift in the cluster landscape. A 5-fold cross validation was therefore conducted, whereby the data was randomly allocated to 1 of 5 groups. The data was then re-clustered 5 times, each time excluding one of the groups. Each time the data was re-clustered the similarity between the original cluster and the corresponding newly formed cluster was calculated (materials and methods, Fig. 4.2.13 - top panel):

$$\text{Jaccard Similarity Index} = \frac{|A_C \cap B_C|}{|A_C \cup B_C|} \tag{4.2}$$

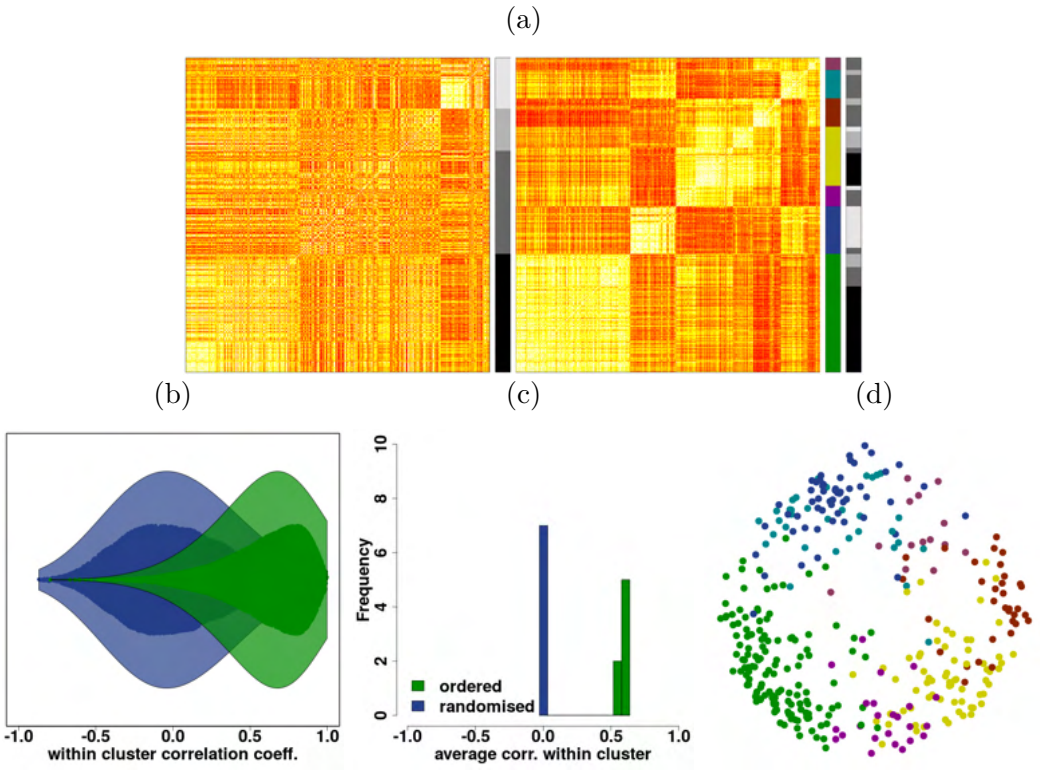

Figure 4.2.12: *Cluster validation.* (a) Left, correlation matrix of all neurons across 4 fish, grey bars demarcate fish identity. Right, correlation matrix ordered according to cluster, coloured bars demarcate cluster membership. (b) Distribution of correlation coefficient for all cells within a cluster (green), compared to the distribution when the data has been randomised (blue). (c) The average within cluster correlation, compared to randomised data. (d) 2-dimensional plot of cell responses using classic multidimensional scaling, each cell is colour coded according to cluster membership.

where A_C represents the set of IDs contained in cluster C for the original clustering and B_C represents the set of IDs contained in cluster C for the cross validation clustering. An similarity of 1 would indicate the cluster has not changed at all, whilst an similarity of 0 indicates there is no similarity between the clusters. After the 5 rounds of cross validation clustering an average similarity for each cluster is then calculated (Fig. 4.2.3). The 7 clusters had an average similarity of 0.71 $\pm$ 0.11 sd, indicating the clusters are relatively stable to the removal of data. The average similarity of the clusters which were removed as outliers was 0.44 $\pm$ 0.10 sd, indicating these clusters are less stable and that is was appropriate to remove them.

This analysis was explored further by removing between 1% and up to 50% of the data. In this case, a certain percentage of the data was randomly removed,

after which the data was re-clustered. This process was repeated 100 times for every percentage of the data removed, and the average similarity for each cluster was calculated at each percentage (Fig. 4.2.13 - bottom panel). As expected, the similarity decreases as the amount of data removed increases. However, the rate at which the similarity decreases differs between the clusters. The clusters removed as outliers show a more rapid decrease in similarity compared to most of the other clusters, except for cluster 8. Furthermore, after the removal of 30% of the data the clusters segregate into 2 groups. The group which is least stable includes the clusters removed as outliers, as well as clusters 3 and 8. The other group includes the remaining clusters and is generally more resistant to the removal of data. The average similarity for the clusters in the stable group after removing 50% of the data is 0.50 $\pm$ 0.07 sd vs 0.18 $\pm$ 0.05 sd for the unstable group, indicating a number of the clusters are consistently present even with much less data.

4.2.4 Similar clusters can be obtained even when removing multiple stimuli

Since, as mentioned in the introduction, it is better to cluster with fewer dimensions, a similar method of cross validation was used to see how removing stimuli affects the clustering. It may be possible to remove some of the sizes whilst retaining the clusters and their core features. To this end, the stimuli were split into small (5°, 10°) and large (26°, 30°) sizes. The data were then re-clustered using one small and one large size stimulus for both directions; this process was repeated using every combination of small and large size. In every case the mid-range size (17°) was removed. The similarity between the original (using 10 stimuli) and new clusters (using 4 stimuli) was then calculated as in Eq. 4.2. There was a range of similarities within the clusters, depending on the combination of sizes used (Fig. 4.2.14). The only cluster which consistently showed a high degree of similarity, irrespective of which combination of sizes were used, was cluster 1 (Fig. 4.2.14). Taking the combination of sizes which gave the highest overall similarity across clusters (5°and 26°) and looking at their response profiles, it seems they do capture the overarching features of each cluster, when compared to clustering with all 10

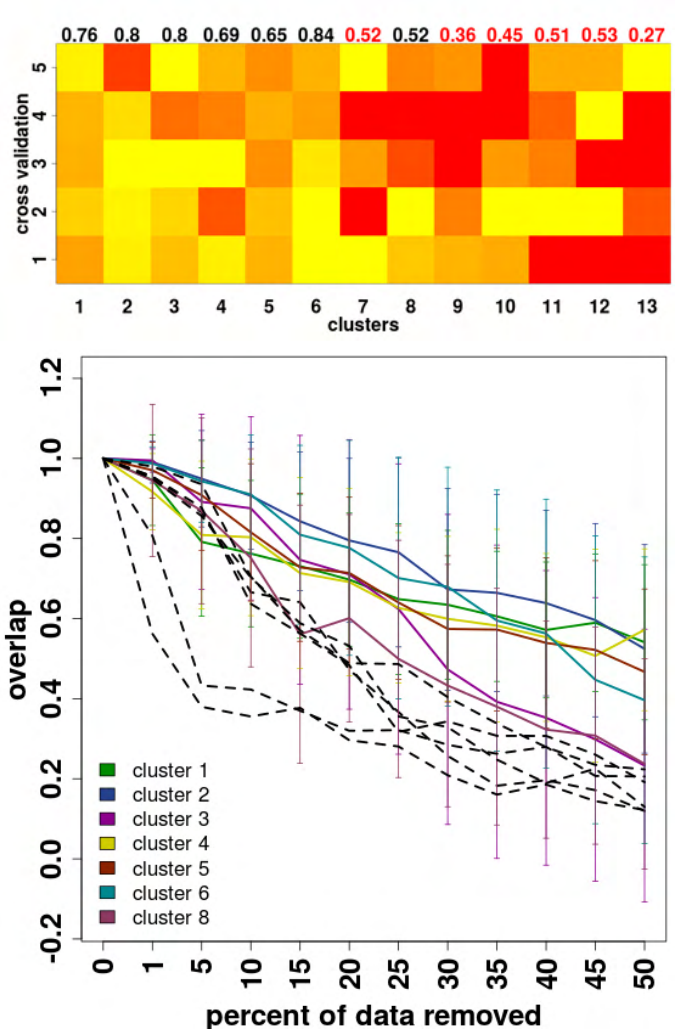

Figure 4.2.13: *Cross validation of clusters.* Top panel: cross validation of clusters. Each column represents one of the 13 clusters (7 clusters, plus 6 which were removed as outliers), each row is one round of cross validation clustering. The heatmap represents the amount of similarity between the original cluster and corresponding cross validation cluster, more yellow indicates a higher degree of similarity. Numbers along top show the average similarity across all of the cross validation steps for each cluster. Numbers in red show clusters which were removed as outliers. Bottom panel: The similarity in each cluster as increasing amounts of data are removed, for each cluster. The black dotted lines show clusters which were removed as outliers.

stimuli (Fig. 4.2.15). This even seems true for clusters which have a low degree of similarity, such as cluster 3. There were also 2 additional clusters, not represented in the original clustering (Fig. 4.2.16 - cluster 8 and 9). Furthermore, 6 out of 9 clusters are now present in all 4 fish (Table 4.2), compared to only 1 fish when using 10 stimuli (Table 4.1). When validating these clusters as above there is a higher degree of within cluster correlation, compared to when clustering on all sizes (Fig. 4.2.17a). Again, there is also a clear localisation of the clusters when projecting

the responses into a 2-dimensional space (Fig. 4.2.17b). Altogether, these results demonstrate it may be possible to reduce the number of sizes used to cluster with, and thereby reduce the dimensionality of the data, without affecting the overarching output from the clustering.

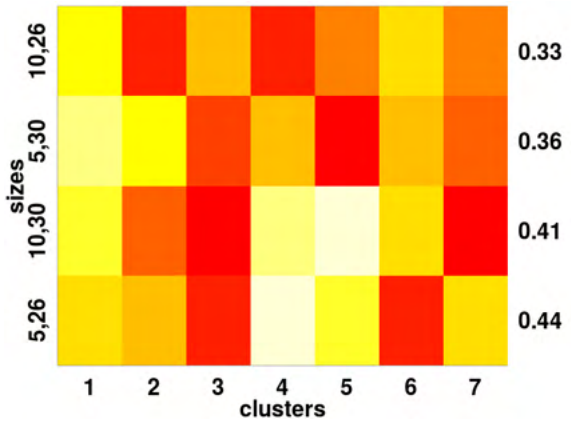

Figure 4.2.14: *Cross validation of stimuli.* The figure shows the similarity of the clusters between using the original 10 stimuli (5 sizes, 2 directions), and a reduced set of 4 stimuli (2 sizes and 2 directions). Each column represents a cluster, and each row shows the sizes that were used for re-clustering (both directions of each size were used). More yellow indicates a higher degree of similarity with the original 10 stimuli. The numbers on the right show the average similarity across all the clusters when using a given pair of sizes.

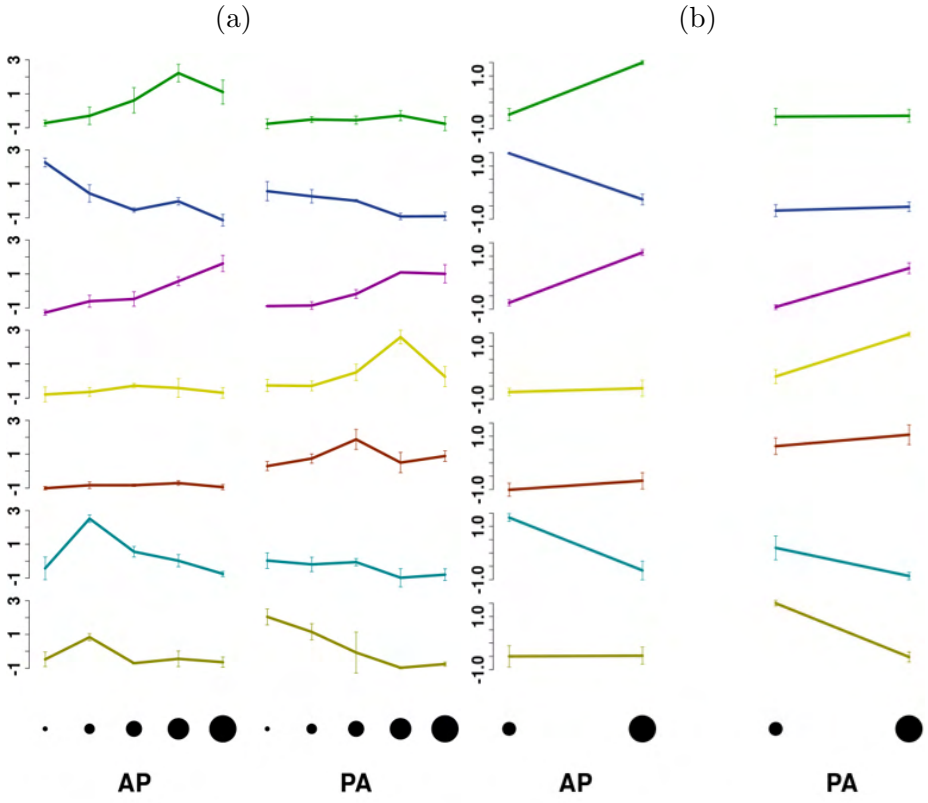

Figure 4.2.15: *The essential features of the clusters can be retained whilst reducing the number of stimuli.* (a) Normalised average response of clusters, colour coded according to cluster membership, across all 10 stimuli. (b) Normalised average response of clusters, when clustered using only sizes 5°and 26°. Error bars show standard deviation $n = 4$ fish.

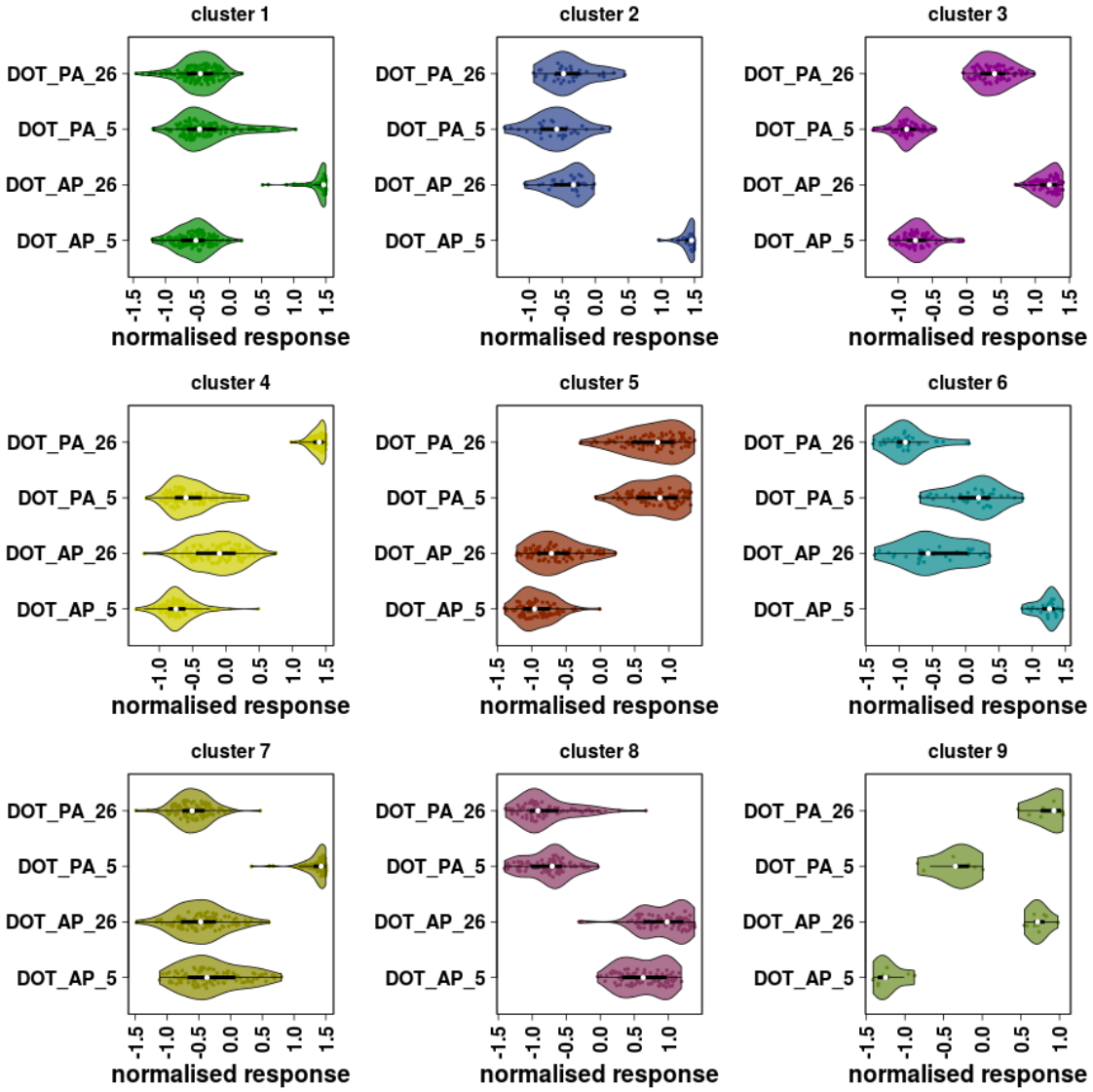

Figure 4.2.16: *Normalised response of the clusters when using a reduced stimulus set.* The white dot shows the median response. The final two clusters on the bottom row are not associated with any of clusters generated when using all 10 sizes. $n = 4$ fish

cluster	cells/fish	fish	description
1	33 ± 14	4 of 4	AP motion and large size selective
2	16 ± 12	2 of 4	AP motion and small size selective
3	17 ± 9	4 of 4	Large size selective
4	27 ± 18	4 of 4	PA motion and large size selective
5	20 ± 15	4 of 4	PA motion selective
6	11 ± 5	3 of 4	AP motion and small size selective
7	24 ± 8	4 of 4	PA motion and small size selective
8	22 ± 13	4 of 4	AP motion selective
9	9	1 of 4	Large size selective

Table 4.2: *Cluster summary for reduced number of stimuli.* Summary of the mean number of cells per fish (± sd) for each cluster, how many fish each cluster is found in and a short description of the cluster.

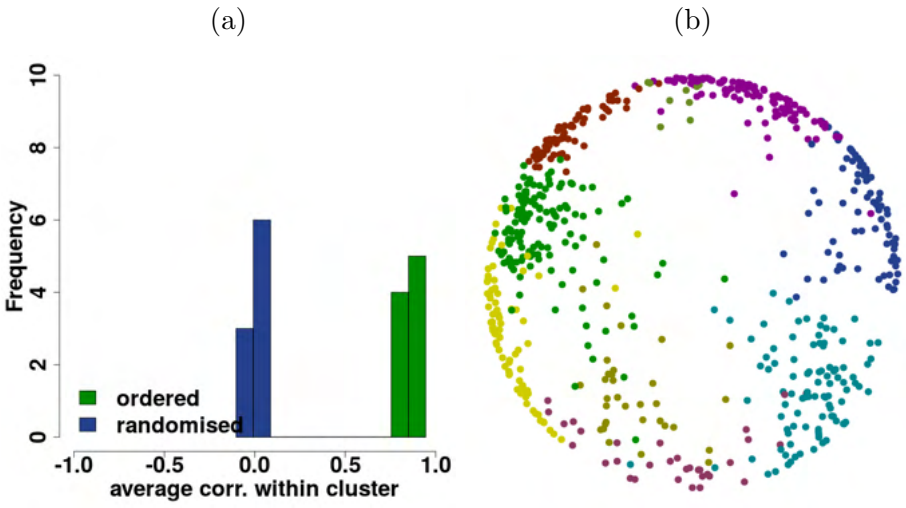

Figure 4.2.17: *Cluster validation when clustering with a reduced stimulus set.* (a) The average within cluster correlation, compared to randomised data when clustering using sizes 5°and 26°. (b) 2-dimensional plot of cell responses using classic multidimensional scaling, each cell is colour coded according to cluster membership.

4.2.5 Summary

1. Most neurons in the tectum prefer dots to bars when matched for direction, size, contrast and speed.

2. There are neurons in the tectum which show selectivity for the combination of both size and direction.

3. Cross validation demonstrates many of the clusters are stable and resistant to the removal of data.

4. Similar clusters can be obtained from the data even when reducing the number of stimuli used for clustering.

4.3 Discussion

4.3.1 Neurons are selective for the shape of a stimulus

A question in visual neuroscience is how complex visual features are represented in the brain. Of particular interest is whether their exists in the brain specialised neurons which respond specifically to prey like stimuli, or whether their detection is via the combined action of multiple neuronal subtypes, with each subtype encoding a particular feature of the stimulus such as its size, direction of motion, or contrast etc. This chapter demonstrated that many neurons in the tectum respond preferentially to dot stimuli, compared to a bar when matched for size, speed, direction and contrast. This indicates that shape is important for inducing strong neuronal responses. Furthermore, since a number of the clusters are size and direction selective there are neurons which require a conjunction of these visual features.

The preference for dots may not be surprising since this kind of stimulus has been shown to be able to elicit hunting behaviour (Bianco and Engert 2014). These kind of spot detectors are reminiscent of the 'bug detectors' outlined in Lettvin's seminal paper: What the Frog's Eye Tells the Frog's Brain (Lettvin et al. 1968) and also type S tectal neurons found in the zebrafish (Sajovic and Levinthal 1982a). These

neurons show a sustained response to spots in their receptive fields, which diminished when the size of the dot expands to match the size of the neuron's receptive field (Sajovic and Levinthal 1982b). Since the bars transerve the entire length of the elevational axis of the visual field, it is possible that this preference for dots comes from surround inhibition in the underlying neural circuitry. It is interesting to note there seems to be a different distribution in the dot selectivity of the SINs, with a more equal distribution across the range of selectivity. The SINs are thought to play a role in discrimination of object size, and be able to switch the state of the zebrafish to either hunting or escape 'mode' depending on the size of the stimulus (Del Bene et al. 2010, Preuss et al. 2014). However, the fact that SINs display selectivity to an array of features, such as shape and direction, as well as size, indicates they may play a role beyond simply size filtering of retinal inputs.

4.3.2 Neurons are selective for a conjunction of visual features

Two visual features which are necessary for the larvae to be able to detect are the size and direction of an object. Previous studies in zebrafish have analysed these two features separately, finding neurons in the tectum which are able to encode for a range of sizes (Del Bene et al. 2010, Preuss et al. 2014) and directions (Gabriel et al. 2012, Grama and Engert 2012, Hunter et al. 2013). Using the clustering algorithm these two features are able to be analysed together. The clusters which emerge when classifying responses based on size and direction to the dot stimuli indicate a mixed selectivity. For example, there are a number of clusters which are selective for a specific combination of size and direction of the stimulus, whilst others show selectivity for only one of the two features, either size or direction. This is in line with previous research which shows there are neurons selective for a conjunction of size, contrast and direction (Bianco and Engert 2014). Where, or how, this selectivity is generated is not known. It has been shown that direction (Nikolaou et al. 2012) and size selectivity (Preuss et al. 2014) arise already in the retina, and that the tectum may simply inherit their selectivity from these inputs. However, it is thought that direction selectivity can also arise *de novo*, within the tectum itself (Abbas et al.

2017, Hunter et al. 2013). The circuit mechanisms which give rise to neurons with mixed selectivity to both visual features are not understood, and it is not known whether they are present already at the level of the retina.

4.3.3 Reducing the dimensionality of the data

When clustering with fewer stimuli the essential features of the original clusters were maintained, even if some had relatively little similarity with the cells contained in the original clusters. There was also an additional 2 clusters found, not present when clustering with all 10 stimuli. In general there is an inherent advantage with clustering in a lower dimensional space (meaning, in this case, with fewer stimuli). As more dimensions are added the volume of the response space rapidly increases, meaning the data becomes increasingly sparse rendering an accurate density estimation more difficult. Therefore, it is preferable to cluster with 4 stimuli, rather than 10, if the essential features of the clusters can be maintained.

By reducing the number of size stimuli used it is likely some information is lost; choosing the sizes of 5° and 26° will necessarily favour neurons which have a tuning curve centred on these sizes. The question is whether it is valid to split 'size', as a visual feature, into two discrete levels. For direction selectivity it is known that, in the zebrafish tectum, there are 4 discrete response types (the 4 cardinal directions) (Hunter et al. 2013), which makes it an ideal feature to cluster on. Similarly for contrast selectivity, there are ON, OFF, and ON-OFF response types. Since one of the roles of the tectum appears to be to distinguish between prey (small) and predator (large) stimuli, it may be reasonable to split the size feature into two categories, and indeed the sizes of 5° and 26° do correspond to the sizes which evoke prey capture and predator avoidance in some experiments (Semmelhack et al. 2014, Bianco et al. 2011, Temizer et al. 2015). However, it is not clear whether the distribution of size selectivities within the tectum do fall into two non-continuous populations (Preuss et al. 2014). Furthermore, the sizes used here don't correspond to the sizes used to elicit behaviour in all experimental set ups (Bianco and Engert 2014, Dunn et al. 2016b). In the future it may be beneficial to determine which

sizes would be best to use based on the behavioural response of the zebrafish.

Overall, this chapter has demonstrated the clustering algorithm is able to classify neurons which have mixed selectivity for multiple visual features and a number of ways to validate these clusters.

Chapter 5

Determining reproducibility of tectal cell responses

5.1 Introduction

In the last chapter the clustering algorithm was applied to multidimensional *in vivo* calcium imaging data, from which a number of size- and direction-dependent clusters emerged. There are, however, a number of caveats to the methodology that need to be addressed:

First, since the lightsheet microscope works on the basis of one photon excitation, the necessary wavelength to excite the GCaMP fluorophore is 465 nm, which means that the zebrafish is able to see the laser, which in turn may affect the neuronal response properties during the visual stimulation.

Second, due to technical issues with the lightsheet, there was only the possibility to do single plane imaging, meaning there were fewer neurons to cluster per fish and none of the clusters could be analysed in terms of their dorsoventral (DV) distribution.

Third, in the previous chapter none of the stimuli were repeated during a given experiment. Therefore, it is impossible to know with any given certainty that the

response of a neuron to a stimulus is actually visually driven, or whether it is spontaneous activity that happens to coincide with the presentation of the stimulus. Multiple presentations of the same stimulus would mitigate this and would help with the analysis in two ways. First, if a neuron responds reliably to multiple presentations of the same stimulus, it increases the certainty that the response is stimulus driven. Second, neurons may respond to multiple presentations of the same stimulus in different ways (habituation, sensitization, or no change) and these features themselves can be used to classify the diversity of neuronal types. It would therefore be beneficial to be able to quantify the amount of variability across repetitions of the same stimulus, and to use the knowledge of this variability when clustering. In the following chapter the experimental approach was modified to address these issues:

First, due to the new availability of a 2-photon microscope the experimental setup was moved from the lightsheet. 2-photon microscopy has the advantage that the fish is unable to see the excitation laser due to it being in the infrared range. Furthermore, in contrast to the lightsheet, the spatial resolution is uniform across the field of view.

Second, although the acquisition speed of the 2-photon microscope is slower than the lightsheet microscope, it is possible to collect a volumetric image of 7 planes, which span the entirety of one tectal hemisphere, with a 10 µm interval between each plane, at 7.28 Hz per volume. This speed is sufficiently fast given that responses are compared across epochs of approximately 10 seconds. Since it is possible to do volumetric imaging with the 2-photon microscope, the anatomical location of the clusters can be probed in terms of the DV axis and more neurons are available for clustering per fish.

Third, to be certain that the neurons being clustered are truly responding to the visual stimuli, and to ascertain how similar a neuron's response is to multiple repetitions of a given stimulus, 10 repetitions of each stimulus were added.

To test this new experimental setup and analysis pipeline a simple barrage of 3 visual stimuli were chosen. The stimuli were chosen to be as different from each other as possible in terms of their features. Therefore, the stimuli were: a black dot

covering 5° of visual angle moving in the 90° direction (dot); a wholefield grating of 26° spatial frequency moving at 1 Hz in the 270° direction (grat); and a rectangular white bar which covers the whole visual field in the vertical dimension and covers 15° of visual angle in the orthogonal dimension, moving in 180° direction (LB/lightbar).

5.2 Results

5.2.1 Classifying neurons based on robustness of response to visual stimuli

Image registration, calcium signal extraction, and neuron segmentation were conducted using suite2p (Pachitariu et al. 2017). Imaging over 7 planes, covering one whole tectal hemisphere, allowed the near simultaneous imaging of 1336 ± 137 neurons per fish. The data presented here come from 2 fish, imaged and analysed using the analysis pipeline described in the previous chapters.

Since 10 repetitions of each stimulus are now included in the barrage it is possible to determine how reliably a neuron responds to multiple presentations of the same stimulus. To calculate this, the response quality index (QI) was calculated (Baden et al. 2016):

$$QI = \frac{Var[\langle C \rangle_r]_t}{\langle Var[C]_t \rangle_r} \tag{5.1}$$

where C is a t x r (time by repetition) response matrix, with $\langle\ \rangle_x$ and $Var[\ ]_x$ denoting the mean and variance across either the time or repetition dimension. The QI determines how similar a neuron's response is over all of the repetitions and will equal 1 if the responses across all repetitions are equal (Baden et al. 2016). The QI was calculated for every neuron over the three stimuli. For each stimulus the neurons were then split into 2 groups based on their $QI_{stimulus}$ score using k-means clustering (Fig. 5.2.1a) and classified as either robust or not. This can be thought of as automatically choosing a threshold for QI, allowing it to be different for each stimulus. Example traces of neurons which were classified as robust after

thresholding based on the $QI_{stimulus}$ value can be seen in Fig. 5.2.2. The ratio of neurons kept after thresholding on each stimulus can be seen in Fig. 5.2.1b. The percentage of neurons which were classified as having a robust response was 7% for the dot stimulus, compared to 22% for the grating and 16% for the lightbar (Fig. 5.2.1b). Taking all of the neurons that were classified as robust to at least one of the stimuli, the majority were robust to only one stimulus, with very few being robust to all three (Figs. 5.2.1c & 5.2.1d). The number of neurons that were robust to two stimuli was greatest between the lightbar and grating stimuli, indicating these are more similar and the dot stimulus is the most distinctive (Fig. 5.2.1c & 5.2.1d).

5.2.2 Robust visually responsive neurons are asymmetrically distributed throughout the tectum

Similar to when using the lightsheet microscope, the NCC (see chapter 3, section 3.2.2) can be calculated for each neuron, which can be used to split the data into noisy and reliable neurons (Fig. 5.2.3). Again, there seems to be a propensity for reliably responsive neurons to be located in the centre of the tectum, compared to the periphery. In terms of the DV axis, there is a higher mean NCC in the more ventral portion of the tectum (Fig. 5.2.4a). Furthermore, of all segmented neurons per imaging plane, a larger proportion are classified as reliable in more ventral planes indicating there is higher distribution of reliable visually responsive neurons in the ventral tectum (Fig. 5.2.4b).

The distribution of QI scores throughout the tectum can be seen in Figs. 5.2.5 to 5.2.7, along with which neurons were classified as robust. To analyse the spatial distribution of these robust neurons 20 points were fitted along the anterior-posterior (AP) axis of the tectum (Fig. 5.2.8a and materials & methods). For each neuron that was classified as robust to a given stimulus the Euclidean distance to all 20 points along the AP axis was calculated. Each neuron was then assigned to its closest point (Figs. 5.2.8b - 5.2.8d). From this the average position along the AP axis of all the robust neurons, for a given stimulus, can be calculated and compared to a null distribution (Fig. 5.2.9 and materials & methods). In both fish, neurons

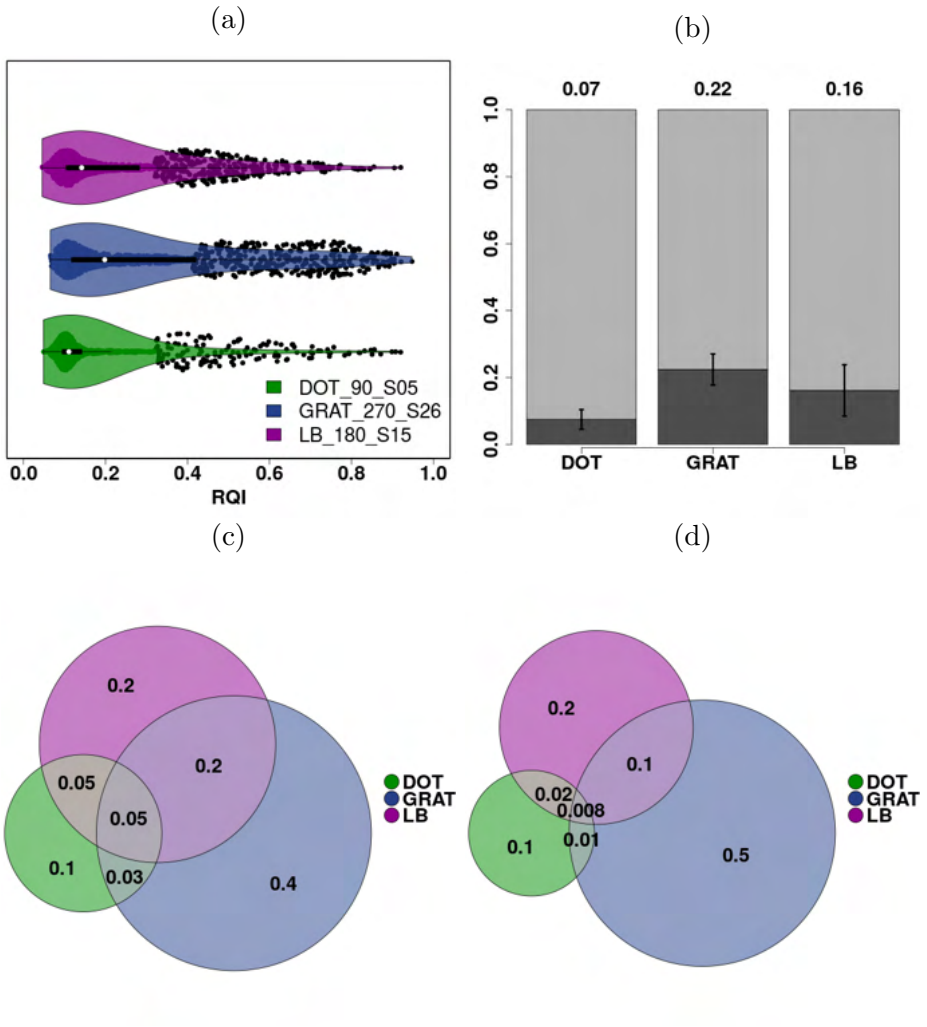

Figure 5.2.1: *The RQI score can be used to threshold neurons.* (a) The distribution of QI scores within one fish for the three stimuli, the white dot represents the median QI score for each stimulus. The large black dots represent neurons that were kept after thresholding on the QI score for that stimulus. (b) The proportion of neurons that were kept after thresholding (dark grey) based on the QI scores, error bars show standard deviation, $n = 2$ fish. (c & d) Venn diagrams showing the proportion of neurons which were classified as robust to either 1, 2 or all 3 stimuli. Each Venn diagram shows one fish.

which responded robustly to the dot and lightbar stimulus had a more posterior bias compared to the null distribution (with less than 0.5% probability that this is due to chance), with the dot stimulus having the most posterior distribution. The neurons which responded robustly to the grating stimulus had a more uniform distribution across the tectum, with a posterior bias in one fish, whilst in the second fish the position fell within the null distribution indicating there is no bias in the spatial distribution of these neurons (Fig. 5.2.8d).

It is also possible to analyse the spatial distribution of these neurons along the DV

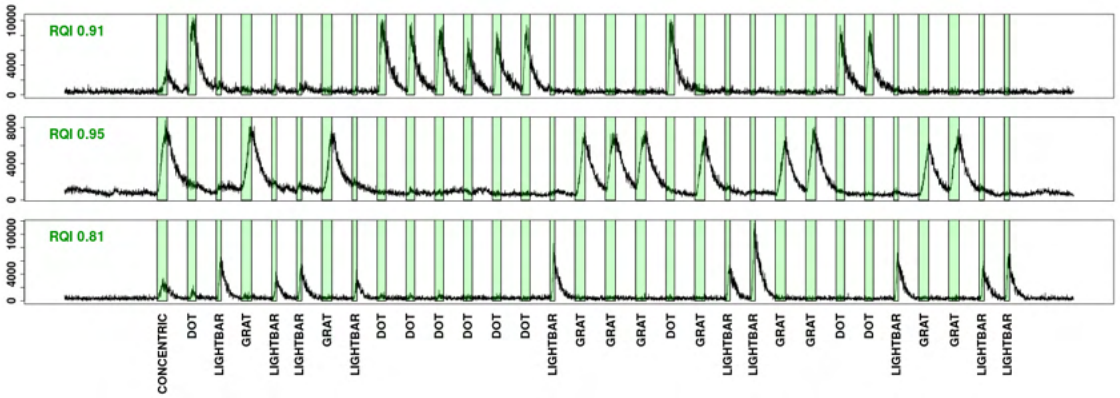

Figure 5.2.2: *Example of calcium traces of neurons kept after thresholding on their QI score.* Top to bottom: dot, grating, lightbar. Green bars indicate when a visual stimulus was being presented.

axis. Of all segmented neurons, a larger proportion of those in the more ventral plane are robust to the dot stimulus, compared to those in the more dorsal planes (Fig. 5.2.10a). This, however, does not seem to be the case with the other two stimuli. In this case, the proportion of neurons which are robust to the lightbar and grating stimuli seems relatively constant across the DV axis (Fig. 5.2.10b & 5.2.10c).

5.2.3 Quantifying the optimal number of stimulus repetitions

In these experiments, 10 repetitions of each stimulus were given. However, it is not clear whether this number of repetitions is necessary to be able to correctly classify neurons using the QI score. Whilst too few repetitions reduces the accuracy to which the robustness of a neuron can be calculated, too many repetitions unnecessarily increases the length of imaging time and size of the data set. To determine the effect of removing repetitions on the ability to classify the robustness of neurons, the QI score was recalculated after removing repetitions. From 1 upto 8 repetitions were removed, with QI_x indicating the QI score calculated using x number of repetitions. This process was repeated 10 times, randomly sampling which of the repetitions were removed each time, and the average QI_x used. The ratio:

(a)

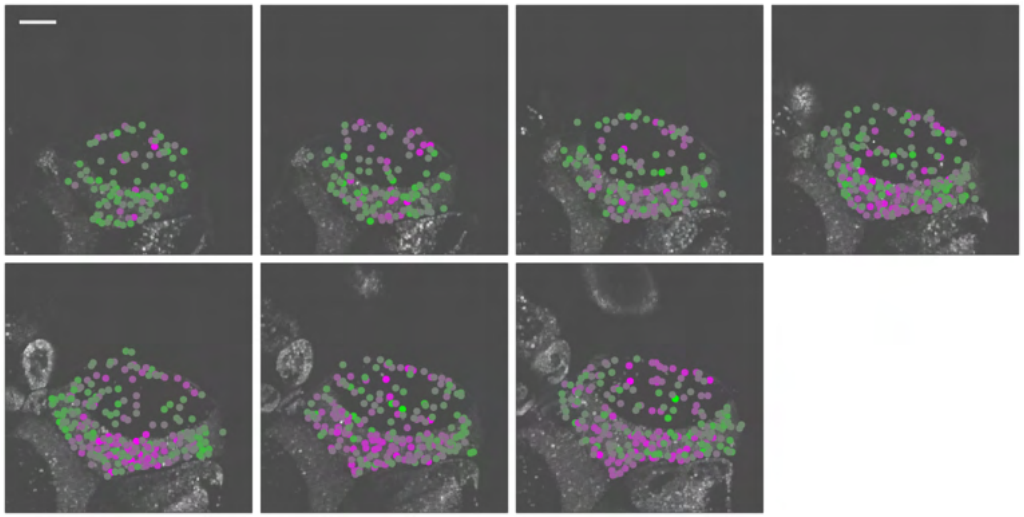

(b)

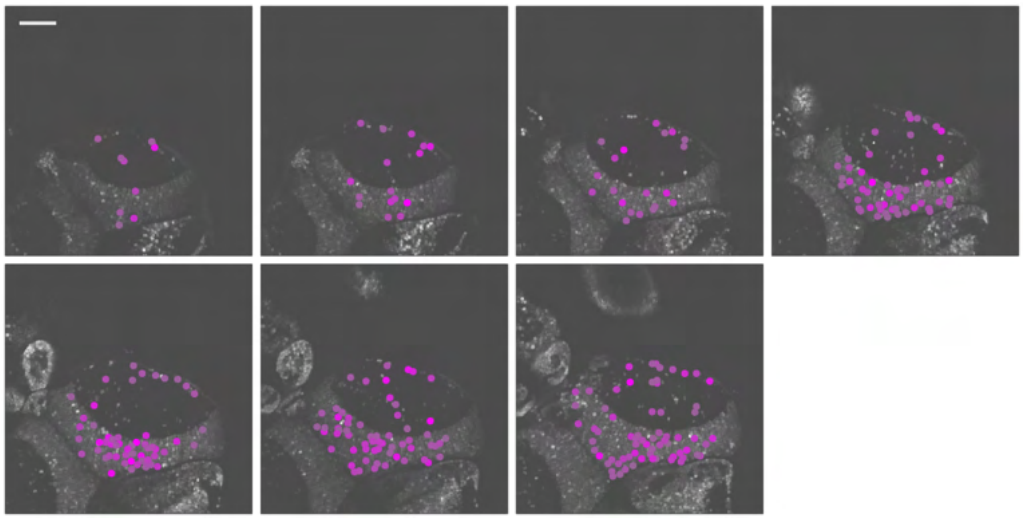

Figure 5.2.3: *Distribution of the NCC across the tectum.* (a) heatmap of the NCC index across the tectum of one fish. Each image is one imaging plane, and more purple indicates a higher NCC value. (b) All the neurons that were kept after thresholding based on the the NCC. Scale bars show 50µm unless otherwise specified.

$$QI_{10}/QI_x \tag{5.2}$$

was calculated for each neuron, with a value of 1 indicating its QI score remains unchanged by removing repetitions (Fig. 5.2.11). As can be seen from the top panel of Fig. 5.2.11, most neurons show a linear decrease in their QI score across all of the three stimuli. However, for each stimulus, there is a population of neurons which have a stable QI even with the removal of several repetitions (Fig. 5.2.11).

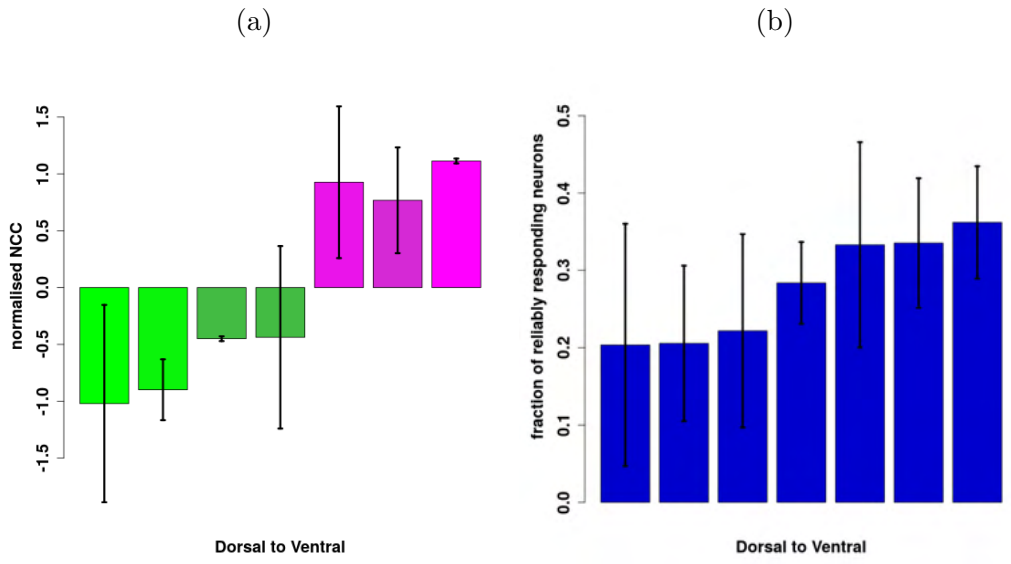

Figure 5.2.4: *More dorsal regions of the tectum have a higher average NCC value.* (a) mean normalised NCC response of all neurons across the dorso-vental axis, colour coded according to mean NCC (b) percentage of neurons within an imaging plane classified as reliable based on their NCC. $n = 2$ fish

When colour coding the neurons according to whether they were classified as robust based on their initial QI_{10} value it can be seen that neurons which are robust to the stimuli with 10 repetitions, tend to maintain a stable QI value even when several repetitions are removed (Fig. 5.2.11). To quantify this, the variance of the QI_{10}/QI_x ratio across all the robust neurons was calculated (Fig. 5.2.12a). As expected the variance increases as the number of repetitions removed increases, however, it remains relatively low for up to 4 repetitions, with a more rapid increase thereafter (Fig. 5.2.12a).

A further way of looking at the number of repetitions necessary is to reclassify the neurons as to whether or not they are robust, based on their QI_x score, and then compare this to their classification using the QI_{10} score. The percentage of cells which were classified the same, for a given stimulus, as when using QI_{10} is shown in Fig. 5.2.12b. Despite changes in the QI value when repetitions are removed, the percentage of neurons which are classified the same as when using QI_{10} does not drop below 95%, indicating only a few repetitions are necessary to 'correctly' classify a neuron. The small percentage of neurons that were not classified correctly can be split into two groups: either false positives or false negatives. That is to say they were either wrongly classified as robust or wrongly classified as not robust,

(a)

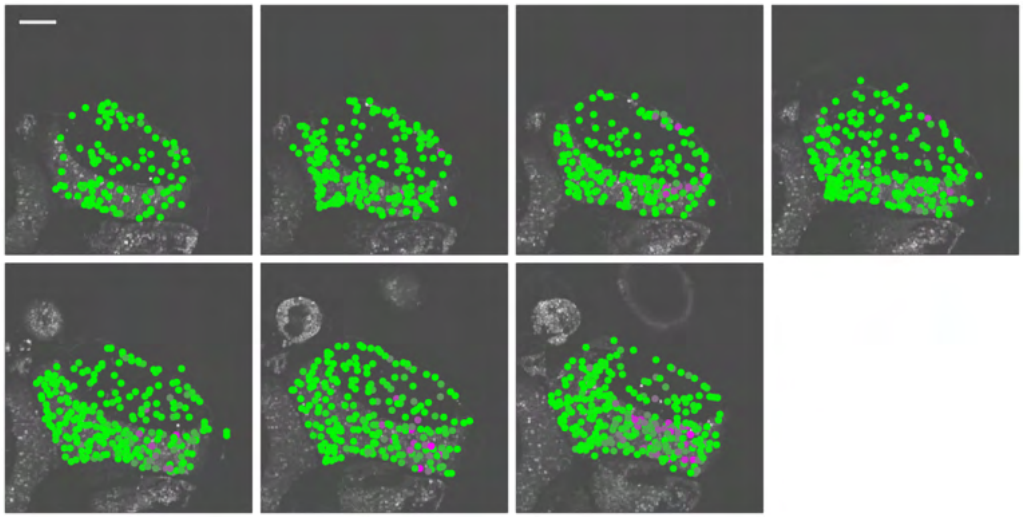

(b)

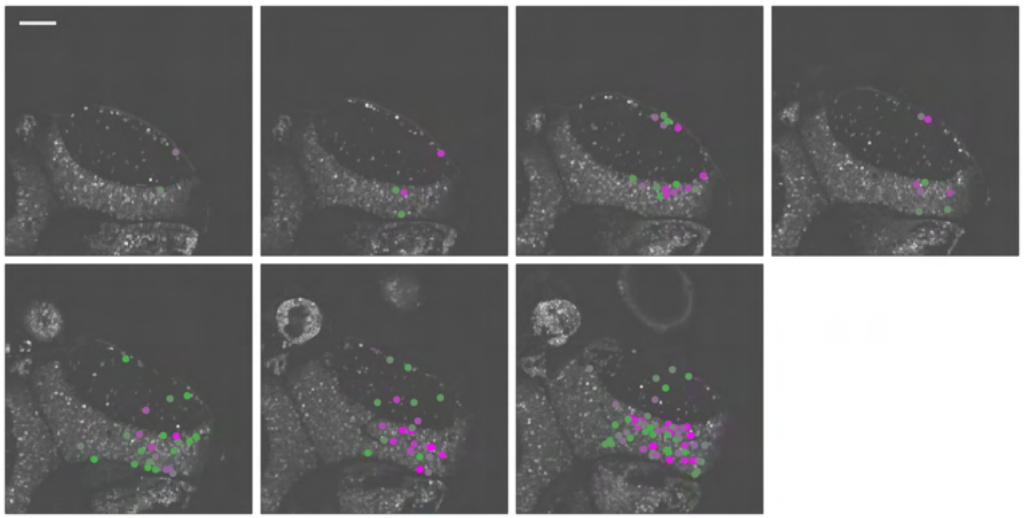

Figure 5.2.5: *Distribution of the QI_{dot} score across the tectum.* (a) Heatmap of the distribution of QI_{dot} score for one example fish, more purple indicates a higher QI_{dot} score. (b) All the neurons that were kept after thresholding based on the the QI_{dot}.

respectively. For all misclassfied neurons, the percentage of false negatives compared to false positives was calculated. There seems to be no bias towards either type over the different stimuli and number of repetitions removed (Fig. 5.2.12c).

5.2.4 Clustering visually responsive neurons

Prior to clustering it is necessary to remove any neuron which is not considered to be responding to the visual stimuli. With the inclusion of repetitions there is a choice

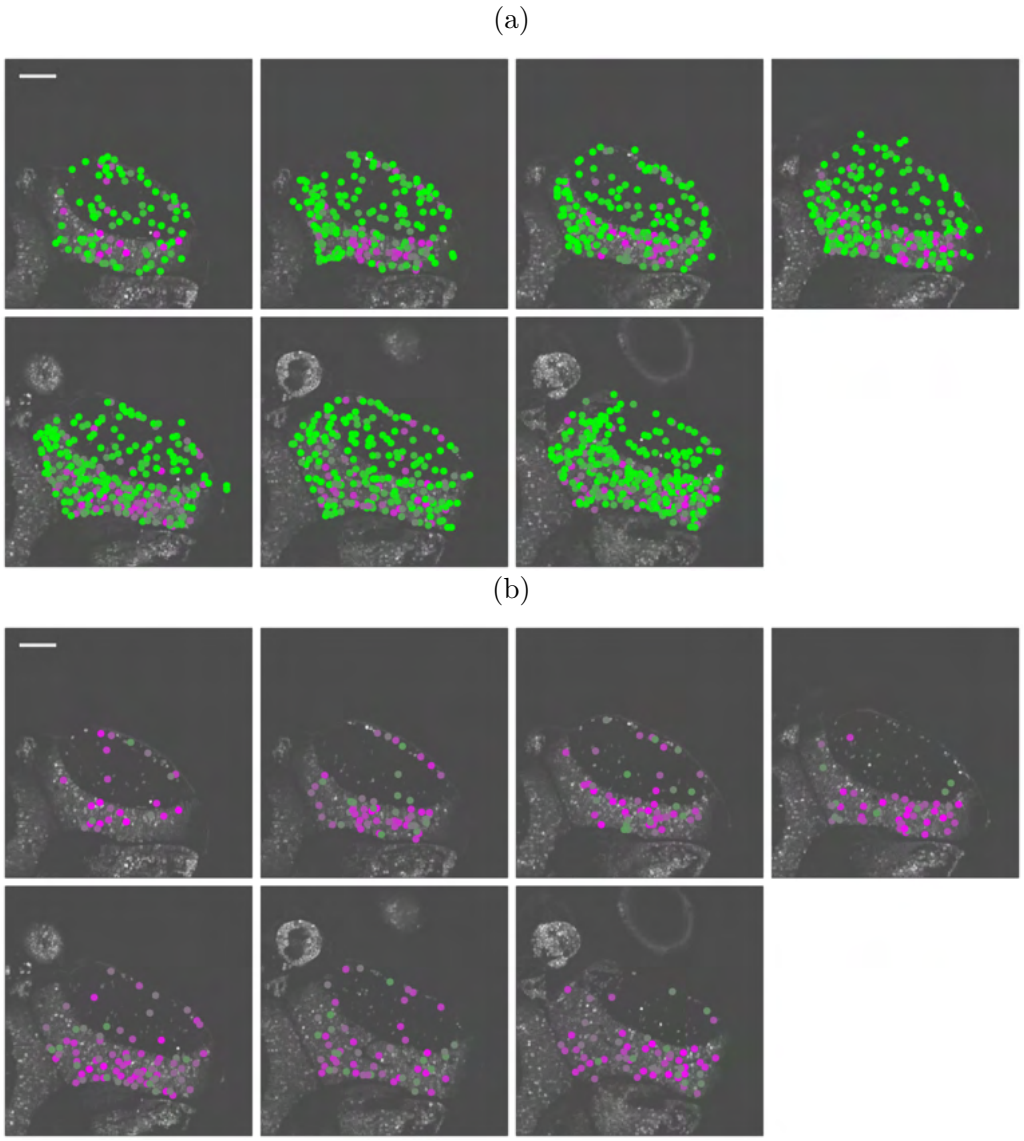

Figure 5.2.6: *Distribution of the $QI_{grating}$ score across the tectum.* (a) Heatmap of the distribtution of $QI_{grating}$ scores across the tectum for one example fish, more purple indicates a higher $QI_{grating}$ score. (b) All the neurons that were kept after thresholding based on the the $QI_{grating}$.

of thresholds, either the NCC, QI, or some combination of both. When looking at the neurons which are either excluded or kept using the NCC and QI it becomes apparent that in 83.3% $\pm$ 1.8% of cases the two thresholds are in agreement (Fig. 5.2.13) (when using the QI as a threshold, a neuron would be kept if it was classified as robust to at least one stimulus). When looking at those neurons in which the thresholds are not in agreement, they tend to have a number of features which make the accurate estimation of either the NCC or QI difficult, such as low signal-to-noise ratio, high spontaneous activity such that the neuron very rarely returns to

(a)

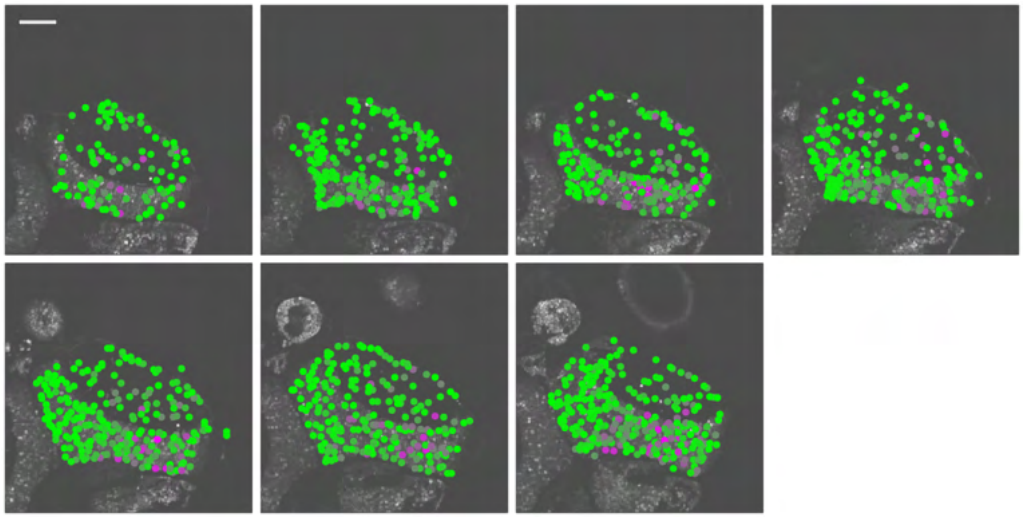

(b)

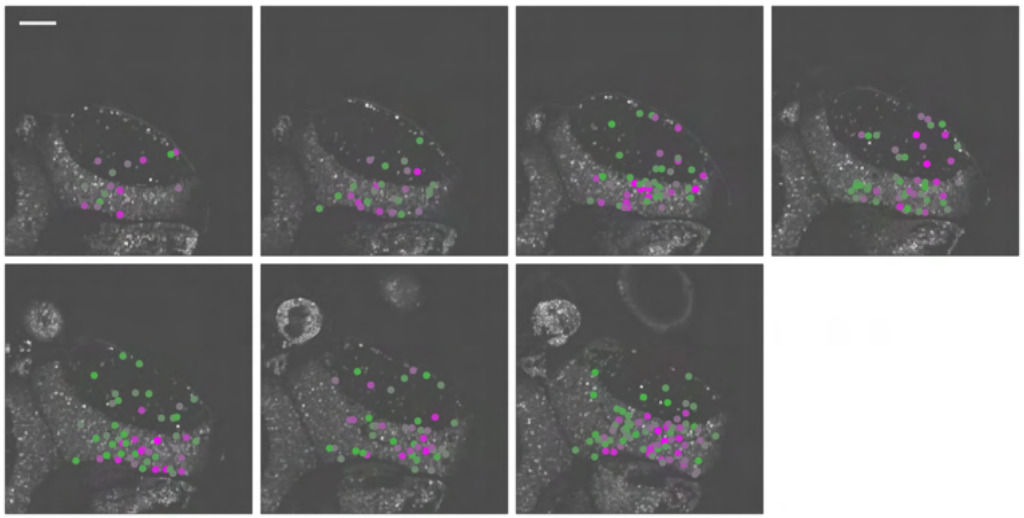

Figure 5.2.7: *Distribution of the $QI_{lightbar}$ score across the tectum.* (a) Heatmap of the distribtution of $QI_{lightbar}$ scores across the tectum for one example fish, more purple indicates a higher $QI_{lightbar}$ score. (b) All the neurons that were kept after thresholding based on the the $QI_{lightbar}$.

its baseline value, or prolonged visually evoked activity which extends after a visual stimulus has ended. The NCC value was chosen to threshold neurons for clustering as it removes the most number of neurons using only one threshold. However, the choice is somewhat arbitrary, and a comparison of the two thresholds should also be applied when using different stimuli and/or number of repetitions, as this may affect the outcome.

Neurons were clustered based on their responses to the stimuli as laid out in chapter 3. However, since only two fish were imaged it was not possible to do the two step

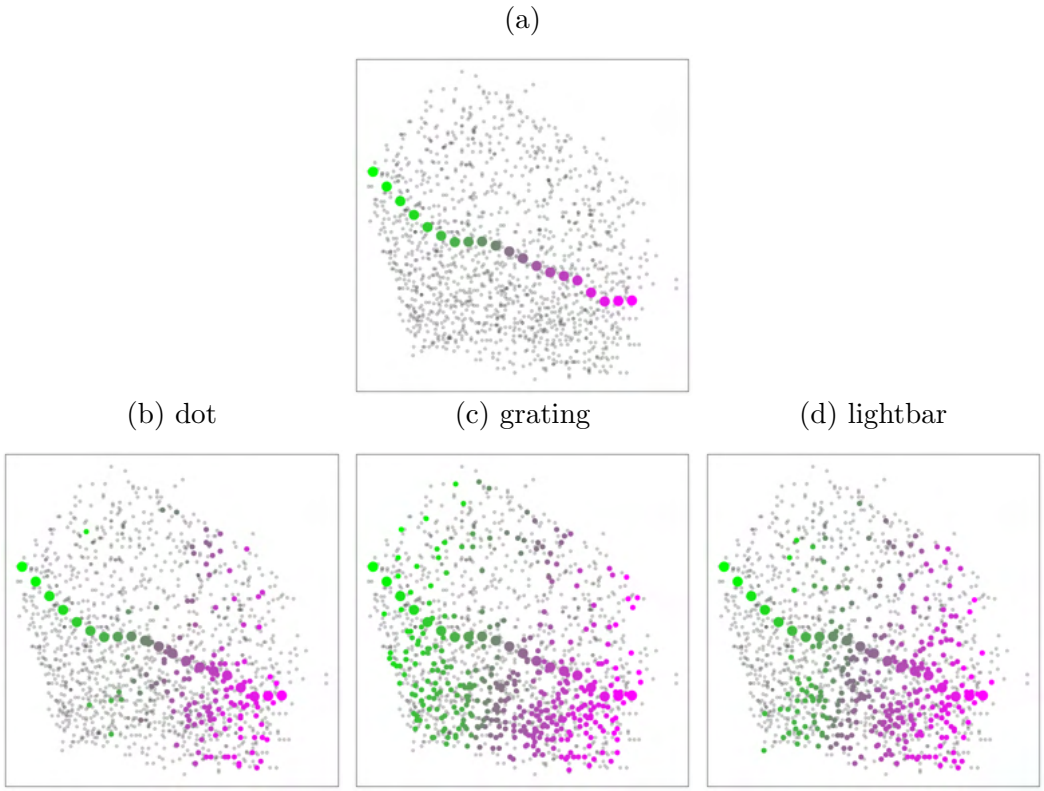

Figure 5.2.8: *Calculating the anterior-posterior bias.* (a) 20 points fitted along the AP axis of the tectum, grey dots show all of the neurons in the tectum across all imaging planes. (b-c) all the neurons which were thresholded based on their QI scores for a given stimulus, colour coded according to their position along the AP axis.

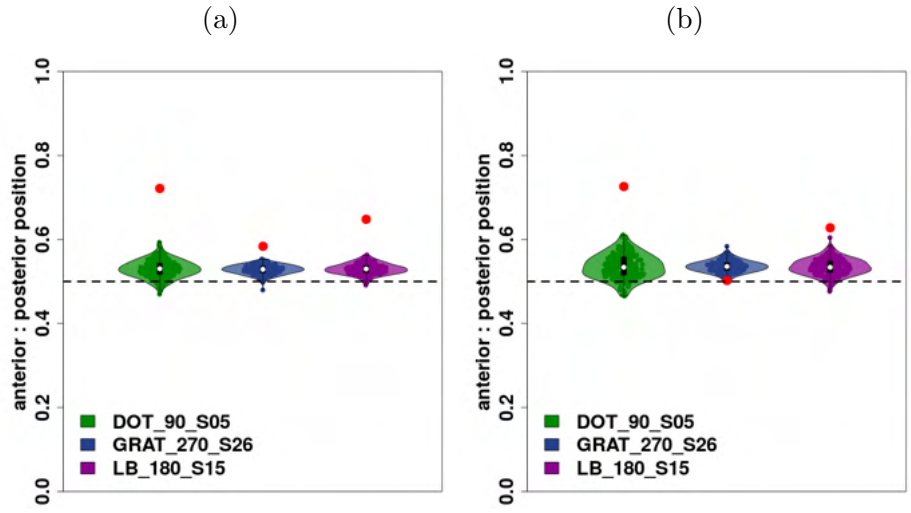

Figure 5.2.9: *Dots and bars are non-uniformly distributed along the anterior-posterior axis.* (a-b) The position along the AP axis of the tectum, with 1 indicating posterior and 0 indicating anterior. The dotted lines shows 0.5. The red dot shows the average position along the AP axis of all the neurons thresholded based on their QI scores for a given stimulus. The violin plots show a null distribution from randomly sampled neurons. Each plot shows one fish.

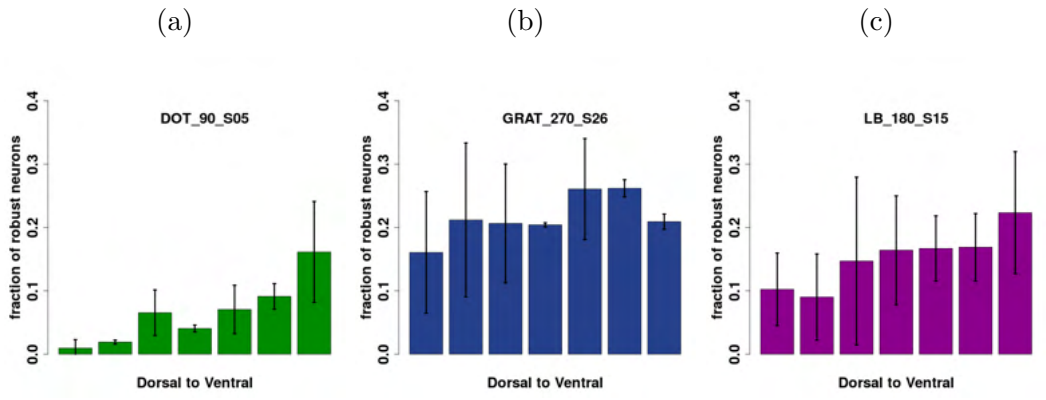

Figure 5.2.10: *Dot responsive neurons are non-uniformly distributed along the dorso-ventral axis.* The proportion of neurons classified as robust along the dorsoventral axis for the (a) dot, (b) grating, or (c) lightbar stimulus. Error bars show standard deviation. n = 2 fish.

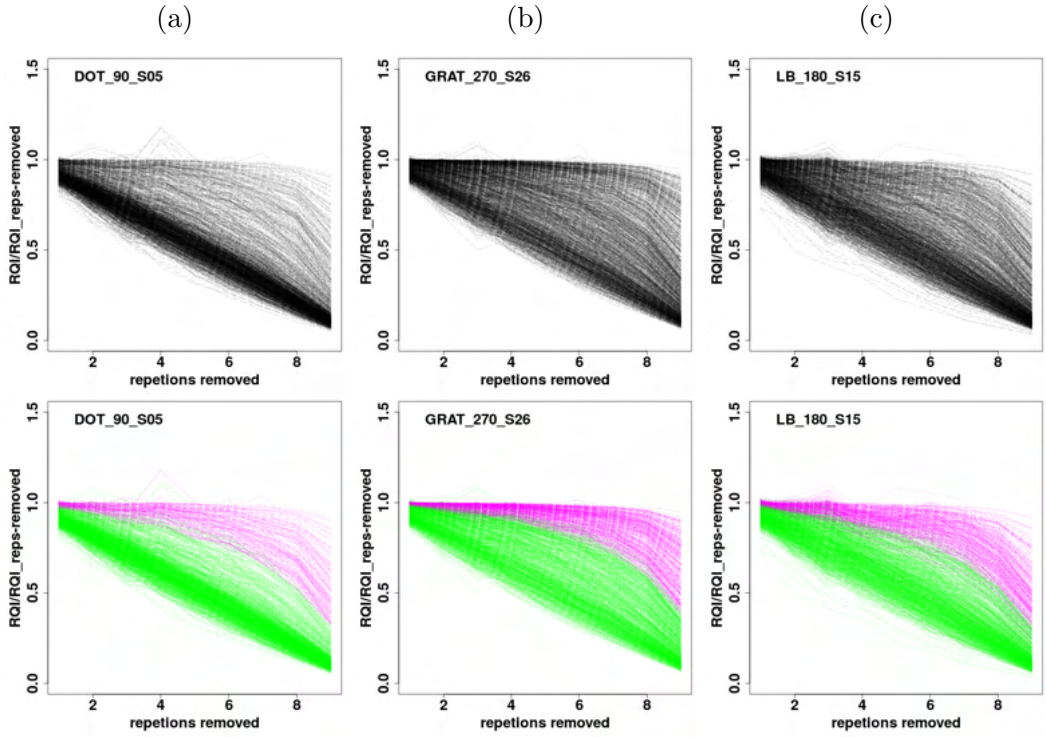

Figure 5.2.11: *Robust neurons are resistant to the removal of repetitions.* (a-c) Shows the change in QI score as repetitions are removed for each of the 3 stimuli for one example fish. The bottom row shows the neurons colour coded according to whether or not they were classified as robust, based on their QI_{10} score. Magenta indicates the neurons were classified as robust.

clustering method, therefore, each fish was clustered independently. Furthermore, since each stimulus now has 10 repetitions, the mean response over the repetitions was used to cluster and the Euclidean distance between neurons was normalised to the standard deviation of the neurons' response as in Eq. 3.4.

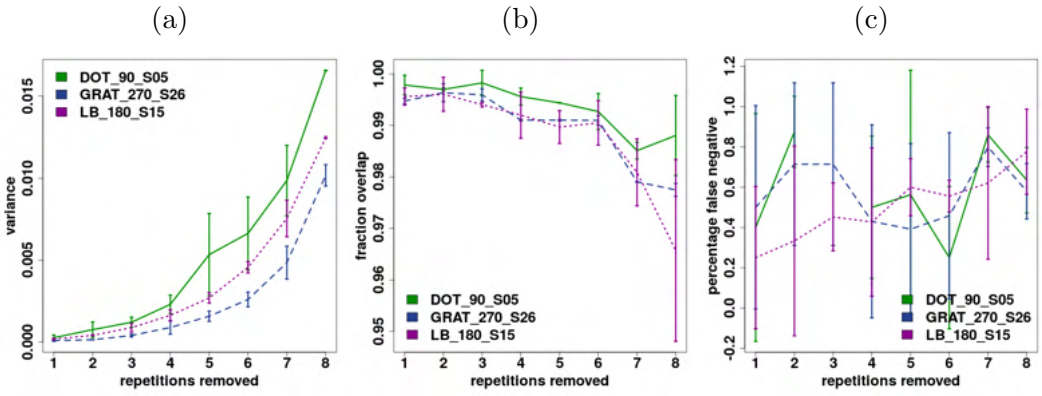

Figure 5.2.12: *Only a small number of repetitions are needed to classify neurons as robust* (a) The variance in the QI_{10}/QI_x score from all neurons that were classified as robust, based on their QI_{10} score, as the number of repetitions removed increases. (b) The percentage match between neurons being classified as robust or not, based on their QI_{10} and QI_x score. (c) The percentage of neurons which were classified as a 'false negative' for all neurons whose classification of robustness wasn't matched between their QI_{10} and QI_x score. $n = 2$ fish

Both fish generated 3 clusters, with the same cluster types easily identifiable across fish (Figs. 5.2.14 & 5.2.15). For each fish, one cluster was found to respond preferentially to dots, a second to gratings and a third to gratings and lightbars. Also, despite not using the QI scores to threshold, when looking at the distribution of the QI scores for all of the neurons in a given cluster, they tend to be higher than average for stimuli which define the cluster response type, e.g. clusters which show a preferential response to the dot stimulus are composed of neurons with a higher than average QI score for dots, and average QI scores for the lightbar and grating stimuli (Figs. 5.2.14 & 5.2.15).

The distribution of clusters within the tectum can be seen in Figs. 5.2.16 to 5.2.18, and Figs 5.2.19 to 5.2.21 for fish 1 and 2, respectively. Neither of the clusters which respond preferentially to the grating stimulus (clusters 2 and 3) have a posterior bias along the AP axis (Fig. 5.2.22). Only cluster 1, whose response is defined by the dot, shows an AP posterior bias compared to the null distribution in both fish. There may also be a bias along the DV axis, with a higher relative fraction of cells present in the ventral tectum, for the dot selective cluster, compared to the other two clusters (Fig. 5.2.23). Given the clustering algorithm reflects what is seen with the QI_{dot} further indicates that it is able to pick out salient features of the data.

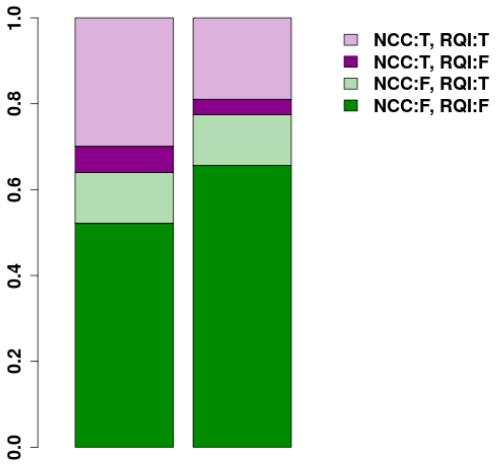

Figure 5.2.13: *The NCC and RQI show agreement on which neurons to threshold.* The proportion of neurons that were removed (F) or kept (T) after thresholding based on the NCC and QI scores. Each bar represents all the segmented neurons from one fish.

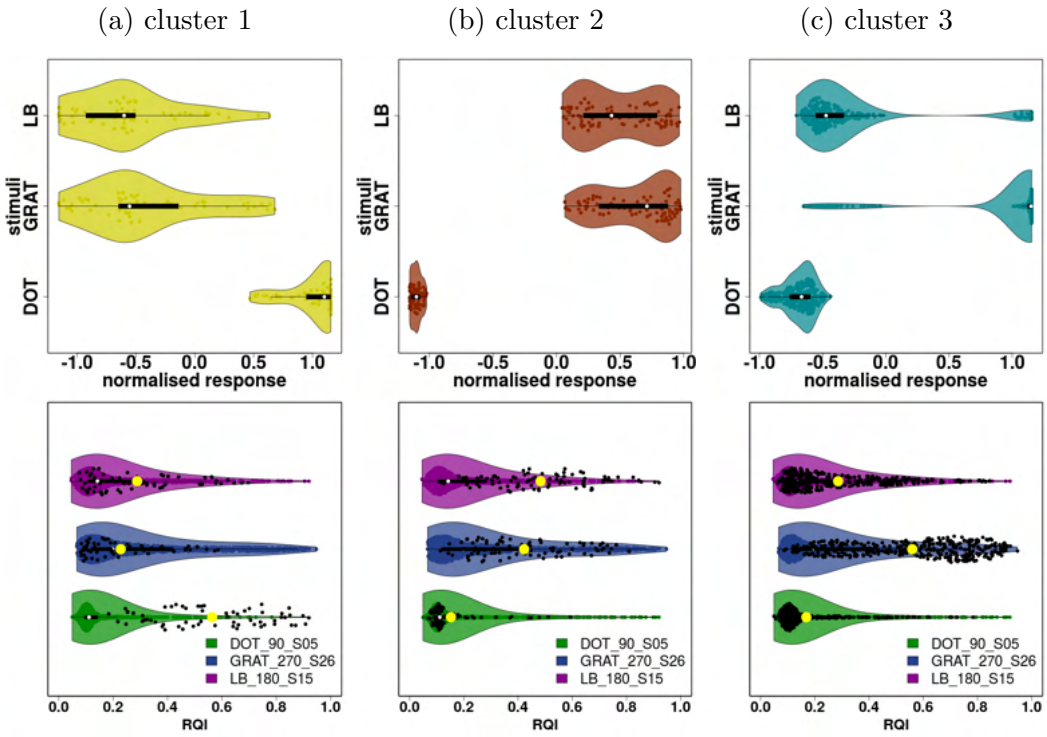

Figure 5.2.14: *Cluster responses for fish 1.* (a-c) The top panel shows the normalised response to the stimuli of all the neurons in a cluster, the white dot shows the median response. The bottom panel shows the distribution of QI scores, the larger black points show the neurons which belong to each cluster from the top panel. The yellow point shows the mean QI score for the neurons in the cluster. $n = 1$ fish.

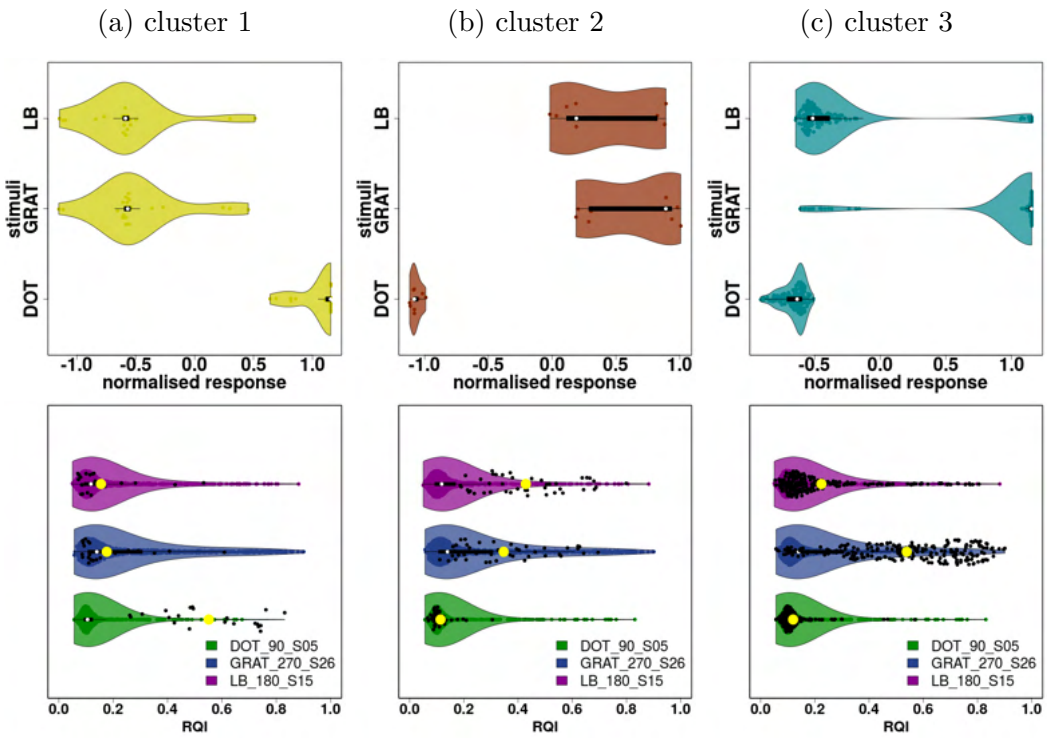

Figure 5.2.15: *Cluster responses for fish 2.* Same as 5.2.14 for second fish.

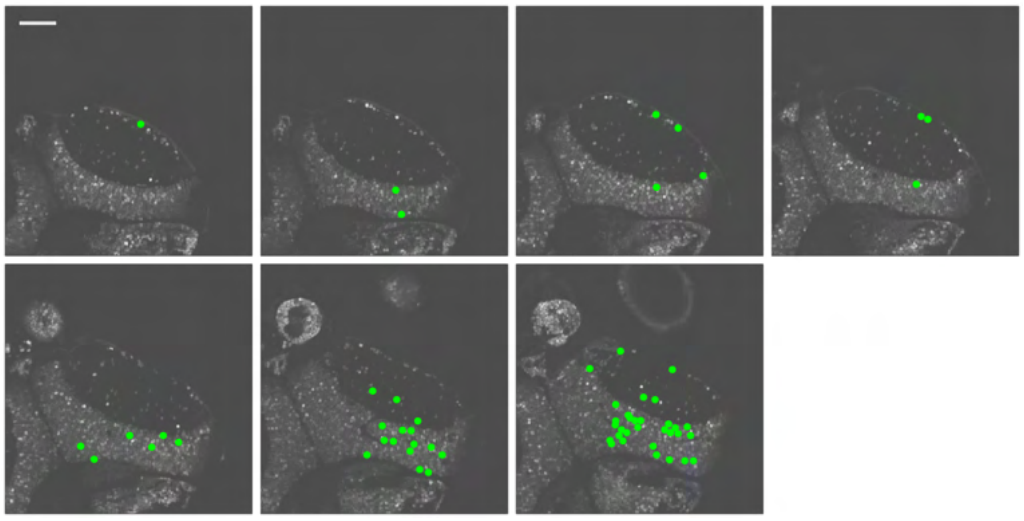

Figure 5.2.16: *Fish 1 tectal distribution of neurons found in cluster 1 from Fig. 5.2.14a*

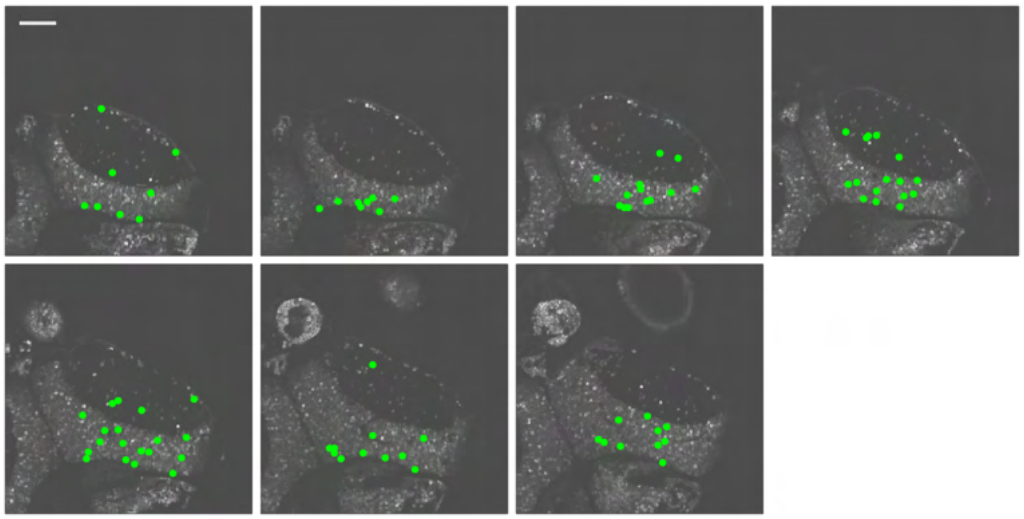

Figure 5.2.17: *Fish 1 tectal distribution of neurons found in cluster 2 from Fig. 5.2.14b*

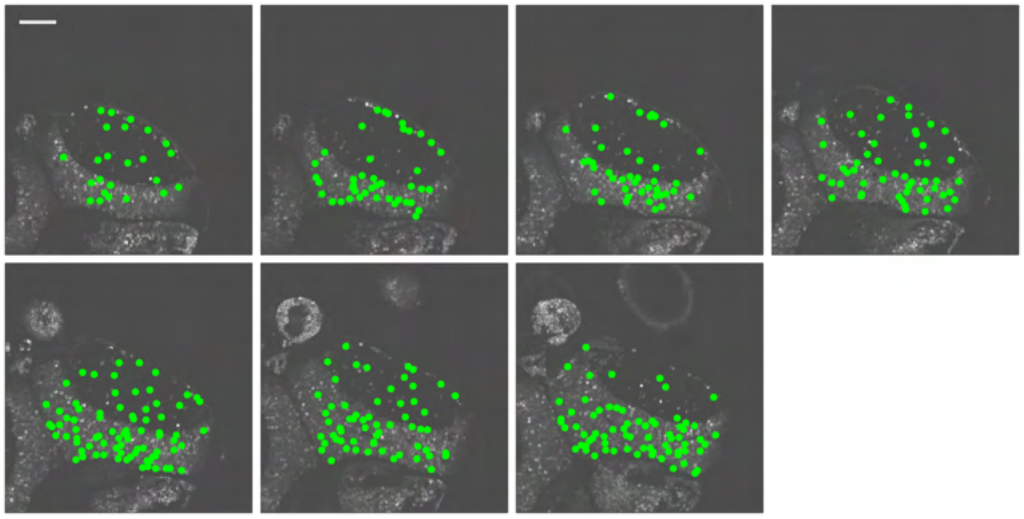

Figure 5.2.18: *Fish 1 tectal distribution of neurons found in cluster 3 from Fig 5.2.14c*

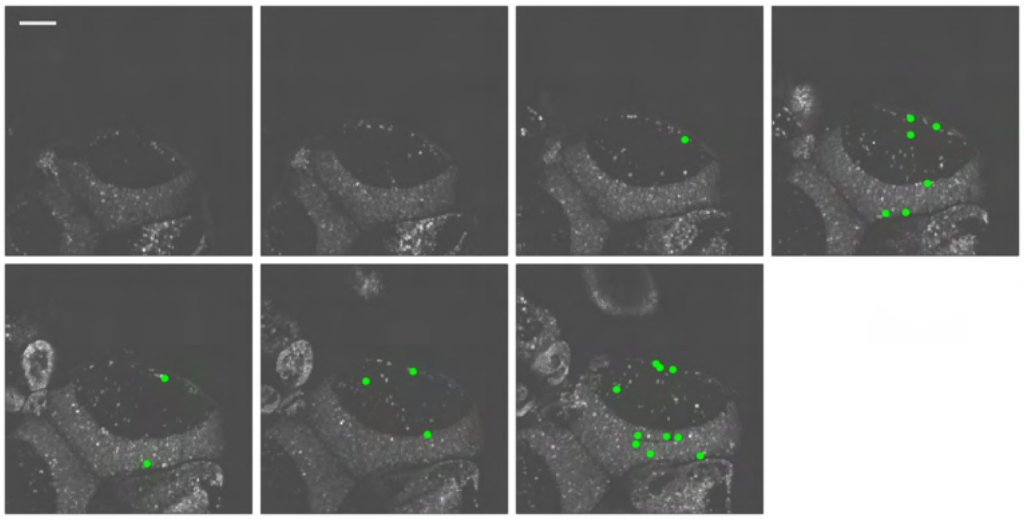

Figure 5.2.19: *Fish 2 tectal distribution of neurons found in cluster 1 from Fig. 5.2.15a*

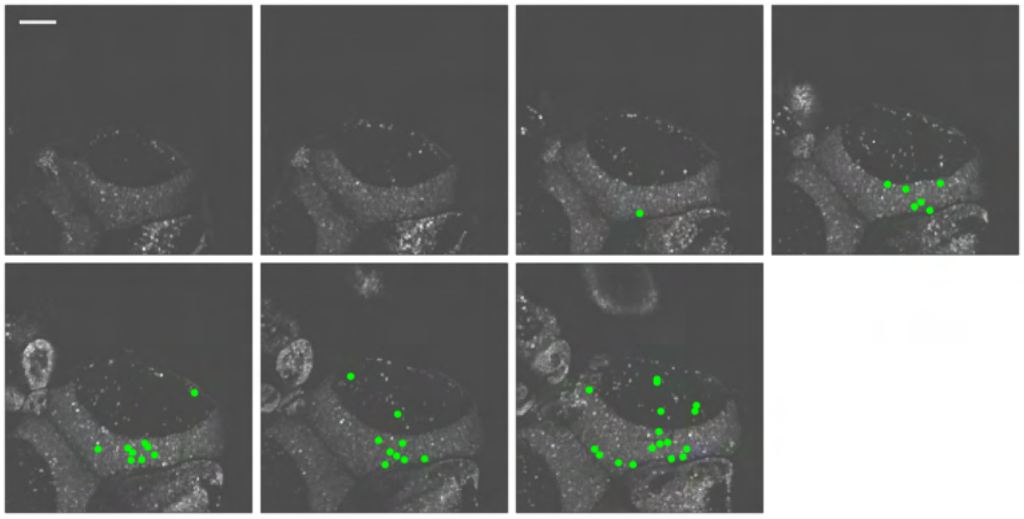

Figure 5.2.20: *Fish 2 tectal distribution of neurons found in cluster 2 from Fig. 5.2.15b*

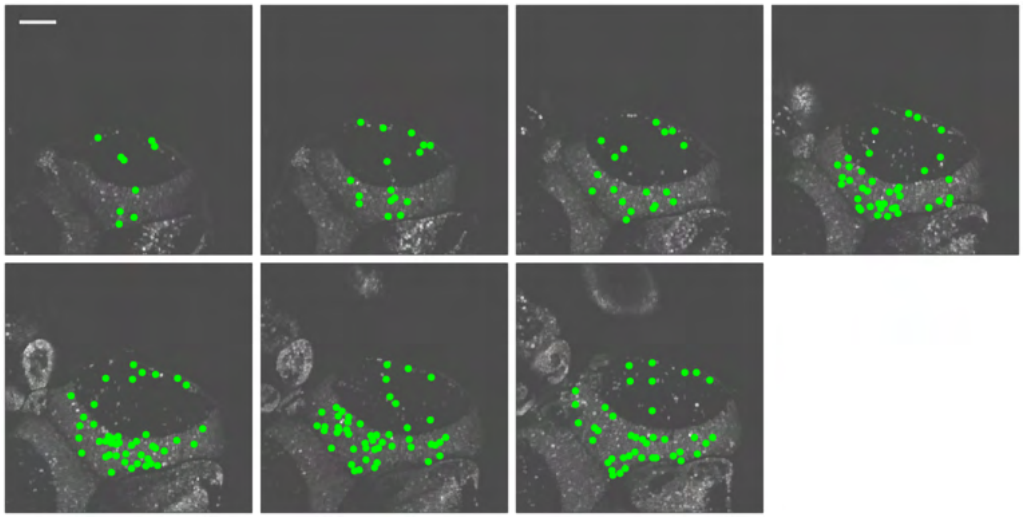

Figure 5.2.21: *Fish 2 tectal distribution of neurons found in cluster 3 from Fig 5.2.15c*

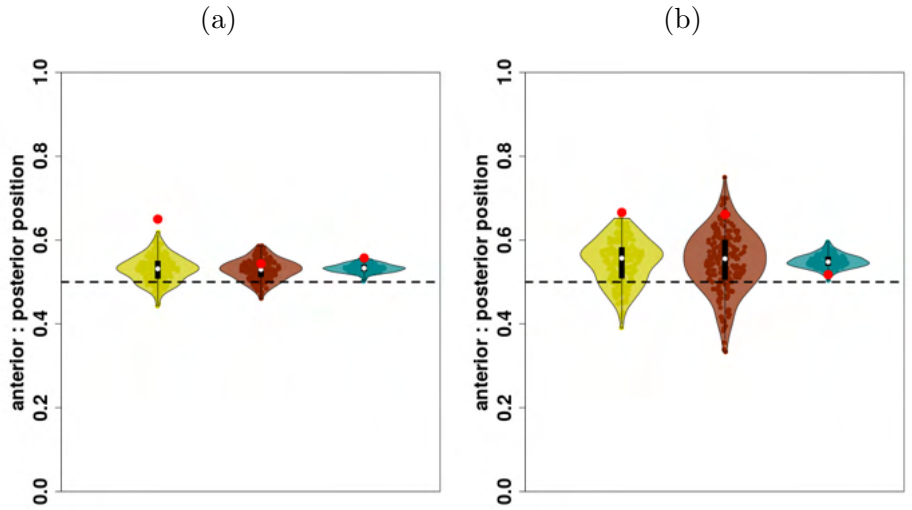

Figure 5.2.22: *Dot selective clusters are non-uniformly distributed along the anterior-posterior axis.* (a-b) The average position along the AP axis of the tectum of all the neurons in each cluster, with 1 indicating posterior and 0 indicating anterior. The dotted lines shows 0.5. The red dot shows the average position along the anterior posterior axis of the tectum of all the neurons in a cluster. The violin plots show a null distribution from randomly sampled neurons. Each plot shows one fish. Plots colour coded to cluster membership.

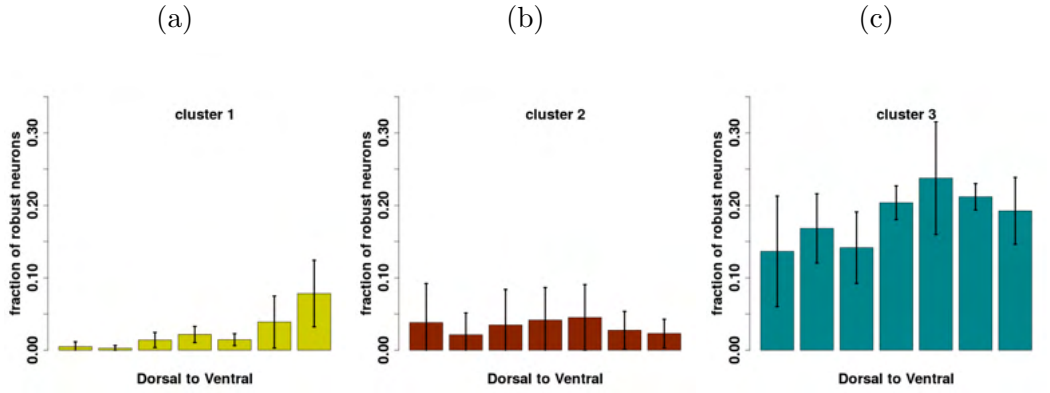

Figure 5.2.23: *Dot selective clusters are non-uniformly distributed along the dorso-ventral axis.* The proportion of neurons belonging to each cluster along the dorsoventral axis for each cluster. Error bars show standard deviation. $n = 2$ fish.

5.2.5 Summary

1. Neurons can be classified based on how reliably they respond to repetitions of the same stimulus (robustness) using the QI index (Baden et al. 2016).
2. Neurons tend to respond robustly to just one stimulus.
3. Neurons which respond robustly to the dot stimulus are more likely to be found in the ventral and posterior portions of the tectum.
4. It is possible to remove many repetitions without affecting the classification of neurons as to whether or not they are robust.
5. Clustering each fish independently gives rise to similar clusters across both fish.

5.3 Discussion

5.3.1 Moving from the lightsheet to the 2-photon microscope

In this chapter the experimental set up and pipeline for the clustering algorithm has been adapted to try and improve performance. One of the biggest changes was switching from lightsheet to 2-photon microscopy, and although a direct comparison of functional imaging data from these two setups is beyond the scope of this analysis, it was thought that the ability of preventing the fish from seeing the laser, and the possibility of conducting volumetric analysis meant it would be worth switching to a new microscope.

One metric that does allow a comparison across these two experimental set ups, however, is the NCC. When looking at the spatial distribution of reliable neurons according to the NCC it seems there is a higher prevelance in the centre of the tectum in both conditions. The fact a similar distribution is present in both the lightsheet and 2-photon imaging data, using different sets of visual stimuli, provides

some validation that the effect is real and not an artifact of a specific imaging setup (see 3.3 for discussion).

5.3.2 Analysing how neurons respond to multiple presentations of the same stimulus

In the previous chapter no repetitions were included in the data. As discussed in the introduction this raised a number of issues, such as the inability to distinguish visually evoked from non-visually evoked activity during the presentation of a stimulus, or the inability to measure how robust a neuron's response is to repetitions of the same stimulus. To make sure the clusters truly represent the underlying response profiles of the neurons, the variability of a neuron's response to a stimulus should be considered in the clustering procedure. By including 10 repetitions, the average response of the neuron could be used to cluster and it's variance across repetitions used as a normalising factor. Furthermore, to quantify the distribution of 'robustness' throughout the tectum the QI (Baden et al. 2016) of the neuron was calculated for each stimulus.

When looking at the data, most neurons were classified as robust for only one stimulus. Those that were robust to two stimuli were in the minority and most of them were found to overlap between the grating and lightbar stimulus. This indicates, first, that robustness is not a general property of the neuron; a neuron's robustness can be altered by presenting it with different visual features. Second, most neurons have a relatively high degree of selectivity for a given visual stimulus. Third, the dot stimulus is the most distinctive of the 3 stimuli, although this may be explained by the fact that the bar and grating extend across the whole of the vertical axis of the screen, whilst the dot doesn't.

In these preliminary experiments 10 repetitions were given for each of the 3 stimuli. For future experiments with a larger number of stimuli, the inclusion of many repetitions may lead to a prohibitively long imaging time. It seems, however, that the removal of repetitions has a negligible effect on the ability to correctly classify neurons as robust, at least to the 3 stimuli which were presented in this study. Indeed,

even removing all but 2 repetitions still enabled the correct classification of around 95% of the neurons suggesting that 10 repetitions is not necessary for this manner of classification.

A further way to analyse the data, which was not explored in this chapter, would be to look at how a neuron's response changes to repetitions of the same stimulus. Neurons can undergo facilitation (Cooke et al. 2015) or habitutation (Glanzman 2009, Simons-Weidenmaier et al. 2006, Weber et al. 2002) in response to stimulus repetition, and deriving metrics which specifically look for these changes in the neural response would provide a further way to classify neurons. This would be particularly useful if the behavioural output of the zebrafish was also being recorded, as it would be possible to correlate changes in neural activity with behavioural habituation.

5.3.3 Spatially localised dot detectors

Since the data from the 2-photon microscope includes multiple imaging planes it was possible to look at the distribution of NCC and QI values across the dorsoventral (DV) axis, as well as along the anteroposterior (AP) axis, of the whole tectal hemisphere. The NCC data indicates there is a bias in the spatial distribution of reliable visually responsive neurons along the DV axis, with a higher prevalence of more reliable neurons in the more ventral regions of the tectum. Furthermore, when looking at the $QI_{stimulus}$ scores, it is apparent that neurons which respond robustly to the dot stimulus are located in more ventral and posterior portions of the tectum, whereas this effect doesn't seem to be apparent for the other two stimuli, indicating there may be a specialised region in the tectum dedicated to detecting dot stimuli.

Whilst there is previous research on the functional properties of dot selective neurons in the zebrafish tectum (Bianco and Engert 2014), a bias in their spatial localisation has not been reported before, and generally it has been thought that subtypes are randomly distributed throughout the tectum (Chen et al. 2018, Portugues et al. 2014, Randlett et al. 2015, Romano et al. 2015). However, the finding of this regional specialisation in the tectum seems to fit in with an emerging picture that

visual features are non-uniformly represented across the visual system. For example, mouse genetic labelling of specific RGC subtypes has demonstrated that many of them have a non-uniform distribution across the retina (Bleckert et al. 2014, El-Danaf and Huberman 2019, Hughes et al. 2013). This includes W3 neurons, which have the highest density in the ventral retina, corresponding to the upper visual field (Zhang et al. 2012). The reason for their prevalence in the ventral retina is thought to be due to them playing a role in the detection of birds of prey overhead, which is supported by the fact that a looming stimulus triggers escape behaviour in mice only when it is presented in the upper visual field (Yilmaz and Meister 2013). A recent paper has also demonstrated region specific separation of motion selectivity in the mouse superior colliculus (Malmazet et al. 2018), indicating that a non-uniform distribution of subtypes exists across different visual areas.

Research in the zebrafish retina has also demonstrated a non-uniform distribution of neurons already at the level of the photoreceptors (Zimmermann et al. 2018), with the variation in the distribution of cones matching the variation in the chromatic content of light across the visual field. The authors also describe an area of the retina which has a high density of UV sensitive photoreceptors which they term the 'strike zone', and may act to enhance prey detection (Yoshimatsu et al. 2019, Zimmermann et al. 2018). It would be interesting to map the projection patterns which links these photoreceptors to other brain regions, or to see if the receptive fields of the putative spot detectors in the posterior portion of the tectum correspond to the region of the visual scene which is activated by the 'strike zone'. Interestingly, local stimulation of the zebrafish tectum also indicates there is a specialisation of the posterior tectum, with escape behaviours being elicited only when the more posterior regions of the tectum are optogenetically activated (Helmbrecht et al. 2018). Further work will hopefully elucidate whether the localised spot detectors found in this study play a role in either prey capture or predator avoidance.

A further question is whether these spatially localised neurons are actually selective for the stimulus i.e do they respond specifically to a dot, and no other stimuli? There are several lines of evidence which suggest this may be the case. First, in this chapter most neurons which responded robustly to one stimulus, didn't respond robustly to

the other stimuli, implying there is a degree of selectivity in the neurons. Second, from the previous chapter it is known that many neurons respond preferentially to a dot over a bar, when matched for size, speed, direction and contrast. Third, when clustering on the 3 stimuli presented in this chapter, both fish had a cluster which responded selectively to the dot stimulus, with both clusters being localised to the ventral and posterior regions of the tectum, matching what was seen with QI_{dot} robust neurons. Altogether, this suggests there may be spatially localised neurons selective for dot stimuli in the zebrafish tectum. This is in keeping with the previous literature which suggests there are spot detectors in the tectum of multiple species including frog (Lettvin et al. 1968) and zebrafish (Sajovic and Levinthal 1982b) and, since the size of the dot used in the barrage matches the range of values which are reported to elicit hunting in zebrafish larvae (Bianco et al. 2011; Semmelhack et al. 2014), may have implications for linking neural circuits to behaviour.

5.3.4 Clustering with repetitions

Due to only having imaged 2 fish, it was not possible to do the 2 step clustering procedure. Therefore, each fish represents an independent round of clustering. Despite this, there is a remarkable degree of similarity between fish in both the response profiles of the clusters, as well as their distribution in the tectum. This is likely due to having multiple repetitions of each stimulus, meaning it was possible to filter out non-timelocked neurons, and cluster only those which demonstrate a reliable response to the stimulus.

Each fish generated 3 clusters, and in both fish the clusters were defined by their response to one of: the dot stimulus, the grating stimulus, or a combintion of the grating and lightbar stimuli. The fact that both fish generated similar clusters is promising and implies the pipeline is able identify common neuronal subtypes across fish. Looking at the distribution of QI scores in the clusters it can be seen that neurons tend to have a higher than average QI for the stimulus which defines the cluster, e.g in cluster 1, which is defined by its response to the dot stimulus, the neurons have high QI_{dot} scores, but average $QI_{grating}$ and $QI_{lightbar}$ scores. Whilst

not necessarily surprising, this is a confirmation that the algorithm is clustering together neurons which behave in a similar manner to one another. Furthermore, it is also possible to use the inverse QI score for each stimulus to normalise the Euclidean distance calculated between neurons, instead of the variance. In this case the clustering gives a weight against non-robust neurons. The resulting clusters are very similar as if normalising using the variance (data not shown).

When looking at the QI scores, it is apparent that a small percentage of neurons do respond reliably to all 3 stimuli (Fig. 5.2.12b). However, no cluster came out which reflected this. The reason for this is likely due to the small number of neurons which are in this group per fish, meaning they are unable to be detected as a cluster. Imaging more fish, and clustering them all together, should mitigate this problem and will enable the method to discover rarer subtypes.

Similar to looking at the distribution of QI scores along the AP axis of the tectum, the dot selective cluster has a posterior bias in both of the fish. Although this property was distinguishable without clustering, it may be possible to see other specialised regions of the tectum when clustering with more stimuli, that are not discernible when looking at the response properties of any given stimulus. A problem does arise when there are very few neurons in a cluster, as the null distribution becomes increasingly large, and the accuracy with which a bias can be detected is reduced (see Fig. 5.2.22b for an example). To mitigate this, it is possible to collate the neurons from multiple fish and register them to a common co-ordinate space, as has been done previously in drosophila (Jefferis et al. 2007), mouse (Leiwe et al. 2016) and zebrafish (Randlett et al. 2015). This will increase the ability with which specialised regions within the tectum can be discerned.

Chapter 6

Conclusions and perspectives

6.1 Summary

The aim of this thesis was to develop a method to classify visually responsive neurons in the zebrafish optic tectum. One of the prerequisites of the method was the ability to categorise neurons in an unbiased manner to a wide range of different visual features, with no underlying assumptions about the distribution of the data. To that end:

1. A density based clustering method (Rodriguez and Laio 2014) was adapted in such a way as to allow the detection of visually responsive neuronal subtypes across multiple fish (Fig. 6.1.1)
2. The method was validated on a range of synthetic and *in vivo* calcium imaging data to ensure it would pick out biologically meaningful clusters.
3. The importance of stimulus selection, data pre-processing, and determining the reliability of neuronal responses was also explored.

Overall, the work has demonstrated a robust pipeline for the detection of neuronal subytpes which can, in the future, be applied to a wide variety of visual stimuli.

In addition to the development of the clustering pipeline a number of features were

observered with respect to the response properties of neurons in the optic tectum. First, the clustering procedure revealed the presence of neurons which are selective for the conjunction of two visual features - direction and size, which is in keeping with previous data (Bianco and Engert 2014). Second, apart from the SINs, most neurons show an increased neural response for dots over bars. Third, there is a spatial bias in the distribution of visually responsive neurons throughout the tectum. This effect seems specific for dots, with a higher prevalence of neurons which respond reliably to the dot stimulus in the ventro-posterior portion of the tectum.

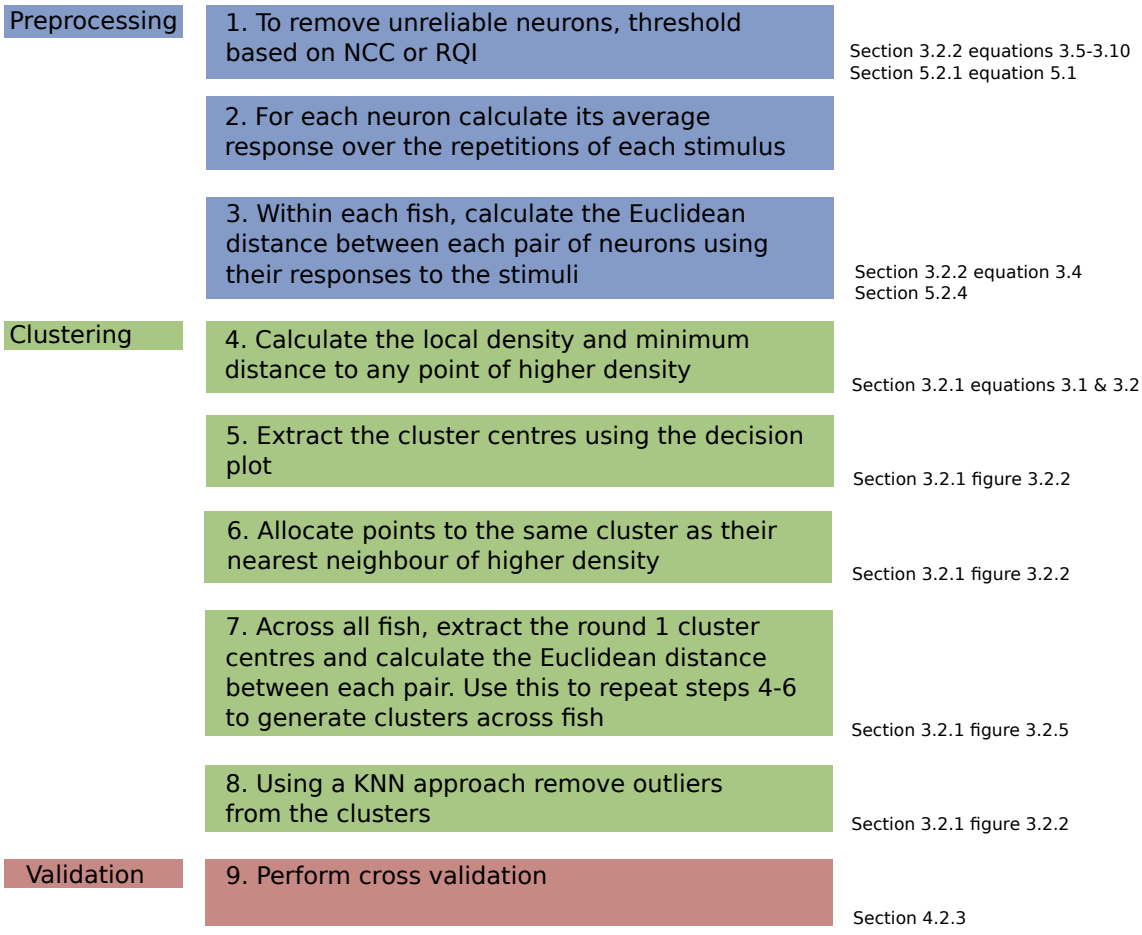

Figure 6.1.1: Overview of the clustering procedure, including preprocessing and validation

6.2 Determining the optimal visual stimuli

The main focus of this thesis has been the development of a method to robustly classify visually responsive neuronal subtypes. The previous chapter demonstrated

the ability to find common subtypes across fish with a small barrage of 3 stimuli, even when clustering each fish independently. In an effort to get a more comprehensive overview of the subtypes present in the tectum, it is necessary to increase the variety and number of stimuli. Two important questions are: how many, and what types, of stimuli are best to include? This is not a insignificant problem, on the one hand, the aim is to define as many subtypes as possible, whilst on the other hand, the ability to accurately cluster the data suffers as the number of stimuli increase. The most efficient scheme for designing the stimuli would be to use a 'factorial experiment'. This experimental design consists of multiple factors, with each factor being composed of multiple discrete values or 'levels'. Each stimulus would be composed of one level from every factor, with the full range of stimuli accounting for all possible combinations of the levels across factors. This design was used in chapter 4 when looking at size and direction selective neurons. In this case size and direction are factors, whilst the levels would correspond to, in the case of size, small and large, and in the case of direction, AP and PA motion. The total number of stimuli is given by the number of levels raised to the power of the number of factors, in this case 2^2.

Deciding what each factor and level should comprise of is based primarily on knowledge of the zebrafish visual system. For example, direction selectivity is prevalent in the tectum, with discrete populations centred on the 4 cardinal directions (Hunter et al. 2013), making it an ideal factor with easily defined levels. Furthermore, a contrast factor can be divided into black and white levels to correspond to the ON and OFF subtypes (Sajovic and Levinthal 1982a). The levels for a size factor could be determined in a behavioural manner, with two sizes chosen that elicit either a hunting or escape response (Bianco et al. 2011, Dunn et al. 2016b, Temizer et al. 2015). A further factor would be motion perception, with local and global motion each being a level. Based on the results in chapter 4, a spot would be used for a local stimulus, whilst wholefield gratings would be used for the global stimulus. Using this method of analysis is particularly useful as first, it allows any change in the response properties of a neuron to be isolated to a specific visual feature and second, it allows the interactions between visual features to be analysed.

6.3 Validation of clusters

There is an inherent difficulty in validating the output of unsupervised clustering since there is no ground truth to compare the results to. Methods for validating the data were demonstrated in chapter 4, such as by projecting the clusters into a lower dimensional space and cross validation. However, further methods of validation which take into account other biological properties of the neurons are also possible. For instance, Baden et al (2016) validated functional mouse RGC classes by demonstrating neurons within a cluster had similar morphological properties, that their receptive fields tiled the retinotopic map, and also by linking clusters to genetically defined populations of neurons. Demonstrating that neurons classified on their functional responses share similar genetic and morpholgical properties increases the likelihood that the clusters are actually a cohesive population. A similar method of validation can also be done in zebrafish: using post hoc immunostaining and non-rigid body alignment it is possible to correlate functional responses with an array of molecular markers (Lovett-Barron et al. 2017), allowing a dissection of the underlying molecular properties of the clusters.

6.4 Extending the analysis to the RGCs

An open question in visual neuroscience is how information is integrated and transformed from the retina to other brain regions, such as the optic tectum. A number of studies have previously compared the response properties of retinal and tectal neurons (Gabriel et al. 2012, Grama and Engert 2012, Nikolaou et al. 2012, Dunn et al. 2016b). However, these studies focused on only one neuronal subtype - direction selective neurons, or in the case of Dunn et al (2016), loom detectors. Furthermore, the analysis of the retinal and tectal response properties was either done in separate fish (Dunn et al. 2016b, Nikolaou et al. 2012), or was analysed in single neurons using single cell electrophysiology (Gabriel et al. 2012, Grama and Engert 2012). An ideal scenario would be the ability to record population activity from both the RGCs and tectal neurons simultaneously to an array of visual stimuli. Using the

method laid out in this thesis to classify both tectal neurons and RGCs would then allow a direct comparison of how information is transformed from one brain region to another. The simultaneous acquisition of retinal and tectal activity may be possible by combining the nuclear localised elavl3:H2B-GCaMP6s line, which was used in this thesis, with a line which expresses GCaMP in the presynaptic terminals of RGC axons (Nikolaou et al. 2012). Using these two fish lines would ensure the GCaMP signal from both the RGC and tectal populations were not mixed, as the RGC signal would be contained in the neuropil region and the tectal signal would be contained primarily within the SPV layer. This method would, therefore, allow a direct comparison of neuronal subtypes contained within these two brain regions, helping to understand what information is inherited directly from the retina and what emerges *de novo* in the tectum.

6.5 Mapping from neural activity to behaviour

Simply classifying tectal (and RGC) neurons is not sufficient to understand visuomotor transformations. Whilst correlating neural activity to defined visual features provides information about how a visual percept is encoded in the brain, to understand how the perception of a stimulus gives rise to behaviour it is necessary to correlate this activity to a behavioural readout. Fortunately, there are a number of ways to monitor the behavioural output of a zebrafish larva whilst simultaneously monitoring its neural activity. Extracellular recordings along the descending axial motor neurons in restrained larvae allow 'fictive swims' to be measured, from which the directionality of motion can be inferred (Vladimirov et al. 2014). Alternatively, it is possible to release the tail of the fish from the surrounding agarose; the freed tail can then be recorded and the kinematics correlated to the presentation of different visual stimuli (Temizer et al. 2015). Although previous work has recorded population activity in response to both prey and predator like stimuli whilst monitoring behaviour (Bianco and Engert 2014, Dunn et al. 2016b, Semmelhack et al. 2014, Temizer et al. 2015), there is still not a precise understanding of exactly what information the visuomotor neurons are encoding. Are they composed of specialised

single neuronal subtypes, or are they assemblies of multiple subtypes, each responding to a different facet of the visual scene? Furthermore, whilst there are neurons in the tectum which respond preferentially to prey like stimuli (Bianco and Engert 2014), how their response is related to prey capture behaviour is still not clear. Are they purely sensory, responding irrespective of whether the fish initiates a prey capture sequence, or are they only activated if the decision to enact a prey capture sequence is reached? In terms of escape behaviour, there is still a debate as to whether there are RGCs which respond selectively to looming stimuli or whether it is a emergent property of the tectal neurons (Dunn et al. 2016b, Temizer et al. 2015). Furthermore, a detailed comparison of the neural activity underlying these two opposing behaviours is still lacking. By classifying visually responsive neurons to the visual stimuli using the method laid out in this thesis, and combining it with behavioural analysis, it will be possible to address these issues.

Bibliography

Abbas, Fatima et al. (2017). "A Three-Layer Network Model of Direction Selective Circuits in the Optic Tectum". In: *Frontiers in Neural Circuits* 11, p. 88.

Ahmadlou, Mehran et al. (2017). "Visual cortex limits pop-out in the superior colliculus of awake mice". In: *Cerebral Cortex*.

Ahrens, Misha B et al. (2013). "Whole-brain functional imaging at cellular resolution using light-sheet microscopy". In: *Nat Methods* 10.5, pp. 413–420.

Allman, J et al. (1985). "Stimulus Specific Responses from Beyond the Classical Receptive Field: Neurophysiological Mechanisms for Local-Global Comparisons in Visual Neurons". In: *Annual Review of Neuroscience* 8.1, pp. 407–430.

Armañanzas, Rubén and Giorgio A. Ascoli (2015). "Towards the automatic classification of neurons". In: *Trends in Neurosciences* 38.5, pp. 307–318.

Baden, Tom et al. (2013). "Spikes in Mammalian Bipolar Cells Support Temporal Layering of the Inner Retina". In: *Current Biology* 23.1, pp. 48–52.

Baden, Tom et al. (2016). "The functional diversity of retinal ganglion cells in the mouse". In: *Nature* 529.

Barlow, Horace B. (1953). "Summation and inhibition in the frog's retina." In: *Journal of Physiology* 119, pp. 69–88.

Basso, M and P May (2017). "Circuits for Action and Cognition: A View from the Superior Colliculus." In: *Annual Review of Vision Science* 15.3, pp. 197–226.

Ben-Tov, Mor et al. (2015). "Pop-out in visual search of moving targets in the archer fish". In: *Nature Communications* 6.1, p. 6476.

Bianco, I and F Engert (2014). "Visuomotor Transformations Underlying Hunting Behavior in Zebrafish". In: *Current Biology* 25.7, pp. 831–846.

Bianco, I et al. (2011). "Prey Capture Behavior Evoked by Simple Visual Stimuli in Larval Zebrafish". In: *Frontiers in Systems Neuroscience* 5, p. 101.

Blanchard, D. C. et al. (1981). "Taming of wild Rattus norvegicus by lesions of the mesencephalic central gray". In: *Physiological Psychology* 9.2, pp. 157–163.

Bleckert, Adam et al. (2014). "Visual Space Is Represented by Nonmatching Topographies of Distinct Mouse Retinal Ganglion Cell Types". In: *Current Biology* 24.3, pp. 310–315.

Boulanger-Weill, Jonathan et al. (2017). "Functional Interactions between Newborn and Mature Neurons Leading to Integration into Established Neuronal Circuits". In: *Current Biology* 27.12, pp. 1707–1720.

Brockerhoff, Susan E et al. (1995). *A behavioral screen for isolating zebrafish mutants with visual system defects*. Tech. rep., pp. 10545–10549.

Buzsáki, György (2010). *Neural Syntax: Cell Assemblies, Synapsembles, and Readers*.

Cang, Jianhua and David Feldheim (2013). "Developmental mechanisms of topographic map formation and alignment." In: *Annual review of neuroscience* 36, pp. 51–77.

Cang, Jianhua et al. (2018). "Visual Function, Organization, and Development of the Mouse Superior Colliculus". In: *Annual Review of Vision Science* 4.1, pp. 239–262.

Carandini, M and D Ferster (2000). "Membrane potential and firing rate in cat primary visual cortex." In: *The Journal of neuroscience : the official journal of the Society for Neuroscience* 20.1, pp. 470–484.

Carrillo-Reid, Luis et al. (2019). "Controlling Visually Guided Behavior by Holographic Recalling of Cortical Ensembles". In: *Cell* 178.2, pp. 447–457.

Chandrasekaran, Anand R et al. (2005). "Development/Plasticity/Repair Evidence for an Instructive Role of Retinal Activity in Retinotopic Map Refinement in the Superior Colliculus of the Mouse". In:

Chen et al. (2018). "Brain-wide Organization of Neuronal Activity and Convergent Sensorimotor Transformations in Larval Zebrafish". In: *Neuron* 100.4, pp. 876–890.

Chiang, Ann-Shyn et al. (2011). "Three-dimensional reconstruction of brain-wide wiring networks in Drosophila at single-cell resolution." In: *Current biology : CB* 21.1, pp. 1–11.

Cooke, Sam F. et al. (2015). "Visual recognition memory, manifested as long-term habituation, requires synaptic plasticity in V1". In: *Nature Neuroscience*.

Cornide-Petronio, María Eugenia et al. (2011). "Retinotopy of visual projections to the optic tectum and pretectum in larval sea lamprey". In: *Experimental Eye Research* 92.4, pp. 274–281.

Costa, Marta et al. (2016). "NBLAST: Rapid, Sensitive Comparison of Neuronal Structure and Construction of Neuron Family Databases". In: *Neuron* 91.2, pp. 293–311.

Cronin, Beau et al. (2010). "Hierarchical Bayesian modeling and Markov chain Monte Carlo sampling for tuning-curve analysis." In: *Journal of neurophysiology* 103.1, pp. 591–602.

Cui, He and Joseph G. Malpeli (2006). "Activity in the Parabigeminal Nucleus During Eye Movements Directed at Moving and Stationary Targets". In: *Journal of Neurophysiology* 89.6, pp. 3128–3142.

El-Danaf, Rana N. and Andrew D. Huberman (2019). "Sub-topographic maps for regionally enhanced analysis of visual space in the mouse retina". In: *Journal of Comparative Neurology* 527.1, pp. 259–269.

De Franceschi, Gioia et al. (2016). "Vision Guides Selection of Freeze or Flight Defense Strategies in Mice". In: *Current Biology* 26, pp. 2150–2154.

Defelipe, Javier et al. (2013). "New insights into the classification and nomenclature of cortical GABAergic interneurons". In: *Nature Reviews Neuroscience*.

Del Bene, Filippo et al. (2010). "Filtering of visual information in the tectum by an identified neural circuit." In: *Science (New York, N.Y.)* 330.6004, pp. 669–73.

DesJardin, J. T. et al. (2013). "Defense-Like Behaviors Evoked by Pharmacological Disinhibition of the Superior Colliculus in the Primate". In: *Journal of Neuroscience* 33.1, pp. 150–155.

Dhande, Onkar S. and Andrew D. Huberman (2014). *Retinal ganglion cell maps in the brain: Implications for visual processing*.

Diana, Giovanni et al. (2018). "Bayesian inference of neuronal ensembles". In: *BioRXiv*.
Doubell, Timothy P et al. (2003). "Functional connectivity between the superficial and deeper layers of the superior colliculus: an anatomical substrate for sensorimotor integration." In: *The Journal of neuroscience : the official journal of the Society for Neuroscience* 23.16, pp. 6596–607.
Druckmann, Shaul et al. (2013). "A hierarchical structure of cortical interneuron electrical diversity revealed by automated statistical analysis." In: *Cerebral cortex (New York, N.Y. : 1991)*.
Dunn, T et al. (2016a). "Brain-wide mapping of neural activity controlling zebrafish exploratory locomotion." In: *eLife* 5, e12741.
Dunn, T et al. (2016b). "Neural Circuits Underlying Visually Evoked Escapes in Larval Zebrafish". In: *Neuron* 89.3, pp. 613–628.
Duong, Tammy M. et al. (2017). "Response of adult dragonflies to artificial prey of different size and colour". In: *PLOS ONE* 12.6. Ed. by Daniel Osorio, e0179483.
Egger, Robert et al. (2012). "3D Reconstruction and Standardization of the Rat Vibrissal Cortex for Precise Registration of Single Neuron Morphology". In: *PLoS Computational Biology* 8.12.
Engelken, E J and K W Stevens (1989). "Saccadic eye movements in response to visual, auditory, and bisensory stimuli." In: *Aviation, space, and environmental medicine* 60.8, pp. 762–8.
Euler, Thomas et al. (2014). "Retinal bipolar cells: elementary building blocks of vision". In: *Nature Reviews Neuroscience* 15.8, pp. 507–519.
Ewert, J P (1974). "The neural basis of visually guided behavior." In: *Scientific American* 230.3, pp. 34–42.
— (1987). "Neuroethology of releasing mechanisms: Prey-catching in toads". In: *Behavioural and Brain Sciences* 10, pp. 337–405.
— (1997). "Neural correlates of key stimulus and releasing mechanisms: a case study and two concepts". In: *Trends in Neurosciences* 20.8, pp. 332–338.
Finlay, Barbara L. et al. (1980). "A neuroethological approach to hamster vision". In: *Behavioural Brain Research* 1.6, pp. 479–496.
Franke, Katrin et al. (2017). "Inhibition decorrelates visual feature representations in the inner retina". In: *Nature* 542.7642, pp. 439–444.
Furigo, I.C. et al. (2010). "The role of the superior colliculus in predatory hunting". In: *Neuroscience* 165.1, pp. 1–15.
Gabriel, Jens P. et al. (2012). "Layer-Specific Targeting of Direction-Selective Neurons in the Zebrafish Optic Tectum". In: *Neuron* 76.6, pp. 1147–1160.
Gahtan, Ethan et al. (2002). "Evidence for a Widespread Brain Stem Escape Network in Larval Zebrafish". In: *Journal of Neurophysiology* 87.1, pp. 608–614.
Gahtan, Ethan et al. (2005). "Journal of Neuroscience". In: *J. Neurosci.* 16.2, pp. 843–852.
Galant, Sonya et al. (2016). "Embryonic origin and lineage hierarchies of the neural progenitor subtypes building the zebrafish adult midbrain". In: *Developmental Biology* 420.1, pp. 120–135.
Gale, Samuel D and Gabe J Murphy (2014). "Distinct representation and distribution of visual information by specific cell types in mouse superficial superior colliculus." In: *The Journal of neuroscience : the official journal of the Society for Neuroscience* 34.40, pp. 13458–71.

Ghosh, Krishna K. et al. (2004). "Types of bipolar cells in the mouse retina". In: *Journal of Comparative Neurology* 469.1, pp. 70–82.

Glanzman, David L. (2009). "Habituation in Aplysia: The Cheshire Cat of neurobiology". In: *Neurobiology of Learning and Memory* 92.2, pp. 147–154.

Grama, Abhinav and F Engert (2012). *Direction selectivity in the larval zebrafish tectum is mediated by asymmetric inhibition*.

Groh, Jennifer M and David L Sparks (1996). *Saccades to Somatosensory Targets. II. Motor Convergence in Primate Superior Colliculus*. Tech. rep. 1.

Gur, Moshe et al. (n.d.). "Orientation and Direction Selectivity of Neurons in V1 of Alert Monkeys: Functional Relationships and Laminar Distributions". In:

Hattar, Samer et al. (2006). "Central projections of melanopsin-expressing retinal ganglion cells in the mouse". In: *The Journal of Comparative Neurology* 497.3, pp. 326–349.

Helm, Jessica et al. (2013). "Subgroups of parvalbumin-expressing interneurons in layers 2/3 of the visual cortex". In: *Journal of Neurophysiology* 109.6, pp. 1600–1613.

Helmbrecht, Thomas O. et al. (2018). "Topography of a Visuomotor Transformation". In: *Neuron* 100.6, pp. 1429–1445.

Herrero, L. et al. (1998). "Tail and eye movements evoked by electrical microstimulation of the optic tectum in goldfish". In: *Experimental Brain Research* 120.3, pp. 291–305.

Hong, Y. Kate et al. (2011). "Stereotyped axonal arbors of retinal ganglion cell subsets in the mouse superior colliculus". In: *The Journal of Comparative Neurology* 519.9, pp. 1691–1711.

Hosp, Jonas A. et al. (2014). "Morpho-physiological criteria divide dentate gyrus interneurons into classes". In: *Hippocampus*.

Hoy, Jennifer L et al. (2019). "Defined cell types in superior colliculus make distinct contributions to prey capture behavior in the mouse". In:

Hubel, D H and T N Wiesel (1959). "Receptive fields of single neurones in the cat's striate cortex." In: *The Journal of physiology* 148, pp. 574–591.

Huberman, Andrew D. et al. (2008). "Architecture and Activity-Mediated Refinement of Axonal Projections from a Mosaic of Genetically Identified Retinal Ganglion Cells". In: *Neuron* 59.3, pp. 425–438.

Hughes, Steven et al. (2013). "Nonuniform Distribution and Spectral Tuning of Photosensitive Retinal Ganglion Cells of the Mouse Retina". In: *Current Biology* 23.17, pp. 1696–1701.

Hunter, Paul R et al. (2013). "Emergent properties of the optic tectum revealed by population analysis of direction and orientation selectivity." In: *The Journal of neuroscience : the official journal of the Society for Neuroscience* 33.35, pp. 13940–5.

Ito, Shinya and David Feldheim (2018). "The Mouse Superior Colliculus: An Emerging Model for Studying Circuit Formation and Function". In: *Frontiers in Neural Circuits* 12, p. 10.

Jang, Eric V. et al. (2016). "Emergence of Selectivity to Looming Stimuli in a Spiking Network Model of the Optic Tectum". In: *Frontiers in Neural Circuits* 10, p. 95.

Jefferis, Gregory S.X.E. et al. (2007). "Comprehensive Maps of Drosophila Higher Olfactory Centers: Spatially Segregated Fruit and Pheromone Representation". In: *Cell* 128.6, pp. 1187–1203.

Jones, Allan R. et al. (2009). "The Allen Brain Atlas: 5 years and beyond". In: *Nature Reviews Neuroscience* 10.11, pp. 821–828.

Jundi, Basil el et al. (2010). "The locust standard brain: A 3D standard of the central complex as a platform for neural network analysis". In: *Frontiers in Systems Neuroscience* 3.FEB.

Kannan, Madhuvanthi et al. (2019). "Optimizing Strategies for Developing Genetically Encoded Voltage Indicators". In: *Frontiers in Cellular Neuroscience* 13, p. 53.

Karagiannis, A. et al. (2009). "Classification of NPY-Expressing Neocortical Interneurons". In: *Journal of Neuroscience*.

Kay, Jeremy N et al. (2011). "Retinal ganglion cells with distinct directional preferences differ in molecular identity, structure, and central projections." In: *The Journal of neuroscience : the official journal of the Society for Neuroscience* 31.21, pp. 7753–7762.

Kim, B. and M Basso (2010). "A Probabilistic Strategy for Understanding Action Selection". In: *Journal of Neuroscience* 30.6, pp. 2340–2355.

Kramer, Anna et al. (2019). "Neuronal Architecture of a Visual Center that Processes Optic Flow". In: *Neuron*.

Kriegel, Hans-Peter et al. (2011). "Density-based clustering". In: *Data Mining and Knowledge Discovery*.

Kubo, Fumi et al. (2014). "Functional Architecture of an Optic Flow-Responsive Area that Drives Horizontal Eye Movements in Zebrafish". In: *Neuron* 81.6, pp. 1344–1359.

Kunst, Michael et al. (2019). "A Cellular-Resolution Atlas of the Larval Zebrafish Brain". In: *Neuron*.

Lang, Stefan et al. (2011). "Simulation of signal flow in 3D reconstructions of an anatomically realistic neural network in rat vibrissal cortex". In: *Neural Networks* 24.9, pp. 998–1011.

Lee and W C Hall (1995). "Interlaminar connections of the superior colliculus in the tree shrew. II: Projections from the superficial gray to the optic layer." In: *Visual neuroscience* 12.3, pp. 573–88.

Leiwe, Marcus N. et al. (2016). "Geniculo-Cortical projection diversity revealed within the mouse visual thalamus". In: *PLoS ONE* 11.1.

Leonardo, A. and Michale S Fee (2005). "Ensemble Coding of Vocal Control in Birdsong". In: *Journal of Neuroscience* 25.3, pp. 652–661.

Lettvin, J Y et al. (1968). "WHAT THE FROG'S EYE TELLS THE FROG'S BRAIN *". In: pp. 233–258.

Li, Xiangning et al. (2018). "Generation of a whole-brain atlas for the cholinergic system and mesoscopic projectome analysis of basal forebrain cholinergic neurons." In: *Proceedings of the National Academy of Sciences of the United States of America* 115.2, pp. 415–420.

Li and M Basso (2005). "Competitive stimulus interactions within single response fields of superior colliculus neurons". In: *Journal of Neuroscience* 25.49, pp. 11357–11373.

Lister, J A et al. (1999). "nacre encodes a zebrafish microphthalmia-related protein that regulates neural-crest-derived pigment cell fate." In: *Development (Cambridge, England)* 126.17, pp. 3757–3767.

López-Cruz, Pedro L. et al. (2014). "Bayesian network modeling of the consensus between experts: An application to neuron classification". In: *International Journal of Approximate Reasoning*.

Lovett-Barron, Matthew et al. (2017). "Ancestral Circuits for the Coordinated Modulation of Brain State." In: *Cell* 171.6, pp. 1411–1423.

Macosko, Evan Z et al. (2015). "Highly Parallel Genome-wide Expression Profiling of Individual Cells Using Nanoliter Droplets." In: *Cell*.

Malmazet, Daniel de et al. (2018). "Retinotopic Separation of Nasal and Temporal Motion Selectivity in the Mouse Superior Colliculus". In: *Current Biology* 28.18, pp. 2961–2969.

Marques, João C and M.B. Orger (2019). "Clusterdv: a simple density-based clustering method that is robust, general and automatic". In: *Bioinformatics* 35.12. Ed. by Jonathan Wren, pp. 2125–2132.

May, P (2006). *The mammalian superior colliculus: Laminar structure and connections*.

Mazurek, Mark et al. (2014). "Robust quantification of orientation selectivity and direction selectivity". In: *Frontiers in Neural Circuits* 8.

McGarry, Laura M et al. (2010). "Quantitative classification of somatostatin-positive neocortical interneurons identifies three interneuron subtypes". In: *Frontiers in Neural Circuits* 4, p. 12.

Mcilwain, James T. (1991). "Distributed spatial coding in the superior colliculus: A review". In: *Visual Neuroscience* 6.1, pp. 3–13.

Miller, Jae-eun Kang et al. (2014). "Visual stimuli recruit intrinsically generated cortical ensembles." In: *Proceedings of the National Academy of Sciences of the United States of America* 111.38, pp. 4053–61.

Miyawaki, Atsushi et al. (1997). "Fluorescent indicators for Ca2+based on green fluorescent proteins and calmodulin". In: *Nature* 388.6645, pp. 882–887.

Monroy, Jenna A. and Kiisa Nishikawa (2011). "Prey capture in frogs: alternative strategies, biomechanical trade-offs, and hierarchical decision making". In: *Journal of Experimental Zoology Part A: Ecological Genetics and Physiology* 315A.2, pp. 61–71.

Mooney, R D et al. (1988). "The projection from the superficial to the deep layers of the superior colliculus: an intracellular horseradish peroxidase injection study in the hamster." In: *The Journal of neuroscience : the official journal of the Society for Neuroscience* 8.4, pp. 1384–99.

Mysore, Shreesh P et al. (2011). "Signaling of the strongest stimulus in the owl optic tectum." In: *The Journal of neuroscience : the official journal of the Society for Neuroscience* 31.14, pp. 5186–96.

Naumann, Eva A et al. (2016). "From Whole-Brain Data to Functional Circuit Models: The Zebrafish Optomotor Response." In: *Cell* 167.4, pp. 947–960.

Neuhauss, S C et al. (1999). "Genetic disorders of vision revealed by a behavioral screen of 400 essential loci in zebrafish." In: *The Journal of neuroscience : the official journal of the Society for Neuroscience* 19.19, pp. 8603–15.

Niell, Cristopher M. and Stephen J. Smith (2005). "Functional imaging reveals rapid development of visual response properties in the zebrafish tectum". In: *Neuron* 45.6, pp. 941–951.

Nikolaou, Nikolas et al. (2012). "Parametric Functional Maps of Visual Inputs to the Tectum". In: *Neuron* 76.2, pp. 317–324.

Oliveira, Ana F and Keisuke Yonehara (2018). "The Mouse Superior Colliculus as a Model System for Investigating Cell Type-Based Mechanisms of Visual Motor Transformation." In: *Frontiers in neural circuits* 12, p. 59.

Orger, M.B. (2016). "The Cellular Organization of Zebrafish Visuomotor Circuits". In: *Current Biology* 26.9, R377–R385.

Orger et al. (2008). "Control of visually guided behavior by distinct populations of spinal projection neurons." In: *Nature Neuroscience* 11.3, pp. 327–33.

Pachitariu, Marius et al. (2017). "Suite2p: beyond 10,000 neurons with standard two-photon microscopy". In: *bioRxiv*, p. 061507.

Panier, Thomas et al. (2013). "Fast functional imaging of multiple brain regions in intact zebrafish larvae using selective plane illumination microscopy". In: *Frontiers in Neural Circuits* MAR.

Patterson, Bradley W et al. (2013). "Visually guided gradation of prey capture movements in larval zebrafish." In: *The Journal of experimental biology* 216.Pt 16, pp. 3071–83.

Portugues, Ruben et al. (2014). "Whole-Brain Activity Maps Reveal Stereotyped, Distributed Networks for Visuomotor Behavior". In: *Neuron* 81.6, pp. 1328–1343.

Preuss, Stephanie J. et al. (2014). "Classification of Object Size in Retinotectal Microcircuits". In: *Current Biology* 24.20, pp. 2376–2385.

Ramon y Cajal, S (1909). *Histologie du système nerveux de l'homme et des vertébrés*. Ed. by A Maloine. Paris Maloine.

Randlett, Owen et al. (2015). "Whole-brain activity mapping onto a zebrafish brain atlas". In: *Nature Methods* 12.11, pp. 1039–1046.

Reichenthal, Adam et al. (2019). "What pops out for you pops out for fish: Four common visual features". In: *Journal of Vision* 19.1, p. 1.

Rhoades, Robert W. et al. (1989). "Organization of the projection from the superficial to the deep layers of the hamster's superior colliculus as demonstrated by the anterograde transport ofPhaseolus vulgaris leucoagglutinin". In: *The Journal of Comparative Neurology* 283.1, pp. 54–70.

Rind, F. Claire et al. (2016). "Two identified looming detectors in the locust: ubiquitous lateral connections among their inputs contribute to selective responses to looming objects". In: *Scientific Reports* 6.1, p. 35525.

Robinson, D.A. (1972). "Eye movements evoked by collicular stimulation in the alert monkey". In: *Vision Research* 12.11, pp. 1795–1808.

Rodriguez, Alex and Alessandro Laio (2014). "Clustering by fast search and find of density peaks". In: *Science* 344.6191, pp. 1492–1496.

Roeser, Tobias and Herwig Baier (2003). "Visuomotor Behaviors in Larval Zebrafish after GFP-Guided Laser Ablation of the Optic Tectum". In: *The Journal of neuroscience : the official journal of the Society for Neuroscience* 23.9, pp. 3726–3734.

Roland, Benjamin et al. (2017). "Odor identity coding by distributed ensembles of neurons in the mouse olfactory cortex". In: *eLife*.

Romano, Sebastián A. et al. (2015). "Spontaneous Neuronal Network Dynamics Reveal Circuit's Functional Adaptations for Behavior". In: *Neuron* 85.5, pp. 1070–1085.

Rybak, Jürgen et al. (2010). "The digital bee brain: Integrating and managing neurons in a common 3D reference system". In: *Frontiers in Systems Neuroscience* 4.

Sahibzada, N et al. (1986). "Movements resembling orientation or avoidance elicited by electrical stimulation of the superior colliculus in rats." In: *The Journal of neuroscience : the official journal of the Society for Neuroscience* 6.3, pp. 723–33.

Sajovic, P and C Levinthal (1982a). *VISUAL CELLS OF ZEBRAFISH OPTIC TECTUM: MAPPING WITH SMALL SPOTS*. Tech. rep. 10, pp. 2407–2426.

— (1982b). "Visual response properties of zebrafish tectal cells". In: *Neuroscience* 7.10, pp. 2427–2440.

Salas, C. et al. (1997). "Tectal codification of eye movements in goldfish studied by electrical microstimulation". In: *Neuroscience* 78.1, pp. 271–288.

Santana, Roberto et al. (2013). "Classification of neocortical interneurons using affinity propagation". In: *Frontiers in Neural Circuits*.

Schapiro, H. and D.C. Goodman (1969). "Motor functions and their anatomical basis in the forebrain and tectum of the alligator". In: *Experimental Neurology* 24.2, pp. 187–195.

See, Jermyn Z et al. (2018). "Coordinated neuronal ensembles in primary auditory cortical columns". In: *eLife*.

Semmelhack, Julia L et al. (2014). "A dedicated visual pathway for prey detection in larval zebrafish." In: *eLife* 3.

Shang, Congping et al. (2015). "BRAIN CIRCUITS. A parvalbumin-positive excitatory visual pathway to trigger fear responses in mice." In: *Science (New York, N.Y.)* 348.6242, pp. 1472–7.

Shang, Congping et al. (2018). "Divergent midbrain circuits orchestrate escape and freezing responses to looming stimuli in mice." In: *Nature communications* 9.1, p. 1232.

Shekhar, Karthik et al. (2016). "Comprehensive Classification of Retinal Bipolar Neurons by Single-Cell Transcriptomics." In: *Cell* 166.5, pp. 1308–1323.

Simons-Weidenmaier, Nadine S et al. (2006). "Synaptic depression and short-term habituation are located in the sensory part of the mammalian startle pathway." In: *BMC Neuroscience* 7.1, p. 38.

Sparks, David L (1988). "Neural Cartography: Sensory and Motor Maps in the Superior Colliculus". In: *Brain, Behavior and Evolution* 31.1, pp. 49–56.

Tang, Fuchou et al. (2009). "mRNA-Seq whole-transcriptome analysis of a single cell". In: *Nature Methods* 6.5, pp. 377–382.

Tardif, Eric et al. (2005). "Intrinsic connectivity of human superior colliculus". In: *Experimental Brain Research* 166.3-4, pp. 316–324.

Temizer, Incinur et al. (2015). "A Visual Pathway for Looming-Evoked Escape in Larval Zebrafish". In: *Current Biology*.

Thompson, A. W. et al. (2016). "Characterisation of sensitivity and orientation tuning for visually responsive ensembles in the zebrafish tectum". In: *Scientific Reports* 6, p. 34887.

Villalobos, Claudio A. et al. (2018). "Parvalbumin and GABA Microcircuits in the Mouse Superior Colliculus". In: *Frontiers in Neural Circuits* 12, p. 35.

Vladimirov, Nikita et al. (2014). "Light-sheet functional imaging in fictively behaving zebrafish". In: *Nature Methods* 11.9, pp. 883–884.

Vries, Saskia E.J. de and Thomas R. Clandinin (2012). "Loom-Sensitive Neurons Link Computation to Action in the Drosophila Visual System". In: *Current Biology* 22.5, pp. 353–362.

Wagner, Allon et al. (2016). *Revealing the vectors of cellular identity with single-cell genomics.*

Wang, Kun et al. (2019). "Selective processing of all rotational and translational optic flow directions in the zebrafish pretectum and tectum". In: *BMC Biology* 17.1, p. 29.

Wassle, H. et al. (2009). "Cone Contacts, Mosaics, and Territories of Bipolar Cells in the Mouse Retina". In: *Journal of Neuroscience.*

Weber, Maruschka et al. (2002). "Synaptic plasticity in the acoustic startle pathway: the neuronal basis for short-term habituation?" In: *The European journal of neuroscience* 16.7, pp. 1325–32.

Wei, Pengfei et al. (2015). "Processing of visually evoked innate fear by a non-canonical thalamic pathway". In: *Nature Communications* 6.1, p. 6756.

White, Brian J. et al. (2017). "Superior colliculus neurons encode a visual saliency map during free viewing of natural dynamic video". In: *Nature Communications* 8.1, p. 14263.

Wurtz, R H and M E Goldberg (1971). "Superior colliculus cell responses related to eye movements in awake monkeys." In: *Science (New York, N.Y.)* 171.3966, pp. 82–4.

Yilmaz, Melis and Markus Meister (2013). "Rapid Innate Defensive Responses of Mice to Looming Visual Stimuli". In: *Current Biology* 23.20, pp. 2011–2015.

Yoshimatsu, Takeshi et al. (2019). "Cellular and molecular mechanisms of photoreceptor tuning for prey capture in larval zebrafish". In: *BioRXiv.*

Yuste, Rafael (2015). "From the neuron doctrine to neural networks". In: *Nature Publishing Group* 16.

Zeng, Hongkui and Joshua R. Sanes (2017). "Neuronal cell-type classification: challenges, opportunities and the path forward". In: *Nature Reviews Neuroscience* 18.9, pp. 530–546.

Zhang, Y. et al. (2012). "The most numerous ganglion cell type of the mouse retina is a selective feature detector". In: *Proceedings of the National Academy of Sciences* 109.36, E2391–E2398.

Zhao, Xinyu et al. (2014). "Visual cortex modulates the magnitude but not the selectivity of looming-evoked responses in the superior colliculus of awake mice." In: *Neuron* 84.1, pp. 202–213.

Zhaoping, Li (2016). "From the optic tectum to the primary visual cortex: migration through evolution of the saliency map for exogenous attentional guidance". In: *Current Opinion in Neurobiology* 40, pp. 94–102.

Zimmermann, Maxime J.Y. et al. (2018). "Zebrafish Differentially Process Color across Visual Space to Match Natural Scenes". In: *Current Biology* 28.13, pp. 2018–2032.

Zivotofsky, A. Z. et al. (1996). "Saccades to remembered targets: the effects of smooth pursuit and illusory stimulus motion". In: *Journal of Neurophysiology* 76.6, pp. 3617–3632.